University of Stavanger

Faculty of Science and Technology

MASTER'S THESIS

Study program/ Specialization: Master in Industrial Economics Specialization: Drilling	Spring semester, 2013 Open
Writer: Ole Martin Valderhaug	…… (Writer's signature)
Faculty supervisor: Aly Anis Hamouda External	
Title of thesis: Investigating EOR for SS by Low Salinity Water	
Credits (ECTS): 30	
Key words: - Enhanced Oil Recovery - Low Salinity Waterflooding - Wettability - Dissolution of kaolinite - Sulfate - Magnesium - Spontaneous Imbibition - Sandstone	Pages: 132 + enclosure: 7 Stavanger, 15.06.2013 Date/year

Abstract

Water flooding has for a very long time been used to improve oil recovery, in the recent years researchers have become aware of the effects from controlling the salinity and composition of the injected water. Low salinity water as a mean to improve oil recovery is now well established. Extensive research on crude oil/brine/rock (COBR) systems has shown that the injected water composition and salinity can acts as a tertiary recovery method by altering reservoir properties. However, due to the complexity of the COBR interactions, the mechanism(s) behind the low salinity EOR is still being discussed, and none of the suggested mechanisms has so far been accepted as a main process. In this work the intention is to contribute to the ongoing discussions.

This thesis contains a literature review, experimental and simulation works. The experimental part studies both core floods and spontaneous imbibition. Cores were flooded with low salinity brine, as well as brines containing only $MgCl_2$ and only Na_2SO_4. The core floods was performed both as primary and secondary oil recovery method. Ion concentration, pH and pressure drop was measured during the flooding. After the flooding sequence the cores were re-saturated with oil and aged, spontaneous imbibition was then performed to observe the effects from the different brines.

Results from the experiments show that low salinity brine has several contributing mechanisms for enhanced oil recovery. Low salinity flooding is related to a wettability alteration towards more water-wet, by a mechanism that involves dissolution of clay and associated release of organic material and other fine material from pore surface, creating new initially water-wet surface.

The clay mineral kaolinite has a dissolution rate that is dependent upon pH, and injection of brines that increase the pH can cause an increased dissolution rate. Release of fines can lead to partial blocking of the pore throat, increasing the pressure drop. The proposed mechanism is supported by pH and pressure drop measurements, ion analysis, simulation, as well as spontaneous imbibition rate and final recovery results.

As a result oil recovery potential of low salinity appears to be sensitive to the rock and brine composition, and should therefore be evaluated for each case.

Acknowledgements

I am thankful to Dr. Aly Anis Hamouda for his guidance, supervision and encouragement during my research work. I appreciate the opportunity to be a part of his studies, and I have achieved lots of positive experiences and learning.

I also very much appreciate the support and enjoyable company of my co-workers at the laboratory, Alireza Roostaei, Håvard Stangeland, and Rinad Munaev.

I wish to thank my family for their patience, support and encouragement during my studies.

Table of Contents

List of Figures

List of tables

Nomenclature

A_H: Hamaker constant
C_i: Molar concentration
D_O: Molecular diffusion coefficient
P_d: Displacement pressure
Z_i: Charge number of ion
k_B: Boltzmann constant
∇P_G: Pressure gradient
A: crossectional area
AN: Acid Number
ASP: Alkaline Surfactant Polymer
BN: Base Number
CEC: Cation Exchange Capacity
CFC: Critical Flocculation Concentration
COBR: Crude Oil Brine Rock
C_s: Spreading coefficient
d: Diameter
dp: Differential Pressure
e: Electron charge
EOR: Enhanced Oil Recovery
FW: Formation Water
g: Gravity constant
H: Height
HS: High Salinity
IC: Ion Chromatograph
IFT: Interfacial Tension
K: Absolute permeability
$K_{r,max}$: End point of relative permeability
K_r: Relative permeability
L_C: Characteristic length
LSW: Low Salinity Water
MIE: Multicomponent ion exchange
N_b: Bond number
N_b^{-1}: Inverse bond number
N_c: Capillary number
N_g: Gravity number
NI: Normalization index
N_o: Corey exponent
N_r: Reynolds number
OOIP : Original oil in place
P: Pressure
P_C: Capillary pressure
PPM: Parts per million
PV: Pore volume
q: Flow rate
Q_w: Total water volume imbibed
r: Radius
S: saturation
SP: Surfactant Polymer
SSW: Synthetic Sea Water
S_{wi}: Initial water saturation

T: Temperature
t: Time
T_D: Dimensionless time
TDS: Total Dissolved Solid
u_t: Total velocity
V_b: Total bulk volume
V_p: Pore volume
WI: Wettability index
Δ: Difference
μ: Viscosity
ρ: Density
σ: Interfacial tension
Φ: Porosity
α: Langmuir adsorption constant
θ: Contact angle
λ: Pore size distribution index
∂: Partial differential

Subscripts

abs : absolute
avg: average
c: characteristic
g : gas
o : oil
og : oil-gas system
r: relative
s: superficial
w: water
wg : water-gas system
wo : water-oil system

1. Introduction

As the natural energy in the reservoir is no longer enough to produce oil at an economic rate, an extra boost may be needed, and water flooding has been used to improve oil recovery. Water floods were first only used as a mean to maintain reservoir pressure and/or sweep the oil towards production wells. The performance of a water flood is typically affected by the following main parameters:

- Reservoir geology and geometry
- Physical properties: porosity, permeability, heterogeneity
- Fluid properties: viscosity, mobility ratio
- Mineralogical properties: Clay type and amount

Over the decades much research has been done to optimize these parameters to be able improve the water flooding process (Ahmed, 2000). The effect of water chemistry on brine-rock interactions was seldom paid any attention, even though the effect of low salinity brine in sandstone rock containing clay was revealed in the 60's.

In recent years controlling the salinity and composition of the injected water has become an emerging enhanced oil recovery (EOR) technique, often described as low salinity (LS) water flooding. Modification of the water composition has shown to be an excellent way to increase recovery from both sandstone and carbonates. Many researchers have reported, both in field and laboratory test, increase in oil recovery by LS floodings. The understanding of the low salinity mechanism is however still debated, and many theories have been proposed. The complexity and amount of parameters behind oil/brine/rock interactions are thought to be the reason.

Tang and Morrow (1999) identified the following necessary conditions for LS effects in Berea-sandstone:

- Significant clay fraction
- Presence of connate water
- Exposure to crude oil to create mixed-wet conditions

However,it would seem like these conditions are not sufficient, as many outcrop sandstones fulfilling the conditions have not shown LS effects, and the cause of such significant differences has yet to be identified.

2. Literature review

2.1 Sandstone

Sedimentary rocks, as sandstone, are molded as an effect of deposition of clastic material or detritus. These depositions are usually attributed to high energy sedimentary environments, and are accumulated in deserts, beaches, flood plains and/or deltas. Sandstone originate from older igneous, metamorphic or sedimentary rock, where fragmentation, erosion and weathering produce the building blocks (Nichols, 2009; Zolotuchin et. al., 2000)

The size range of the grains varies from 63 µm to 2 mm (Nichols, 2009). Diagenesis is any chemical, physical, or biological change undertaken by sediment or sedimentary rock during and after lithification / formation. Lithification is the process in which the sediments compact as the overburden pressure increase as the grains are buried and the chemically dissolved minerals cause compaction and cementation. Quartz (SiO_2) is the most common mineral species in sandstone reservoirs, there are however a range of different minerals that may occur, such as mica feldspar, heavy minerals, lithic fragments, biogenic particles and many other mineral species which have all been observed in sandstones. Sandstones are often denoted as silici-clastic rocks due to their high silica content. The sandstone has some common cementing material that is attached as a coating to the grains, such as silica, calcium carbonate, iron oxide and clay minerals. After diagenesis the resulting rock has a density of about 2.65 g/cm^3 (Zolotuchin et. Al., 2000)

2.2 Clay minerals

Clay is basically described chemically as aluminum silicates, and consists of a range of different materials, such as silica, alumina, water, and frequently with large quantities of iron and magnesium and lesser amount of sodium and potassium. Clays usually found in sandstone reservoirs is made up by a crystal structure with two simple fundamental building units, sheets of tetrahedral silica and octahedral aluminum layers. These layers are linked to each other into planar layers by sharing oxygen ions between Si^{4+} or Al^{3+} ions of the adjacent tetrahedral or octahedral. The space between the oxygen octahedral and tetrahedral are mostly taken by the Si^{4+} and Al^{3+} ions, but to ensure charge balance other cations such as potassium, calcium, magnesium and iron are necessary in the clay structure (Morad et. Al.,2003). The tetrahedral silica and octahedral aluminum layers join together to form the structure of the clay, which defines the units the clay is made up with.

Kaolinite is clay minerals that consist of one tetrahedral layer linked through oxygen atoms to one octahedral layer with no interlayer cations, and is connected by O-H-O bonds in a 1:1 layer structure. The chemical composition is $Al_2Si_2O_5(OH)_4$ (Morad et. Al., 2003, Wikipedia). Kaolinite is typically

described as booklet pages, it can cause pore blockage if mobilized by liquid flow, however, it does not break up under chemical treatment.

Illite is a non-expanding clay mineral and a phyllosilicate or layered alumino-silicate. Its structure is constituted by the repetition of tetrahedral – octahedral – tetrahedral (TOT) layers, termed 2:1 structure. Two opposing tetrahedral layers are connected by O-K-O bonds, and poorly hydrated K^+ mainly occupies the interlayer space, responsible for the absence of swelling. Al^{3+} partially substitutes Si^{4+} in the tetrahedral layer, and a substitution of divalent cations for Al^{3+} in the octahedral layer occurs, the K^+ is required for charge balance. The chemical formula is given as $(K,H_3O)(Al,Mg,Fe)_2(Si,Al)_4O_10[(OH)_2,(H_2O)]$, but there is considerable ion substitution (Morad et. Al., 2003).

Chlorite has a 2:1 sandwich structure, consisting of negatively charged tetrahedral – octahedral – tetrahedral layers. Unlike other 2:1 clay minerals, a chlorite's interlayer space consist of an additional octahedral layer that is positively charged and comprised of cations and hydroxyl ions, (Mg^{2+}, Fe^{3+})$(OH)_6$, commonly described as the brucite -like layer. Chlorite´s structure will then have the following build up; T – O – T – Brucite – T – O – T. (Morad et. Al., 2003)

Montmorillonite, as chlorite, has a 2:1 sandwich structure, two tetrahedral layers sandwiching a central octahedral layer. The particles have an average diameter of about 1 µm, and are plate shaped. Montmorillonite is a member of the smectite family, and is the main component of the volcanic ash weathering product, bentonite. It increases greatly in volume when it absorbs water, and the original water content is variable. The chemical formula is given as $(Na,Ca)_{0.33}(Al,Mg)_2(Si_4O_{10})(OH)_2 \cdot nH_2O$, named hydrated sodium calcium aluminium magnesium silicate hydroxide. Usual substitutes are Iron, potassium and other cations, but the exact ratio of cations varies with source. It often occurs blended with chlorite, muscovite, illite, and kaolinite.

Montmorillonite, Illite, and Chlorite are all formed as a volcanic rock weathering product, especially volcanic glass.

Clay minerals has unbalanced negative charges on the edges of the unit cells, this is a characteristic that separates them from the other silicates. These negative charges originate from the broken bonds at the edges and surface of the clay structure, and from the dissociation of accessible hydroxyl groups, where the isomorphous substitution of Al^{3+} for Si^{4+} occurs. To attain neutrality, these negatively charged sites attract positively charged ions from the surrounding pore fluid. Some materials have the ability to exchange cations, either by absorption to the external surface or between the layers of the structure, and are described as cation exchange materials (Hamilton,

2009). A clays capacity to attract and hold cations from a solution is measured in CEC (Cation exchange capacity). The Cation exchange capacity is defined as the maximum quantity of total exchangeable cations that the clay is capable of holding at a given pH, usually at a pH of 7. CEC is commonly measured in milliequivalent of hydrogen per 100 gram of clay (meq+/100g) (Bergaya et. Al., 2006, Wikipedia). Cations in the solution are attracted and held by weak quasi-bonding forces, including electrostatic and van der Waals forces, and depending on the conditions they are exchanged and not held permanently. Various cations have different relative strengths and replacing power. Weakly adsorbed cations may easily be exchanged, and therefore the relative replacing power of a particular cationic species depends on its strength of binding.

It is believed that the relative replacing power of cations in room temperature is as follows (IDF, 1982, Beaton et. Al., 2011):

$$Li^{+}<Na^{+}<K^{+}<Mg^{2+}<Ca^{2+}<Sr^{2+}<Ba^{2+}<H^{+}<Al^{3+}$$

As a result, at equal concentrations, H^{+} will be more successful to displace Li^{+} from the clay surface, then Li^{+} to displace H^{+}. However, if the relative concentration of the weaker ion is high enough it may be able to replace ions with a relatively higher replacing power. Characteristics from the four most common clays found in sandstone oil reservoir are listed below.

Property	*Kaolinite*	*Illite / Mica*	*Montmorillonite*	*Chlorite*
Structure	1:1	2:1	2:1	2:1:1
Particle sice (micron)	5-0.5	Large sheets to 0.5	2-0.1	5-0.1
CEC (meq/100g)	3-15	10-40	80-150	10-40
Surface area BET (m^2/g)	15-25	50-110	30-80	140

Table 2.1: Clay characteristics and properties (IDF, 1982)

2.3 Oil recovery

Production of a well through its lifetime can be divided into phases, distinguished by the amount of energy in the reservoir. Traditionally these phases are described in a chronological sense as primary, secondary and tertiary recovery. Initially the fluid flows through the wellbore from natural reservoir drive mechanisms, such as gravity, natural water drive, solution gas drive and expansion of fluids and rock. The fluid flow rate and displacement within a porous media is determined by buoyancy, capillary and viscous forces. Pore geometry, fluid properties, interfacial tensions and wettability is important factors affecting the production rate. An ideal situation compared to most efficient and highest recovery rate is when a field can be produced by gravity drainage alone, however, because of low production rates most fields cannot be economically justified by this mechanism alone.

As the production continues the pressure will decrease in proportion to the net volume of fluid that is produced. As the rate declines, the well may not be economically justifiable, to increase performance (increase oil recovery, shorter duration of production time, etc) secondary and tertiary recoveries may be used (Zolotuchin and Ursin, 2000). Even though the stages are considered as chronological in nature, it has become more common to exploit a reservoir as to maximize recovery.

2.3.1 Primary oil recovery

Primary recovery is defined as the first stage in the oil recovery operation, where the main source of energy to produce oil is preexisting natural energy in the reservoir. As mentioned the natural energy sources consist of expansion of fluids and rocks, gravity drainage, natural water drive, solution gas drive, gas-cap drive and compaction drive. Primary oil recovery is often relatively low and rarely exceeds 45%, and the reservoir pressure fall may lead to solution gas formation (Zolotuchin and Ursin, 2000).

Reserves obtained by primary recovery depend on: (Cossé, 1993)

- amount and distribution of oil/gas in place
- characteristics of the fluids and of the rock
- drive mechanisms and production rate
- economic factors

Adding artificial energy (gas lift, electrical pumps) in the wellbore to lift the fluid, if the reservoir energy is not sufficient to do so, are counted as a part of the primary production. (Zolotuchin and Ursin 2000).

2.3.2 Secondary oil recovery

Secondary oil recovery is employed when the pressure inside the well drops to levels that make primary recovery no longer viable. Injection of water, immiscible gas or a WAG (Water Alternating Gas) increases recovery by displacing oil and maintaining pressure (Green et. Al., 1998).

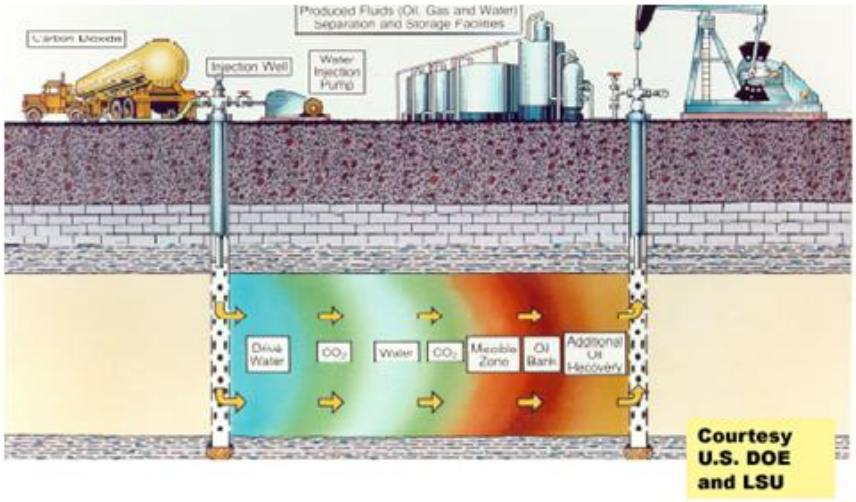

Figure 2.1: Conceptual diagram of an idealized CO_2-WAG process. (D.Rao, spe)

Since immiscible gas flooding is not as efficient, water flooding is preferable. Critical design elements of a successful water flood are: reservoir geometry, lithology, reservoir depth, porosity, permeability, continuity of rock properties, fluid saturations, fluid properties, relative permeabilities, water source and its chemistry (Raymon et.Al., 2006).

Primary and secondary recoveries together give up to 60% from the oil initially contained in the reservoir (Bavière, 1991).

2.3.3 Tertiary oil recovery (EOR)

There are several different definitions of tertiary recovery and Enhanced Oil Recovery (EOR). One definition is that the injected fluid is altered by changing the chemical and/or physical properties to increase the sweep efficiency and increase recovery beyond which is achieved by primary and secondary recovery. Chronologically, tertiary recovery is performed after secondary recovery. However, reservoir operations may not necessarily be performed in a specific order. Tertiary recovery has therefore been replaced by the term enhanced oil recovery.

The Norwegian Petroleum Directorate defines EOR (enhanced oil recovery) as a term used for advanced methods for reducing the residual oil saturation in the reservoir (NPD, 2013).

Enhanced oil recovery techniques have been strategically developed to bring a radical increase in economic recovery by improving pore scale displacement and sweep efficiency using existing well stock. As in primary and secondary recovery the goal is to maintain the reservoir pressure, and reducing the residual oil saturation. Mobilization of oil at pore scale is expressed by the microscopic displacement efficiency, which depends on several physical and chemical interactions occurring between the displacing fluid, gas and oil. The sweep efficiency is the percentage of the total pore volume which is being swept of oil by a displacing fluid, as in water flooding or natural / artificial gas drive. The efficiency may be improved by altering mobility ratios between all displacing fluids, which is accomplished by altering wettability, interfacial tension (IFT), fluid viscosities or by injecting gas/fluid that through favorable phase behavior displaces the oil. Tertiary recovery methods may be categorized into four categories (Green et. Al., 1998, Hourshad et. Al., 2012) :

- Mobility-control process
- Miscible processes
- Chemical processes
- Thermal processes

An example of a proven EOR technique is polymer flooding, which by increasing the water-oil viscosity increases water flooding recovery efficiency. Low Salinity water injection is an emerging technology which enhances the displacement efficiency by mechanisms not currently fully understood. The technique involves the salinity of the injected water to be controlled, as to improve oil recovery vs. conventional higher-salinity water flooding. Tests with core floods and single-well chemical tracer have shown that basic water flood recovery can be improved by about 5-38% (Hourshad et. Al., 2012). Low salinity flooding has been modeled by using salinity-dependent oil/water relative permeability resulting from wettability changes, the approach was based on the established modeling methods of chemical EOR (Jerauld et. Al., 2008). Schemes that is more robust than the individually used methods have been generated by the synergistic behavior of EOR approaches as Surfactant Polymer (SP) and Alkaline Surfactant Polymer (ASP). A polymer or foam is needed as a mobility control agent to make any low interfacial tension chemical EOR successful, which has often been giving disappointing results due to an insufficient amount of injected polymer.

As in the chemical EOR application a combination of polymer flood and low salinity water flood should have added benefits. It is expected that tertiary low salinity floods would be mildly unstable due to low mobility ratio at adverse saturation shocks and presence of capillary pressure (Tripathi et.al, 2007). As an effect it is believed that tertiary low salinity flood improves the stability of the shock front by adding polymer, especially at the shock front. Mohanty, 2011, demonstrated by a core

flooding comparison of high and low-salinity water combined with polymer, that adding polymer to the low-salinity water could increase oil recovery to an extra 10% above the low salinity water flood.

A lot of recent research has been motivated by screening, selecting and developing of polymers for EOR applications that can handle high-salinity and high-temperature reservoirs (Levitt et. Al., 2008; Vermolen et.al.,2011). Numerous polymers with high molecular weight demonstrating high viscosities at high salinities up to 170,000 ppm NaCl and greater than 17,000 ppm $CaCl_2$ were tested, showing that polyacrylamide polymers hydrolyze at high temperatures and are a substance to precipitation by calcium beyond a certain point. As a conclusion the use of polyacrylamide polymers is feasible if calcium concentration is kept below 200 ppm and with reservoir temperatures up to 100^{o}C (Levitt et. Al., 2008). Therefore the combination of low-salinity water and polymer flood would become even more desired, and the applications of these EOR methods would be expanded to high-temperature reservoirs.

2.3.4 Waterflooding

The earliest and most widely used process for increased oil recovery from reservoirs is water flooding. The reservoir pressure is maintained, and oil production is accelerated or the production decline is slowed down as the water flood physically displaces the oil from the reservoir (Cosse, 1993). The performance of a water flood is typically affected by the following main parameters:

- Reservoir geology and geometry
- Physical properties: porosity, permeability, heterogeneity
- Fluid properties: viscosity, mobility ratio
- Mineralogical properties: Clay type and amount
- Presence of chemicals

Over the decades much research has been done to optimize these parameters to be able improve the water flooding process (Ahmed, 2000).

2.3.4.1 Low Salinity Waterflooding

Waterflooding is traditionally considered as a secondary recovery method. However, modification of the water composition has shown to be an excellent way to increase recovery from both sandstone and carbonates, and could therefore be considered as a tertiary recovery method. Compared to other tertiary methods available for sandstone reservoirs, low salinity waterflooding may be one of the cheapest and environmentally friendly approaches. The low salinity method was first discovered in the late 1950`s, when fresh water was injected to increase recovery and displace viscous oil (Martin, C., 1959). Bernard continued the investigation into low salinity brine (Bernard, 1967).

Reservoir and outcrop sandstone cores were flooded with fresh water and brine solutions with different concentration of NaCl, and with a reduction in concentration of NaCl from 1% to 0.1% an increased recovery was observed. It was discovered that the increased recovery was dependent of a salinity range from 0% to 0.1% of NaCl. Several laboratory studies performed lately of low salinity flooding with both outcrop and reservoir cores have shown increased oil recovery (Austad et. Al., 2010; Boussour et. Al., 2009; Cissokho et. Al., 2009; Ligthelm et. Al., 2009; McGuire et. Al., 2005; Morrow et. Al., 1998; Pu et. Al., 2008; Tang and Morrow, 1999a; Tang and Morrow, 1999b; Tang and Morrow, 1997b; Webb et. Al., 2008; Zhang and Morrow, 2006b). Positive test results have also been required from full field studies, single well tracer test and log-inject-log measurements (Batias et.al., 2009; Lager et.al., 2008b; McQuire et.al., 2005; Robertson, 2007; Seccombe et.al., 2008b, Webb et.al., 2004).

2.3.5 Observations and factors affecting low salinity water flooding

2.3.5.1 Mineral surface

Some researchers have reported that low salinity water injection in sandstone cores, enhanced oil recovery is only observed in cores containing clay, and clay has earlier been listed as a requirement to obtain a low salinity effect. Experiments performed on clay-free cores, which were fired at 800^{o}C and acidized to remove the clay, did not show any response to low salinity (Tang et.al., 1999a, Pu et.al., 2008). It has been proposed that the increased oil recovery from low salinity water injection performed as tertiary mode is scalable to the amount of kaolinite clay in the rock. The theory was suggested after laboratory coreflood test, singe-well chemical tracer tests (SWCTT), and a full field test on the Endicott field in Alaska (Lager et.al., 2007, Seccombe et.al., 2009). Secombe et.al., (2008) found a correlation between the kaolinite content and additional tertiary recovery by low salinity waterflooding, using three SWCTT and a core flood. However, other results show that cores lacking kaolinite still had an increase in recovery from low salinity injection (Austad et.al., 2010; Cissokho et.al., 2009). Researchers have observed increased recovery from low salinity flooding on cores containing different clays, such as illite, muscovite and chlorite (Cissokho et.al., 2009). The presence of Chlorite has been related to poor results of low salinity injection, by research on Berea sandstone cores (Zhang et.al., 2006a). Austad et.al.,(2010) also stated that because of its low Cation Exchange Capacity (CEC) kaolinite may be one of the least advantageous clay types. Sandstone cores without clay, but with a content of dolomite crystals have shown positive results from injection of low salinity water (Pu et.al., 2008). A further suggestion is that a negative zeta potential material with cation exchange capacity seems to be related to a successful low salinity flooding of sandstone rock (RezaeiDoust, 2011).

Experiments involving a 3D imaging technique resulted in the observation that low salinity brine was able to mobilize the dolomite and anhydrite crystals in the rocks (Lebedeva et.al., 2009), Pu et.al. (2010) later related low salinity effects to the dissolution of anhydrite and dolomite cements in three different cores. As a result it was suggested that the core becomes more water-wet from the dissolution, and that strongly water-wet cores did not show any low salinity effect. In recent studies it has been concluded that anhydrite dissolution is not the main mechanism behind the improved oil recovery, but rather a contributory mechanism (Romanuka et.al., 2012).

Diluted sea water has been able to improve the recovery in carbonate reservoir rock (80% calcite, 13% dolomite, 6% anhydrite, >1% quartz), the observed effect were explained by some brine-rock interaction increasing the water-wetness of the rock (Yousef et.al., 2011). Reinholdtsen et al. (2011) suggests that the presence of certain plagioclase silicates, increases the pH of formation water and therefore the capacity of clays present to adsorb oil during ageing are reduced. Such a situation would lead to an initially water wet rock and thus prevent the low salinity effect from occurring.

2.3.5.2 Brine

Low Salinity Brine: Composition and Salinity

Several investigations have revealed a lower salinity threshold needed in order to observe an increased oil recovery, which was a good degree less than salinity of the formation brine (Batias et.al., 2009; Cissokho et.al., 2009; Jearuld et.al., 2008; Lager et.al., 2008a; McGuire et.al., 2005). Provided that other required conditions are fulfilled, the research has shown that reducing the salinity of the injected water to 1000-2000 ppm an effect on oil recovery was observed in about all instances. An upper salinity threshold of about 5000 ppm are most commonly acknowledged, in which increased recovery has been obtained (Webb et.al., 2004). It has been observed by some researchers that the low salinity brine must contain some form of divalent and other multivalent cations to work successfully (Lager et.al., 2006; Sharma et.al., 2000). Other research indicate that by injection of water with a high concentration of divalent cations the oil recovery stopped (Jerauld et.al., 2008; Tang et.al., 1999a). On the other hand it has been reported that removing the divalent ions in the injection brine is not sufficient, if the concentration of mono-valent ions is high, for example Na^+ (Ligthelm et.al., 2009; Zhang et.al., 2007b). Some authors have suggested that there should be an optimal low salinity water composition, according to their proposed mechanism responsible for the low salinity effect (Austad et.al., 2010; Lager et.al., 2008).

Formation Brine

It appears that initial water saturation is an important parameter for low salinity recovery methods. Spontaneous imbibition and flooding / forced imbibition experiments on 100% crude oil saturated cores showed no low salinity effect, and it appears that the presence of connate brine or aging brine is a requirement for low salinity effects in core experiments (Tang et.al., 1999a).In addition a higher increase in recovery has been obtained from cores with higher initial water saturation (Jadhunandan et.al., 1995a). Another important parameter in formation brine is the concentration of divalent cations, such as Ca^{2+} and Mg^{2+}, observations seems to indicate that divalent cations must be present to observe any increased recovery by low salinity injection in secondary or tertiary corefloods (Sharma et.al., 2000; Lager et.al., 2006; Ligthelm et.al., 2009).

2.3.5.3 Oil

From experiments with refined oil, and all other parameters kept constant, no extra recovery was observed by adjusting the salinity of the injection brine (Tang et.al., 1999a; Zhang et.al., 2007b). Tang et.al. (1999b) reported that polar components in the oil is a necessary requirement for improved oil recovery, as the use of refined oil without polar components did not show any response to low salinity. Similar results was obtained by RezaeiDoust et al. (2011), oil with different acid / base number were used in floodings, they reported that both high acid number-low basic number oil and low acid number-high basic number oil gave similar low salinity effect, indicating that both acidic and basic oils is usable. Imbibition test with the same core and brine type were conducted with various crude oil, characterized by IFT with formation water, acid / base number, density, viscosity, sulphur content, saturates, aromat, asphaltene stability and resin / asphaltene content. A good correlation between any of the oil properties and tertiary low salinity effect were not discovered, the conclusion were that conventional characterization of the oil properties was not efficient, and it was suggested a fractionation of oil into functional groups (Suijkerbuijk et al., 2012). It is therefore generally accepted that the oil must contain polar components for a low salinity effect.

2.3.5.4 pH in Effluent

Several researchers have discovered an increase in the pH of the effluent in low salinity floodings, typically 1-3 units, for non-buffered systems (Austad et.al., 2010; Cissokho et.al., 2009; McGuire et.al., 2005; RezaeiDoust et.al., 2009). There are two different mechanism behind the increase, mineral dissolution and ion exchange, which cause the formation of excess hydroxyl ions, OH^- (Austad et.al., 2010; Lager et. Al., 2006; McGuire et.al., 2005). Cation exchange is performed between the brine and clay surface, where H^+ ions can exchange with cations adsorbed onto the clay. It is a relatively fast mechanism, and the process requires an existence of surface active cations in the initial formation brine and the presence of cation exchange mineral. Mineral dissolution occurs

mainly of carbonate, such as calcite and dolomite, and is a relatively slow process (RezaeiDoust, 2011).

2.3.5.5 Fines Migration

When low salinity brine is injected the clay is thought to be destabilized, as a result of the critical flocculation concentration (CFC) of the clay is reached. The destabilization is a result of the electrical double layer expanding between clay particles, and the clays ability to screen negatively charged particles decreases. A reduction in the permeability could occur from the mobilization of fines. As a result an increase in pressure drop over the core may be observed, and a production of fines could be expected. It seems this is not a general observation, but it has occurred in some experiments with low salinity flooding, with and without increased recovery (Boussour et.al, 2009; Tang et.al., 1999a).

2.3.5.6 Temperature

Contradictory results have been reported on the effect of aging temperature, even at temperature below 100^0C. Some has stated that an increase in aging temperature did not alter the ability of the core to imbibe water (Buckley, 1996), other experiments reports a less water-wet condition as the aging temperature is increased. Initial wetting of the rock is a very important factor, and a mixed-wetting condition after aging seems to give best LS results (Buckley, 1996; Jadhunandan et.al., 1991; Tang et.al., 1999a). The results obtained from low salinity water flooding also seem to be dependent upon the flooding temperature. Recovery were increased by a higher flooding temperature with a high salinity secondary flooding, while recovery from tertiary low salinity water flooding were reduced (Cissokho et.al., 2009). RezaeiDoust et.al., 2010, conducted low salinity corefloods on North Sea reservoir samples with different aging and flooding temperatures. Cores aged at 60^0C showed no response to tertiary low salinity flooding at 60^0C and 130^0C, while cores aged at 90^0C responded to low salinity flooding at 60^0C, 90^0C, and 130^0C. Cissokho et.al., 2009, aged the cores at 60^0C, followed by flooding with high salinity and tertiary low salinity at 35^0C and 60^0C, observing a low salinity effect only for the core flooded at 35^0C.

Wetting state after aging is known to be temperature dependent. A study of aging temperatures between 25-80^0C revealed that cores were more water-wet at lower temperatures (Jadhunandan et.al., 1995).

Generally flooding experiments have been studied at temperatures below 100^0C, there is therefore a lack of experiments studying the effect of temperature on initial wetting and enhanced oil recovery, more research should be done on this matter.

2.3.5.7 Wettability

It has been suggested that cores become more water wet as the mixed wet clay particles is released by low salinity water (Tang et.al., 1999b). Oil production may be accelerated by a water wet condition, it is however commonly accepted that a mixed wet condition usually produces the least residual oil saturation after injection of several pore volumes (Jadhunandan & Morrow, 1995; Green & Willhite, 1998). An experiment conducted by Berg et al. (2009), visually revealed the release of oil droplets from the clay surface, as the surface were initially exposed to high salinity water, changing to low salinity, the mechanism involved were however not identified. Oil field low salinity injection resulted in two distinct observed water cuts, which may be an indication of a wettability alteration towards a more water wet case (Vledder et.al., 2010).

On the other hand, it has been suggested that the wettability may be altered towards more oil wet from the injection of low salinity water (Fjelde et.al., 2012; Sandengen et.al., 2011), resulting in an insignificant increase in tertiary oil recovery in their experiments, and slower oil production in secondary floods. Due to the wettability change, an increased capillary end effect is expected, and especially with slow rate corefloods the residual saturations may be distorted.

A mechanism of different effects of salinity on wettability has been explained by the basis of the disjoining pressure (Sharma et.al., 2000). According to DLVO theory, salinity may affect the electrostatic forces, as a result lower salinity creates a thicker film, increasing the water-wetness (Israelachvili, 2011). Sharma et.al., 2000, suggested that for some crude oil and polar fractions with large surface density where electrostatic forces dominate, the water-wetness is increased as explained by DLVO theory. They also suggested that for some less polar oils where electrostatic forces are suppressed, the hydration/hydrophobic forces may dominate, hypothesizing that these hydration / hydrophobic forces increases with salinity producing a less water wet surface.

Core flooding experiments on cores with different wettabilities, including water-wet, oil wet, neutral wet and neutral wet towards oil wet, a low salinity effect was observed for all states, after aging and flooding with high salinity. The highest effect was however observed for the water wet core (Ashraf et.al., 2010).

2.4 Displacement Forces

Capillary, viscous and gravity forces are just some of several forces that the oil, gas, and water inside a porous media are subjected to, but they are most likely to be the most important ones, as these forces to a large extent influence the residual saturation that can be obtained in a porous medium.

2.4.1 Gravity forces

If the density difference between the displacing and displaced fluid is large, gravity would play an important role in fluid flow, and in cases where the interfacial tension between oil and water is relatively low (Austad et. Al., 1997). The pressure difference due to density is given in the equations below:

$$\Delta P_G = \Delta \rho g H \tag{2.1}$$

$$\nabla P_G = \Delta \rho g \sin \alpha \tag{2.2}$$

ΔP_G = pressure difference
∇P_G = pressure gradient
$\Delta \rho$ = density difference
g = gravitational acceleration constant
H = height of the column
α = angle of formation dip

When immiscible fluids with different densities co-exist, a buoyancy force is created. The lighter fluid would be pressured upwards, and the fluids would segregate. A potential displacement may result in either gravity override (CO_2 and solvent flooding) or gravity under-ride (waterflood), and the gravity forces would be more severe for a large dip in the formation (Green et.Al., 1998).

2.4.2 Capillary Forces

In a petroleum reservoir the capillary forces are dependent upon several factors, such as pore size and geometry, wetting characteristics of the system, surface and interfacial tension of the rock and fluids (Ahmed, 2000). Capillary pressure is the pressure difference across two immiscible fluids interphase, and is formed due to the tension of the interface (Green et. al., 1998). By definition it is the pressure in the non-wetting phase minus the pressure in the wetting phase, and for a water / oil system, the capillary pressure are defined as the pressure in the oil phase minus the pressure in the water phase. The pressure could be higher in the non-wetting phase, as a result the capillary pressure could be positive or negative depending on which fluid is the wetting phase. Laplace`s equation calculates the capillary pressure between two immiscible phases across a curved surface in terms of the radii of curvature:

$$P_C = P_O - P_W = \sigma_{OW}\left(\frac{1}{R_1} + \frac{1}{R_2}\right) \tag{2.3}$$

P_c = capillary pressure
P_o = pressure in the oil phase
P_w = pressure in the water phase
σ_{OW} = interfacial tension between wetting phase and non-wetting phase
R_1,R_2 = curvature radii of interface between oil and water

For a capillary tube containing two immiscible fluids the capillary pressure can be expressed by equation 2.5 below. The principal radii of the meniscus formed are given by equation 2.4. The parameters are the interfacial tension, size of the capillary and the relative wettability of the fluids.

$$R_s = R_1 = R_2 = \frac{r_t}{\cos\theta} \quad (2.4)$$

$$P_C = \frac{2\sigma_{OW}\cos\theta}{r_t} \quad (2.5)$$

P_c = capillary pressure
σ_{OW} = interfacial tension between oil and water
θ = contact angle
r_t = radius of capillary tube

The surface forces of capillary pressure would either aid or oppose the process of displacing one fluid by another in the pores of a porous medium (Ahmed, 2000). The impact capillary pressure will have on fluid flow is dependent upon if the reservoir is fractured or not. If the reservoir is fractured, the displacement efficiency of a waterflood is strongly dependent upon spontaneous imbibition of water into the matrix because of strong capillary forces. Sandstone reservoirs are rarely fractured, and strong capillary forces may cause trapping of oil and high residual oil saturation for a water flood, known as ”end effect” (Anderson, 1987). Reducing the interfacial tension between the water and oil will however improve the situation.

2.4.3 Viscous Forces

As a fluid flows through a porous medium a certain pressure drop occurs, caused by the viscous forces in the fluid. The magnitude of the viscous forces must be larger than the capillary forces, if not the fluid would not flow through the pore. A porous medium can be compared to a bundle of parallel capillary tubes, and the following equation represents the pressure drop in one capillary tube at laminar flow conditions (Green et.al., 1998):

$$\Delta P = \frac{8\mu L v_{avg}}{r^2 g_C} \quad (2.6)$$

ΔP = pressure difference across capillary tube
μ = viscosity
L = length of capillary tube
v_{avg} = average flow velocity in capillary tube
R = radius of capillary tube

g_C = conversion factor

Darcy`s law give the viscous force for single-phase flow in a porous media, the equation is given below. Phase trapping and mobilization in a two phase setting is determined by the viscous and capillary forces (Willhite, 1986).

$$\nabla P_v = -\frac{\mu u_s}{K} \quad (2.7)$$

∇P_v = pressure gradient due to viscous forces
u_s = superficial velocity
K = permeability of the porous medium

2.4.4 Dimensional Analysis

Dimensional analysis (Buckingham theory) is a general analytical method of determining or finding relations among physical quantities by using their dimensions. The dimensional analysis theory is based on the fact that any equation that describes a relation among a number of physical quantities can be reduced to the following form:

$\Phi(\Pi_1, \Pi_2, \Pi_3, \ldots) = 1$

Here the Π values are independent dimensionless products in the form of the original quantities. As an alternative to individual variables the physical phenomenon is characterized in the form of various dimensionless groups. The performance of spontaneous imbibition will therefore be a function of the dimensionless groups and not to each individual parameter. Dimensionless groups can be used to assess the interplay of different forces involved in fluid flow through porous media. Different forces can be stated as ratios, reducing the number of parameters to be studied. Various dimensionless numbers obtained from literature is listed in table 2.2.

No.	Similarity Group	Formulation
1	Dimensionless time	$t_D = t\sqrt{\frac{k}{\phi}}\frac{\sigma}{\sqrt{\mu_o\mu_w}}\frac{1}{L_C^2}$
2	Bond number (ratio of gravity force to capillary force)	$N_B = \frac{\Delta\rho g H\sqrt{\frac{K}{\phi}}}{\sigma_{OW}}$
3	Inverse Bound number (ratio of capillary force to gravity force)	$N_B^{-1} = C\frac{\sigma_{OW}\sqrt{\frac{\phi}{K}}}{\Delta\rho g H}$
4	Capillary number (ratio of viscous force to capillary force)	$N_c = \frac{v\mu_w}{\sigma_{ow}\cos\theta}$
5	Gravity number (ratio of gravity forces to viscous force)	$N_g = \frac{\Delta\rho g(\frac{k}{\phi})}{v\mu}$
6	Reynolds number (ratio of viscous force to inertia force)	$N_r = \frac{\rho v D p}{\mu}$

Table 2.2: Different dimensionless numbers obtained from literature

The relative magnitude of capillary and viscous forces has a connection with the influence of gravity forces. In order to mobilize discrete ganglia of the oil and coalesce them together to form a continuous oil phase, a certain viscous force is required, and lowering the interfacial tension would mean lowering the viscous forces required (Taber, 1969). Several studies have shown that residual oil saturation is a function of capillary number, which is the dimensionless ratio between the viscous forces and capillary forces:

$$N_C = \frac{u\mu}{\gamma} \quad (2.8)$$

$$N_C = \frac{v\mu_w}{\sigma_{ow}\cos\theta} \quad (2.9)$$

u = darcy velocity
μ = viscosity of displacing fluid
γ = interfacial tension between two phases

As a consequence of this formula, the residual oil saturation in a reservoir is affected by parameters as oil/rock/formation brine interactions (wettability) and rock properties (porosity, permeability) (Chatzis et.al., 1984, Lake, 1989). Capillary pressure can aid or disrupt the fluid displacement during flooding in a porous media, also determining the saturation profile / distribution. During a core

flooding process the boundary condition of the water saturation at the core outlet is determined by the capillary pressure, if S_{we} is sufficiently low the average water saturation in the core at the end of flooding may be distorted. This is usually the case if the core is oil wet, short, and/or the flow rate is low, since high viscous forces are needed to overcome the capillary forces at the rest of the core. This effect is called capillary end effect. When displacing a non-wetting phase an increase in the capillary number beyond a critical value can reduce the residual saturation after a waterflood. The increase can be achieved by increasing the viscosity of the displacing fluid, reducing the interfacial tension, increasing the displacement velocity, or alter the wettability. In a field case, increasing the velocity may not be an option, since the injection of fluid usually is pressure dependent.

The oil displacement mechanism is impacted by the balance between gravity and capillary forces. Schechter et.al., 1994, expressed the relationship as the inverse Bond number:

$$N_B^{-1} = C\frac{\sigma_{OW}\sqrt{\frac{\phi}{K}}}{\Delta\rho g H} \quad (2.10)$$

C = constant
σ_{OW} = interfacial tension between oil and water
H = height of the medium
ϕ = porosity
$\Delta\rho$ = cifference in density between water and oil
K = absolute permeability
g = gravity acceleration constant

In a system with well-defined wetting properties, gravity forces are dominant for $N_B^{-1} \leq 1$, and capillary forces for $N_B^{-1} > 5$. Both capillary and gravity forces can be active in the displacement in the intermediate range, $0.2 < N_B^{-1} < 5$. Oil is produced in a countercurrent flow mode from all surfaces if the capillary forces are dominating the SI process. Gravity forces become more important as the interfacial tension is reduced or the difference in density in increased, thereby reducing the inverse bond number.

2.4.5 Molecular diffusion

If two miscible fluids are in contact with each other by an initially sharp interface, the two fluids will slowly diffuse into one another. This spontaneous diffusion is the outcome of the spontaneous movement of particles from an area of high concentration to an area of a lower concentration, in a certain volume of fluid, either liquid or gas. With time, the sharp interface will turn into a diffuse mixed zone grading from one pure fluid to the other (Perkins and Johnston, 1963). The diffusion is a result from the random motion of the molecules. The net transport of one of the constituents across

any arbitrary plane can be calculated by Fick's first law, assuming steady-state diffusion, given by that the concentration within the diffusion volume does not change with time.

$$(2.11) \quad \frac{dG}{dt} = -D_O A' \frac{\partial c}{\partial x}$$

G = quantity of material diffusing across a plane
t = time [s]
D_O = molecular diffusion coefficient [m^2/s]
A' = cross section area for diffusion [m^2]
c = concentration, fraction of volume
x = distance [m]

For a non-steady state, where the concentration within the diffusion volume changes with respect to time, Fick's second law may be used.

$$(2.12) \quad \frac{\partial c}{\partial t} = D_r \frac{\partial^2 c}{\partial x^2}$$

c = concentration [mol/m^3]
t = time [s]
D_r = diffusion coefficient / diffusivity [m^2/s]
x = position [m]

Normally molecular diffusion is small in porous media, however, as the contact area for diffusion is significantly increased as the dispersive flux through a fracture, it may be of importance in naturally fractured reservoirs (Da Silva et.al., 1989). If inert hydrocarbon gas is injected in a small fracture spacing, the molecular diffusion potential could even overrule viscous forces. Molecular diffusion rates are temperature dependent, and in room temperature the diffusion coefficients of most ions in dilute aqueous solutions are similar, and the values range from 0.6×10^{-9} to 2×10^{-9} m^2/s.

2.4.6 Adsorption

As oil and gas reservoirs are formed, the adsorption of polar components from the hydrocarbon changes the wetting state of the reservoir rock (Collins et.al., 1983; Legens et.al., 1998,1999; Madsen et.al., 1996). Adsorption is defined as the process in which the solute in a gas or liquid accumulates on the surface of a solid or a liquid, forming an atomic or molecular film. An equation was developed by Irving Langmuir (1916), called the Langmuir adsorption equation, which at a fixed temperature relates the coverage or adsorption of molecules on a solid surface to the concentration of a medium or gas pressure above the solid surface.

$$(2.13) \quad \varphi = \frac{\alpha p}{[1+(\alpha p)]}$$

φ = percentage coverage of the surface
p = gas pressure / concentration

α = Langmuir adsorption constant

The constant α increases as the strength of adsorption increases, and with a decreasing temperature. Derived from a starting point with equilibrium between the empty surface sites, particles and filled particle sites.

$$S^* + P \leftrightarrow SP \quad (2.14)$$

S^* = empty surface sites
P = particles
SP = filled surface sites

The equilibrium then becomes:

$$K = \frac{[SP]}{[S^*][P]} = \frac{\theta}{(1-\theta)P} \quad (2.15)$$

Optimized Langmuir equation:

$$\Gamma = \frac{\Gamma_{max} K c}{1+Kc} \quad (2.16)$$

K = Langmuir equilibrium constant
c = aqueous concentration
Γ = amount adsorbed
Γ_{max} = maximum amount adsorbed as c increases

2.5 Wettability

One definition of wetting is the ability of the liquid to maintain contact with a solid surface, or of a solid to liquid, as a result of intermolecular interactions from the two. Adhesive and cohesive force balance determines the degree of wetting. Adhesive forces bond the liquid and surface together, causing the liquid to spread across the surface. Cohesive forces repel the liquid, causing the liquid to form a drop, avoiding contact with the surface. The contact angle between the fluid and solid can be measured to determine the degree of wetting/wettability, and ismeasured where the solid-liquid interface meets the liquid-gas interface. The tendency of a liquid to spread over a solid surface increases as the contact angle decreases, and the contact angle provides an inverse measure of wettability. Two immiscible fluids in contact with a solid surface could have a variety of effects, one of the fluids could spread or adhere to the surface more than the other. If one fluid does not wet the surface completely, the mixed-wetting condition can be measured by the contact angle between the denser liquid and the surface. One example is a water-solid-oil system. At equilibrium Youngs´s equation can be expressed as (Olga Vizika et. Al., 1996):

$$\sigma_{so} - \sigma_{sw} = \sigma_{wo} \cos\theta \quad (2.17)$$

Where σ_{so} is the interfacial tension between the oil and solid, σ_{sw} between the water and solid, σ_{wo} between the oil and water. θ is the contact angle measured through the water phase. The favorably fluid which wets the solid is determined by the adhesion/cohesive tension, a function of interfacial tension. The adhesion tension A_T for water-oil-solid is defined as:

$$A_T = \sigma_{so} - \sigma_{sw} = \cos(\theta)\sigma_{so} \quad (2.18)$$

Water is the favorably fluid to wet the solid surface at a positive adhesion tension (water-wet media). An A_T of zero indicates an equal attraction for the surface (neutral system). A negative A_T indicates that oil preferentially wets the solid surface (oil wet media) (Olga Vizika et.al. ,1996).

The wetting state of a rock is an important parameter that determines distribution of fluid, end point saturations, and relative permeability of the phases (Donaldson et.al., 2008). There are numerous factors affecting wettability, such as rock mineral composition, pore structure, pore geometry, pore size, brine composition, salinity, pH, temperature and oil composition. It is very difficult to isolate these factors in wettability studies, since all parameters influence the wettability in different ways. The interactions responsible for wettability may be listed in the following actions: polar interactions, acid/base interactions, surface precipitation and ion binding (Buckley et.al., 1998).

Wetting Condition	Contact Angle (degrees)
Strongly water-wet	0-30
Moderate water-wet	30-75
Neutrally wet	75-105
Moderatly oil-wet	105-150
Strongly oil-wet	150-180

Table 2.3: Wetting conditions for a water-oil system by contact angle (Fanchi, 2010).

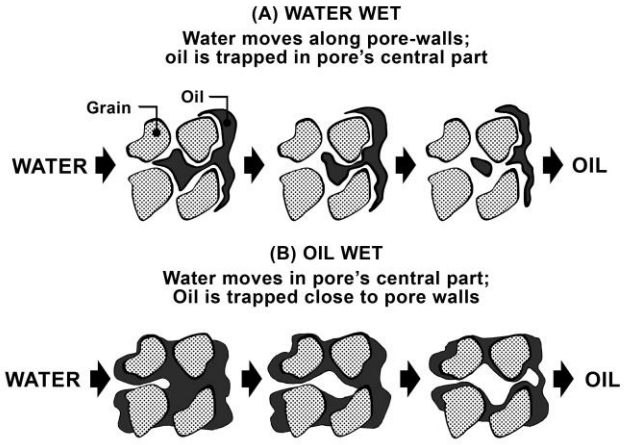

Figure 2.2: Residual oil at water-wet(top) and oil-wet(bottom) surfaces.

Water-wet

If the surface prefers the water phase rather than the oil, the rock can be considered as water-wet. If the rock is completely water-wet, the oil is centered in the large pores as droplets surrounded by water films lining the pore walls. Water may totally occupy the smaller pores, leaving oil phase to reside in the bigger pores. Continued waterflooding potential are low for these systems, with a high recovery at water breakthrough, and only a small recovery increase after breakthrough, because the remaining oil are trapped as globules without hydraulic connections. The contact angle is 0^{o} for these systems (Dandekar, 2006).

Oil-wet

If the surface prefers the oil phase rather than the water, the rock can be considered as oil-wet. The water is centered in the larger pores as droplets, whereas the oil exists on the surface of the rock as a thin film, occupying the smaller pores. An oil-wet rock is associated with a low recovery at water

breakthrough, but since there is no loss of hydraulic connection an extended recovery period is possible after breakthrough (Donaldson et.al., 2008).

Mixed-wet

The larger pores in a mixed-wet rock are wetted by oil, while the smaller pores are occupied by water. Resulting in a smaller recovery at breakthrough, but extended oil production period. The oil phase is not trapped as isolated droplets, as there may exist some connections along the larger pores, therefore a mixed-wet rock is ordinary containing the least amount of residual oil. The figure below shows typical relative permeability and capillary pressure curves for water-wet and mixed wet systems. The dotted curve represents primary drainage (P_C) for both water-wet and mixed-wet conditions, they are identical since most reservoirs are considered water-wet prior to primary drainage. At S_W = 100% the value is positive, specifying that an entry pressure has to be overcome before substantial displacement of water can follow.

Secondary imbibition and drainage capillary pressure curves are positive for a large part of the saturation range for a strongly water-wet system, characterized as spontaneous imbibition of water. For a mixed-wet system the secondary capillary curves is both negative and positive at different water saturation ranges, as a result spontaneous imbibition of both phases is possible. Also, for a mixed-wet system the relative permeability of oil is reduced in the presence of water, since oil must compete with the water in the larger pores. The relative permeability of water increases in the mixed-wet case compared to the water-wet. The true residual saturation may not be so important in a field case, since injection of several pore volumes of fluid is not feasible economically, the saturation at abandonment conditions, such as low pressure or high water cut, must be the deciding factor (Ligthelm et.al., 2009).

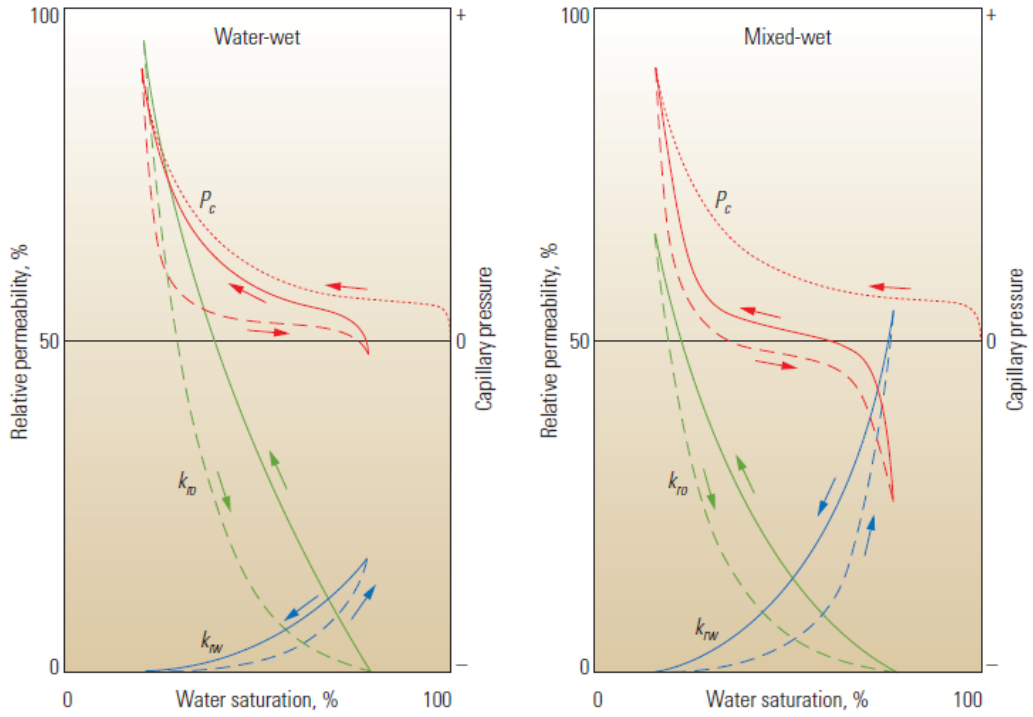

Figure 2.3: Relative permeability and capillary pressure curves for water-wet (Left) and mixed-wet (Right). Showing relative permeability for water (k_{rw}, blue), oil (k_{ro}, green), and capillary pressure (P_c, red). Dotted curves represents primary drainage, the dashed curves are imbibition (increasing water saturation), continuous curves are drainage (reducing water saturation), (Abdallah et.al., 2007).

2.5.1 Spreading Coefficient

The initial spreading coefficient C_s, explains the behavior of a liquid drop on a flat liquid substrate.

$$C_s = \sigma_{wg} - \sigma_{wo} - \sigma_{go}$$

σ_{wg} , σ_{wo} and σ_{go} are the water/gas, water/oil and gas/oil interfacial tensions respectively, measured before the fluids where brought in contact with each other (Blunt et al.,1995). Blunt et.al., 1995, studied three-phase flow from the molecular level upwards in water-wet porous media, and summarized three different things that can happen:

1. $C_s<0$, the three phase contact is stable and the droplet remains on the liquid surface. Medium to long chained alkanes are an example, such as dodecane.
2. $C_s>0$, the contact line is unstable and the oil will spread. This is consistent with observations when gasoline is spilled in a puddle of water, it will then spread until it forms a thin, iridescent film. Many solvents, hydrocarbons and crude oils have a positive spreading.
3. $C_s \approx 0$, the oil film will spread without limit. When the spreading coefficient is approximately zero the oil film is thicker than the range of inter molecular forces. Soltrol 170 is an example of this behavior.

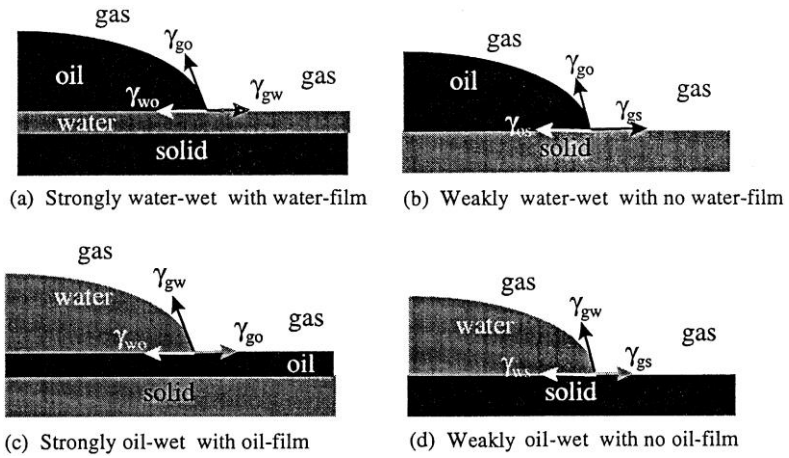

(a) Strongly water-wet with water-film (b) Weakly water-wet with no water-film

(c) Strongly oil-wet with oil-film (d) Weakly oil-wet with no oil-film

Figure 2.4: Configurations of water, oil and gas on a solid flat surface. (a) A strongly water-wet surface coated by a water film; (b) A weakly water-wet surface with no film; (c) A strongly oil-wet surface coated by oil; and (d) A weakly oil-wet surface with no oil film. (Blunt et. Al., 1998)

2.5.2 Mechanism of wettability alteration

There are currently four suggested different mechanisms in which polar crude oil components can alter the rock wettability towards less water-wet condition. The suggested mechanisms are polar interactions, surface precipitation, acid/base interactions and ion binding between charged sites and higher valence ions. The potential for wettability alteration for a given crude oil might be evaluated by API gravity, acid number and base number (Buckley et. Al., 1998).

2.5.2.1 Polar Interactions

Direct adsorption from the asphaltinic portion of the crude oil onto the mineral surfaces has been reported by several researchers, especially clays (Clementz, 1976; Cuiec, 1984a; Denekas et. Al., 1959b). In the absence of a water film between the oil and the rock, adsorption through polar interactions is the predominant adsorption mechanism. The binding mechanism is affected by typical parameters like type of clay, the exchangeable cations on the clay surface, nitrogen content of the crude oil and the solvent in which the polar components are dissolved (Buckley et. Al., 1998). Direct contact between the oil and rock surface becomes possible in cases with specifically hydrophobic oil-wet minerals present in the rock (Anderson, 1986), or in reservoirs where the rock have an organic coating on the pore surface, due to the rock being both source and reservoir (Cuiec, 1986). Aging time and temperature does not affect the extent of polar interaction as studied by the contact angle method, but it is however obviously not equal for different types of crude oil (Buckley, 1996).

2.5.2.2 Surface Precipitation

The wettability conditions of the reservoir rock may be changed by the high molecular polar components of the oil interactions with the rock surface. Crude oil has a reduced capacity to act as a solvent for the asphaltenic fraction, and surface precipitation results as a consequence. The capacity

of the oil to dissolve asphaltenes is indicated by parameters as the refractive index and API gravity (Buckley et.al., 1998). It has been reported that as the oil has a decreasing degree of solvency of asphaltene contents, it leads to a systematic decrease in water wetness of the Berea sandstone (Tang et.al., 1997). Precipitation has however not been proved to effect reservoir wettability on a large scale (Buckley, 1995), it could however plug pore throats and modify reservoir rock structure past its effect on wettability. The oil solubility is naturally greatly affected by oil compositions, temperature and pressure.

2.5.2.3 Acid / Base Interactions

Wettability modifications through acid/base interactions can happen in two ways, adsorption of ionized oil components from the oil / brine interface as the water film which is in contact with the surface of the rock becomes less stable. It has been reported that crude oil / brine interfaces are negatively charged at a high pH and positively charged at low pH (Dubey et. al., 1993). Positively charged nitrogen bases are the components most likely to adsorb due to the fact that sandstone/brine have a negatively charged interface above a pH of 2 (Anderson, 1986). The solubility of oil in water, and vice versa, is very low, as a consequence the process of acidic or/and basic components of the oil adsorbing onto the mineral surface must happen through the water film, and from the oil/water interface. This process will lead to a wettability change for the mineral surface of the rock. In the presence of water, the interfaces of oil/brine and brine/rock will be charged because of acid/base dissociation (Buckley, 1996). Both interfaces can behave as acids or bases by gaining or losing a proton (Cuiec, 1975).

2.5.2.4 Ion Binding

The wetting process of sandstone reservoirs from crude oil with a high acid number and low base number are dependent on ion binding, this process is highly temperature dependent (Buckley et. al., 1998). The mechanism behind ion binding is when cations, such as Ca^{2+}, behave as bridges between the adsorption of negatively charged oil components to the negatively charged sites on the rock surface, like carboxylate and clay surface. The mechanism for ion binding provides the opportunity for negatively charged carboxylates to alter the wetting conditions to less water-wet for the negatively charged clay surface, and it is probably the dominant wetting mechanism in wetting alteration in sandstone reservoirs by acidic oil (Buckley, 1996). In the presence of multivalent cations, such as Ca^{2+}, pH is reported to play a less important role and pure acid/base interactions are masked (Buckley, 1991).

2.6 Permeability

A porous rock has the ability to allow flow of fluid through its interconnected pores. The capacity to transmit fluids is termed permeability, a non-porous rock does not have any permeability, and a reservoir must be able to conduct the petroleum fluids. Permeability is dependent upon mainly effective porosity, which again is affected by many factors, such as packing, degree of consolidation and cementing, grain size, shape and distribution, and the type of clay or cementing material between the grains.

Henry Darcy found an equation that has been one of the standard mathematical tools to describe fluid flow. The equation is expressed in differential form as follows (Erle Donaldson et al., 2004):

$$u = \frac{q}{Ac} = \frac{K}{\mu}\frac{dp}{dl} \quad (2.19)$$

u = fluid velocity
q = flow rate
K = permeability of the porous rock
Ac = cross-sectional area of the rock
μ = viscosity of the fluid
l = length of the rock sample
$\frac{dp}{dl}$ = pressure gradient in the direction of flow

Permeability, K, is measured in Darcy`s. One Darcy is relatively high, most reservoir rocks is less than one Darcy. Therefore a smaller unit, millidarcy (mD) is used in the oil and gas industry. For a flow where more than one fluid is present permeability is measured as effective permeability.

K_o, K_g or K_w being oil, gas, or water effective permeability respectively.

Because the fluids interact with each other as they move through the channels, the sum of effective permeability of all the phases will always be less than the absolute permeability (K). The ratio of effective permeability (K_o, K_w) to the absolute permeability (K) is known as the relative permeability (K_r) of that fluid. Relative permeability for each phase is defined as:

$$K_{ro} = \frac{K_o}{K}, K_{rg} = \frac{K_g}{K}, K_{rw} = \frac{K_w}{K}$$

The familiar Corey type correlations are used as a basic model for relative permeability functions (Corey, 1954). The dimensionless function is given below.

$$k_{rw}(S_w) = k_w^* \left(\frac{S_W - S_{WR}}{1 - S_{OR} - S_{WR}}\right)^{Nk_w}, \; S_{WR} \leq S_W \leq 1 - S_{OR} \quad (2.20)$$

$$k_{ro}(S_w) = k_O^* \left(\frac{1 - S_{OR} - S_W}{1 - S_{OR} - S_{WR}}\right)^{Nk_O}, \; S_{WR} \leq S_W \leq 1 - S_{OR} \quad (2.21)$$

$$(2.22)\quad P_C = P_d\left(\frac{S_w - S_{iw}}{1 - S_{iw} - S_{or}}\right)^{-\left(1/\lambda\right)}$$

$$(2.23)\quad k_{ro} = k_{ro}(S_{iw})[1 - S_W^*]^2\left\{1 - (S_W^*)^{\left(2/\lambda\right)+1}\right\}$$

$$(2.24)\quad k_{rw} = k_{rw}(S_{or})\left\{(S_W^*)^{\left(2/\lambda\right)+3}\right\}$$

$$(2.25)\quad S_W^* = \frac{S_W - S_{iw}}{1 - S_{iw} - S_{or}}$$

S_{WR} = residual water saturation
S_{OR} = residual oil saturation
S_{iw} = irreducible water saturation
Nk_w, Nk_O = corey exponents
λ = pore size distribution index
S_W^* = normalized water saturation based on the mobile oil saturation
$k_{ro}(S_{iw})$ = end point relative permeability for the extrapolated irreducible water saturation from capillary measurements
k_w^*= end point relative permeability for water
k_O^* = end point relative permeability for oil
k_{ro} = relative permeability of oil
k_{rw} = relative permeability of water
P_C = capillary pressure
P_d = displacement pressure, threshold pressure

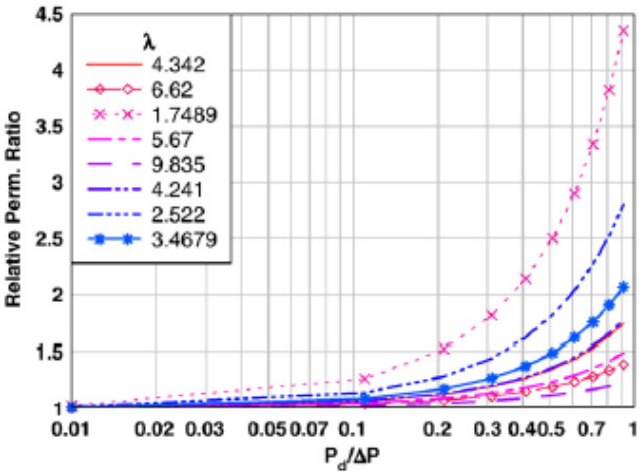

Figure 2.5: Relative permeability ratio as a function of pore size distribution index for different pressures and cores. (A.A, Hamouda et.al., 2008).

2.7 Modeling low salinity waterflood

There are only a few low salinity modeling works presented in the literature to date, and none of the proposed mechanisms has been accepted as a universally working model. However, one model relates the beneficial low salinity effects by directly linking the brine salinity to the flow conditions, such as relative permeability and/or capillary pressure (Yu-shu et.al., 2009; Jerauld et.al., 2008; Tripathi et.al., 2008).

Jerauld et.al.,2008, modeled salt as a single component in the water phase, and by simple linear interpolation the residual saturation is determined by tracking the salinity. By using predetermined low salinity and high salinity residual saturations, a weighting function, θ_W, may be calculated. This weighting function is then used to derive the relative permeability's and capillary pressure as shown in the equation below.

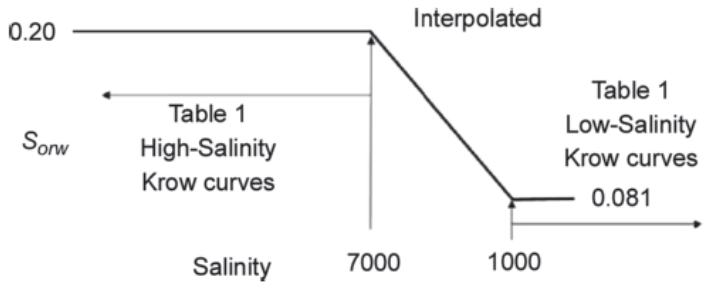

Figure 2.6: Residual saturation dependent upon salinity (Jerauld et.al., 2008).

$$\theta_W = \frac{S_{or} - S_{or}^{LS}}{S_{or}^{HS} - S_{or}^{LS}} \quad (2.26)$$

$$S^* = \frac{(S_o - S_{or})}{(1 - S_{wr} - S_{or})} \quad (2.27)$$

$$k_{ro} = \theta_w k_{ro}^{HS}(S^*) + (1 - \theta_w) k_{ro}^{LS}(S^*) \quad (2.28)$$

$$k_{rw} = \theta_w k_{rw}^{HS}(S^*) + (1 - \theta_w) k_{rw}^{LS}(S^*) \quad (2.29)$$

$$P_C = \theta_w P_C^{HS}(S^*) + (1 - \theta_w) P_C^{LS}(S^*) \quad (2.30)$$

High Salinity Conditions:

$$k^{HS}\langle S\,;\, S_{wr}^{HS} \leftrightarrow S_{or}^{HS}\rangle, \quad k_o^{HS}\langle S\,;\, S_{wr}^{HS} \leftrightarrow S_{or}^{HS}\rangle, \quad S_{WR}^{HS} \leq S_W \leq 1 - S_{OR}^{HS}$$

Low Salinity Conditions:

$$k^{LS}\langle S\,;\, S_{wr}^{LS} \leftrightarrow S_{or}^{LS}\rangle, \quad k_o^{LS}\langle S\,;\, S_{wr}^{LS} \leftrightarrow S_{or}^{LS}\rangle, \quad S_{WR}^{LS} \leq S_W \leq 1 - S_{OR}^{LS}$$

2.7.1 History matching

Sendra (2013.1) is a 1D fully implicit black oil simulator that has an automated history matching routine, which is useful for history matching special core analysis experiments. The simulator is used to obtain water-oil relative permeability (k_r) and capillary pressure (P_c) curves by history matching the experimental production and delta pressure from the core experiments, indicating different wetting state´s during flooding with different brines.

Required input data are:

- Core plug data: Dimensions, porosity, absolute permeability, S_{wi}
- Injection rate
- Fluid viscosities
- Delta pressure
- Production history

The Corey correlation (Corey, 1954) were used to generate best fit water-oil relative permeability, and the Skjæveland correlation (Skjæveland et.al.,2000) were used to generate capillary curves, by implementing end point relative permeability and saturations.

2.8 DLVO theory

Zeta potential is a term for electro kinetic potential in colloidal systems. It is a parameter characterizing electrochemical equilibrium on interfaces, depending on the properties of the liquid and properties of the surface. Zeta potential plays an important role in theory of aggregative stability, DLVO theory. DLVO describes the force between charged surfaces interacting through a liquid medium, and was developed by Derjaguin, Landau (1941) and Verwey, Overbeek(1948). Van der Waals attraction and the electrostatic repulsion due to the double layer of counter-ions are combined in one effect. Different conditions must be taken into account, as a result different equations can be obtained. The process can be simplified by some useful assumptions which are suitable for ordinary circumstances. Simply adding the two parts together is the easy way to derive.

$$V_T = V_A + V_R + V_S \quad (2.31)$$

V_T = total potential energy function
V_A = Van der Waal's attractive force
V_R = double layer repulsive force
V_S = potential energy due to solvent

DVLO theory suggests that the stability of a particle in solution is dependent upon its total potential energy function V_T. The attractive and repulsive contributions is much more important than potential energy from solvents, they are potentially much larger and operate over a much larger distance.

2.8.1 Van der Waals attraction

Van der Waals force is defined as the sum of attractive or repulsive forces between molecules, it includes the attraction and repulsion between atoms, molecules, surface and intermolecular forces. In DLVO theory the van der Waals force are referred to as purely attractive, and is actually the total name of dipole-dipole force, dipole-induced dipole force and dispersion forces. The dispersion forces are always present and are therefore considered to be the most important. It is assumed that the pair potential between atoms or small molecules is purely attractive, and can be defined as:

$$(2.32) \quad W = -\frac{C}{r^n}$$

W = interaction energy
C = constant for interaction energy
n = 6, for van der Waals attraction

Assuming additivity, the sum of the interaction energy between the molecule and every molecule in the surface body will be equal to the net interaction energy between a molecule and planar surface made up of like molecules. For a molecule at a distance D away from the surface the net interaction energy can be derived as follows:

$$(2.33) \quad w(r) = -2\pi C\rho_1 \int_{z=D}^{z=\infty} dz \int_{x=0}^{x=\infty} \frac{x dx}{(z^2+x^2)^3} = \frac{2\pi C\rho_1}{4} \int_D^\infty \frac{dz}{z^4} = -\frac{\pi C\rho_1}{6D^3}$$

W(r) = interaction energy between the surface and molecule
ρ_1 = number density of the surface
z = perpendicular axis with the surface, passing across the molecule
z = 0, the point where the molecule is
z = D, at the surface
x = perpendicular axis with the z-axis
x = 0, at the intersection

For a large sphere with a radius of, R, and a flat surface, the interaction energy can be calculated as:

$$(2.34) \quad W(D) = -\frac{2\pi C\rho_1\rho_2}{12} \int_{z=0}^{z=2R} \frac{(2R-z)zdz}{(D+z)^3} \approx -\frac{\pi^2 C\rho_1\rho_2 R}{6D}$$

$$(2.35) \quad A_H = \pi^2 C\rho_1\rho_2$$

W(D) = interaction energy between sphere and surface
ρ_2 = number density of the sphere
A_H = Hamaker constant

The van der Waals interaction energy can be calculated for particles with different shapes following a similar method.

(2.36) Two spheres: $V(D)_A = -\frac{A}{6D}\frac{R_1 R_2}{(R_1 + R_2)}$

(2.37) Sphere – surface: $V(D)_A = -\frac{AR}{6D}$

(2.38) Two surfaces [per unit area]: $V(D)_A = -\frac{A}{12\pi D^2}$

2.8.2 The Electric Double Layer

A double layer (DL), or an electrical double layer (EDL), is a structure that is formed on the surface of an object when it is placed in liquid (figure 2.8), the model is used to visualize the ionic environment in proximity of a charged surface. Object such as a solid particle, a gas bubble, liquid droplet, or a porous body. The object is surrounded with two parallel layers. The first layer is comprised of ions adsorbed directly onto the object due to the surface charge, either positive or negative. The second layer is made up of ions attracted to the surface charge by coulomb force, and is only loosely associated with the object, since the ions is not firmly anchored but is made up of free ions which move in the fluid under influence of electric attraction and thermal motion. This layer is called the diffuse layer.

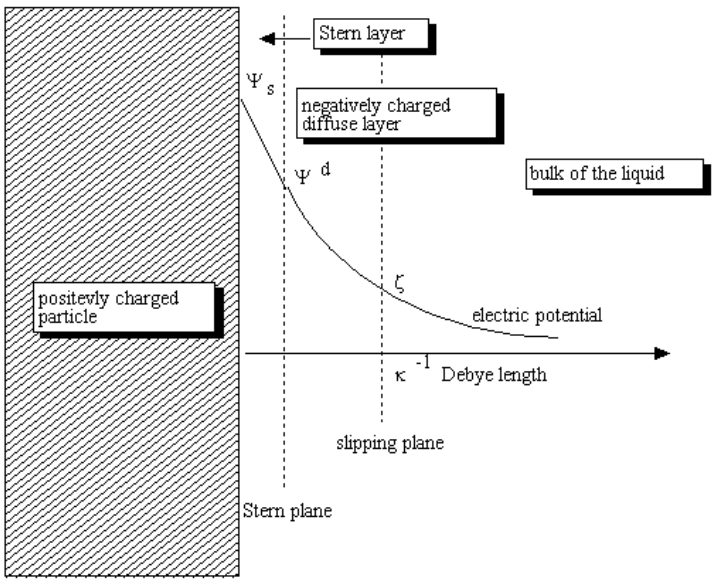

Figure 2.7: Illustration of the Double Layer structure near the surface of the positively charged particles (Wikipedia, picture 1).

The earliest model of the electrical double layer was first discussed by Helmholtz in 1879 (Hunter, 1981). He modeled the double layer mathematically as a simple capacitor, assuming a physical model were a compact layer of ions of opposite sign is adsorbed to the surface. Later Guoy and Chapman (1913) made significant improvements by involving the Boltzmann distribution and a exponentially decrease in electric potential away from the surface to the fluid bulk, a diffuse double layer was introduced in which the accumulated ions extended some distance from the surface. There are however some parts were the Guoy-Chapman models fails.

To solve the problem, Stern (1924), suggested a combination of the Helmholtz and Guoy-Chapman models. As a result the electrified solid-liquid interface combines both the rigid Helmholtz layer, which is fixed to the interfacial surface with an approximately thickness of a single ion, and a diffuse layer that extends some distance into the liquid dispersing phase (Hunter, 1981; Pashley et.al., 2004; Shaw, 1992). Attraction from the charged colloidal particle, based on DLVO theory, causes some of the ions with opposite charge in the solution to form a firmly attached layer around the surface. This firmly attached layer is known as the Stern or Helmholtz layer (Russel et. Al., 1989).

The thickness of the diffuse double layer is known as the Debye screening length (1/k).

$$\kappa = \sqrt{\frac{\sum_i (\rho_{\infty,i} e^2 z_i^2)}{\epsilon \epsilon_0 k_B T}} \qquad (2.39)$$

T = absolute temperature
z_i = valency of the ion
e = electron charge
ϵ, ϵ_0 = electric constant, and relative static permittivity, respectively
k_B = Boltzmann constant
ρ_∞, i = density of the ion I in the bulk solution

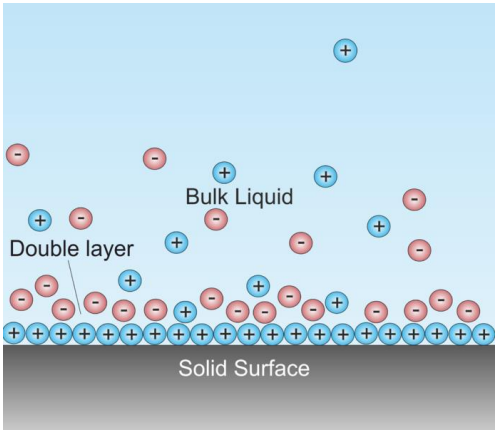

Figure 2.8: Illustration of the double layer and bulk liquid on a solid surface (Wikipedia, picture 2).

2.8.3 Ionic Strength

The ionic strength, *I*, of a solution is a function of the concentration of *all* ions present in that solution.

$$I = \frac{1}{2}\sum_{i=1}^{n} C_i Z_i^2 \quad (2.40)$$

Z_i = charge number of ion
C_i= molar concentration

2.9 Low Salinity Mechanisms

The effect from low salinity flooding seems to be complicated, and may be the results of different mechanism contributing together or operating at different conditions. Wettability alteration in chalk by injection of sea water seems to be a less complicated phenomenon (Puntervold et.al., 2007; RezaeiDoust et.al., 2009; Strand et.al., 2006; Strand et.al., 2008; Zhang et.al., 2007a). Wettability alteration is among the most generally accepted mechanism behind the improved oil recovery by low salinity injection, however, explanations by physical mechanisms also exists. As double layer expansion, migration of fines and fluid flow due to osmotic pressure caused by salinity gradient. The different proposed mechanisms will be discussed and presented below.

2.9.1 Increase in pH

An increase in the pH of 1-3 units has been reported in laboratory water flooding and several single well chemical tracer tests. It has been proposed that injection of low salinity brine is similar to alkaline flooding, were the main reason for extra oil recovery is reduction in interfacial tension between the oil and water phase and in-situ generation of surfactants (McGuire et.al., 2005). In laboratory experiments with low salinity water flooding an increase in the pH of the effluent brine from 6-7 to 9 or above has been observed for several studies with non-buffered systems. The pH increase might be explained by dissolution of the small amount of cementing material, carbonate, and cation exchange between the mineral surface and brine phase. Both of the reactions below are drastically accelerated when low salinity brine is injected into the reservoir.

Ca^{2+} - Clay + H_2O = H^+ - Clay + Ca^{2+} + OH^- Cation Exchange

$CaCO_3$ + H_2O = Ca^{2+} + HCO_3^- + OH^- Carbonate Dissolution

It has been proposed that the acidic components of the crude oil are saponified at a high pH. The saponification results in in-situ generation of surfactants, which could cause a reduction of the interfacial tension and oil-in-water emulsification. Reduction of capillary forces that cause lower

residual oil saturation may be one of the reasons behind the increase in oil recovery, especially for laboratory experiments conducted with short cores and a high end effect (Baviere, 1991; McGuire et.al., 2005). Another consequence of the increase in pH is increase in water wetness of the rock (Buckley, 1996)

A higher concentration of divalent ions, such as Ca^{2+} and Mg^{2+}, have been shown to reduce the low salinity effect (Jerauld et.al., 2008). Divalent cations in high concentration will precipitate the surfactants and thus block them from lowering the IFT and increasing the oil recovery. However, the surfactants will continue to be effective in low salinity brines which usually have a lower concentration of divalent cations (Anderson, 1986a; McGuire et.al., 2005).

Test have been performed with an increase in recovery but with only a small increase in pH (Zhang et.al., 2007b). In addition significant increases in pH but without any increase in oil recovery have also been reported (Cissokho et.al., 2009).

Crude oils with an acid number higher than 0.2 mg KOH/g are required to generate enough surfactant to influence recovery through IFT reduction and emulsion formation in alkaline water flooding (Ehrlich et.al., 1977). However, in North Sea reservoir with an acid number less than 0.05 increases in oil recovery of up to 40% of OOIP have been reported (Lager et.al., 2008a), this contradicts the proposed mechanism and no correlation between the acid number and increase in oil recovery have yet been found. Also, increases in oil recovery at reservoir temperature and pressure with live oil performed by BP resulted in increased oil recovery without any recorded increase in the pH (Lager et.al., 2008a).

2.9.2 Double-layer Effects

It has been proposed that in high salinity brine there are sufficient cations available to screen-off the negative charge of the oil/water interface and the clay surface to cause a suppression of the electrostatic repulsive force (Ligthelm et.al., 2009). It is believed that multivalent cations, such as Mg^{2+} and Ca^{2+}, act as bridges between the negatively charged oil/brine interface and the negatively charged clay minerals (Anderson, 1986; Arnarson et.al., 2000; Buckley et.al., 1998; Lager et.al., 2006; Lager et.al., 2008a; Sposito, 1989). The high salinity brine reduces the zeta potential of the minerals surface, as described by DLVO theory. This will result in oil components adsorbing onto the clay surface by forming organo-metallic complexes, reducing the water-wetness of the rock. The ability of the cations to screen-off the negative charges on the clay surface is reduced as low salinity brine is injected, as a result the electrical double layer is expanded and repulsive forces between the mineral surface and oil/water interface is increased. The oil will desorb from the surface when the repulsive force between the mineral surface and oil phase increases above the binding forces for the organo-

metallic complexes, this will occur at a certain salinity level. The electrostatic repulsive forces within the clay itself will exceed the binding forces if the salinity is further reduced, and may lead to deflocculation and formation damage. Increased oil recovery could be achieved by lowering the salinity to certain levels (RezaeiDoust, 2011).

Ligthelm et.al., 2009, made several observations supporting the proposed mechanism. During flooding experiments, after oil production had stopped with high salinity brine containing sodium, calcium and magnesium, the brine composition was changed to a content of only sodium chloride, with the same ionic strength, and a small increase in oil recovery was observed. The results were associated to cation exchange mechanism, as the pure sodium chloride brine stripes off the divalent cations attached to the rock surface. The brine was then diluted to 100 times lower salinity, and a following large increase in recovery was observed, believed to be related to the expansion of the electrical double layer. The contribution from the cation exchange mechanism was believed to be small, compared to the expansion of the electrical double layer.

2.9.3 Migration of fines

In certain experiments small amounts of solid particles have been observed in the effluent, these are called fines, and are mainly built up of kaolinite clay. It has been reported that a sharp increase in pressure across the core was observed when injecting low salinity brine into Berea Cores (Tang et. Al., 1999a). Tang et. Al. suggested that mobile fines is an important part of the mechanism that causes increased recovery, and a permanent reduction in permeability were typically observed with the production of fines.

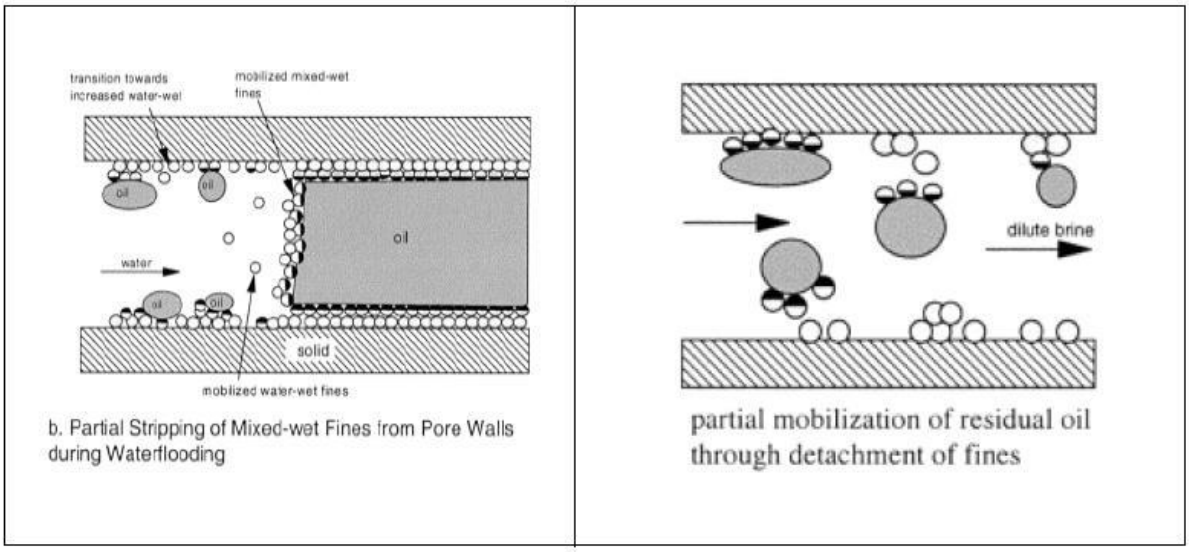

Figure 2.9: Migration of fines as suggested by Tang et.al., 1999a.

Adsorption of heavy polar components on the outer surface of clay particles attached to the sandstone is governing for the initial wetting condition (Salathiel, 1973). A partial mobilization of mixed-wet particles as the low salinity brine is injected may reduce the residual oil saturation and increases the oil recovery. A balance between mechanical forces keeps the clay particles attached to the surface, including capillary forces and colloidal forces (Israelachvili, 1991). The attractive and repulsive colloidal forces depend on the balance of van der Waals and electrostatic forces, see previous section on DLVO theory. The clay maintains a certain degree of equilibrium and are undisturbed by the injection of high salinity brine, and the wetting state is preserved (Lager et.al., 2006). Tang et.al., 1999a, showed that injection of low salinity brine into sandstone cores containing clay makes them more water wet, the electrical double layer in the water phase is expanded as the low salinity brine is injected, which may cause stripping of clay particles. The pH of the effluent have been observed to increase in several experiments performed with non-buffered systems, this is also a contributing factor to the instability of the clays (Khilar et.al., 1983).

A proposed explanation for the increased oil recovery in low salinity brine injections is improved microscopic sweep efficiency, associated to an analogy with the enhanced oil recovery technique using linked polymer solutions. Skauge et.al., 2008, suggested that the microscopic sweep efficiency is improved due to the release of clay particles , the partial mobilization of fines will block pore throats and divert the flow into non-swept pores. It has been verified by a number of laboratory and field test in china that injection of linked polymer gels improves oil recovery above the level obtainable with ordinary polymer flooding, even though linked polymer particles are much smaller that the pore throats in sandstone (Li, 2008; Skauge et.al., 2008). As a result the improved oil recovery may not be caused by wettability modification, but rather by improved microscopic sweep efficiency.

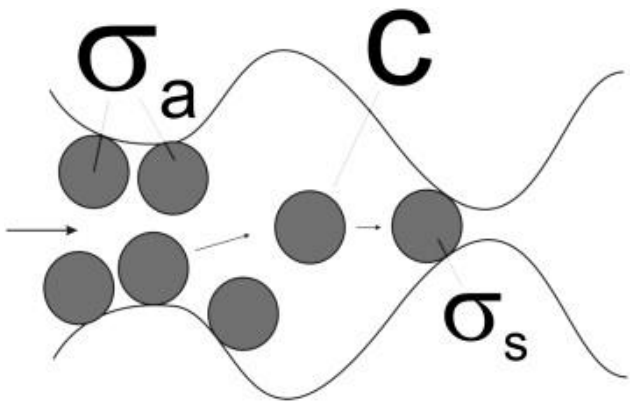

Figure 2.10: Straining of particles and permeability reduction during fines migration (Zeinijahromi et.al., 2012)

Several experiments have observed a production of clay fines, increase in pressure drop across the core and permanent permeability reduction from injection of low salinity brine. Tang et.al., 1999a, analyzed the solid particles and reported it to be mainly kaolinite. Stabilizing the clay inside the core by firing rendered the core insensitive to the salinity of the injection of brine both in spontaneous imbibition and water flooding experiments, supporting the proposed mechanism (Tang et.al., 1999a). Another reason behind the mechanism is the direct relation between the amount of clay in the core and the level of increased oil recovery observed. The increase in oil recovery stopped when calcium was added to the injection brine, and was explained by flocculation and/or re-attachment of fines at the pore walls (Tang et.al., 1999a).

Low salinity flooding test have been performed without any production of solid particles and any increase in pressure drop (Lager et.al, 2006; Pu et.al., 2008; Zhang et.al., 2006a). In addition core floods with increased pressure drop and with a production of solid particles, but without any increased oil recovery have been reported (Boussour et. al., 2009). Cissokho et.al., 2009, performed injection of low salinity brine in kaolinite free sandstone cores, containing only illite and chlorite, and observed an increase in recovery of about 10% (OOIP%). This result seems to contradict that kaolinite is essential for improved oil recovery.

2.9.4 Multi-component Ionic Exchange (MIE)

Soil science investigates the trends of adsorption and desorption of organic material on mineral surfaces. Eight different mechanisms for adsorption of organic functional group on soil minerals are proposed (Sposito, 1989).

Mechanisms	**Organic functional group involved**
Cation Exchange	Amino, ring NH, heterocyclic N (aromatic ring)
Protonation	Amino, heterocyclic N, carbonyl, carboxylate
Anion Exchange	Carboxylate
Water Bridging	Amino, carboxylate, carbonyl, alcoholic OH
Cation Bridging	Carboxylate, amines, carbonyl, alcoholic OH
Ligand Exchange	Carboxylate
Hydrogen Bonding	Amino, carbonyl, carboxyl, phenolic OH
Van der Waals Interactions	Uncharged organic units

Table 2.4: Adsorption mechanisms of organic materials onto clay minerals (Sposito, 1989)

Studies performed on the magnitude and mechanisms of adsorption of marine pore water materials onto montmorillonite led to the conclusion that van der Waals interactions, ligand exchange and cation bridging are the dominant adsorption mechanism out of the eight proposed by Sposito (Arnarson et.al., 2000). According to DLVO theory high ionic strengths give low electrostatic repulsion forces, as the van der Waals attractive forces are significant at high ionic strengths, the particles are thereby allowed to be located close to each other.

Ligand exchange occurs when carboxylate groups of acidic material substitute hydroxyl groups on the surface (RezaeiDoust, 2011). Cation bridging is when negatively charged surface and functional groups of the organic material is connected by a cation acting as a bridge, this is a weak adsorption mechanism (Arnarson et.al., 2000). During injection of low salinity brine two different observations was made, the first was that the presence of divalent cations in the formation brine, especially Ca^{2+}, was essential in order to observe an increase in recovery (Lager et.al., 2006; Ligthelm et.al., 2009). The second was that the effluents from low salinity test showed a strong reduction in the concentration of Mg^{2+}, indicating a strong adsorption to the rock matrix. From the knowledge of the dominant mechanism and these two observations, Lager et.al., 2006, suggested that the increase in oil recovery was caused by competition of all the ions in the brine for ionic exchange with the rock surface. In low salinity flooding four of the eight identified mechanisms for organic adsorption to the clay mineral were affected by possible cation exchange, these mechanisms were cation exchange, ligand bonding/ligand bridging, water and cation bridging. There are two different mechanism in which the polar components can adsorb onto the clay, one is where polar components adsorb onto the clay by multivalent cations and forming an organo-metalic complex. The second is direct adsorption by displacing the most labile cations at the clay surface (Lager et.al., 2006). Direct adsorption is a bridging mechanism where the negatively charged clay surface and negatively charged molecules in the oil are bridged together by divalent cations (Buckley et.al., 1998; Seccombe et.al., 2008).

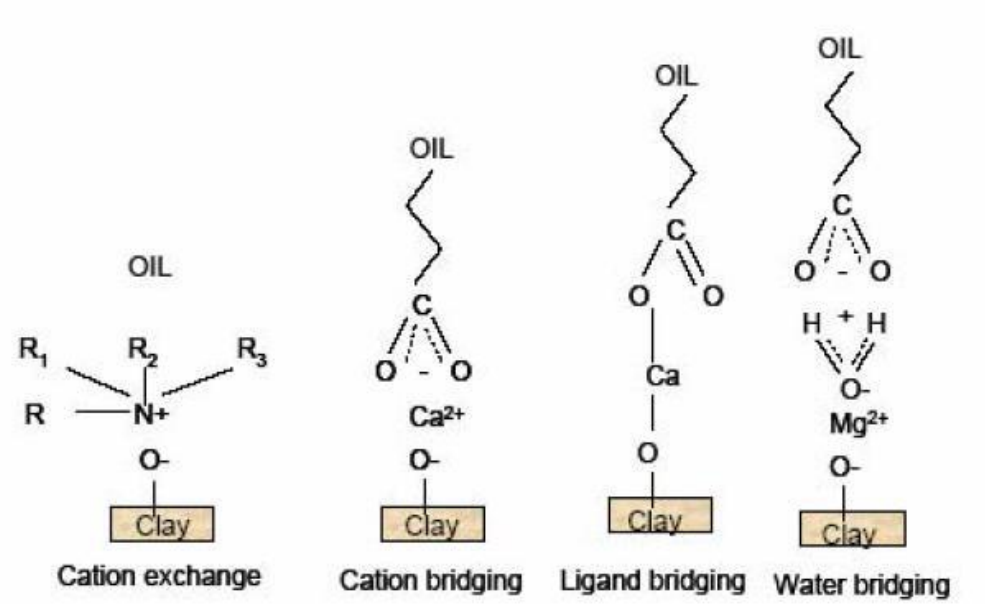

Figure 2.11: Four of the proposed adsorption mechanisms of organic materials onto clay surface (Lager et.al., 2008b)

Injection of brine containing low concentrations of Ca^{2+} and Mg^{2+} may trigger multi-component ionic exchange (MIE) to occur between clay mineral surfaces, cations in the in-situ brine and adsorbed crude oil components. A change in the ionic equilibrium causes an exchange with either cationic organic complexes or with bases, and the divalent cations from the low salinity invading brine. The result is a removal of organic polar compounds and organo-metallic complexes from the clay surface, increasing oil recovery and water-wetness of the clay. The multi-component ionic exchange mechanism due to the injection of low salinity brine may result in an expansion of the electrical double layer, increasing oil recovery and water-wetness by desorption of oil from the clay (RezaeDoust, 2011).

2.9.5 Desorption of the adsorbed organics from mineral surface

2.9.5.1 Mineral dissolution

Some researchers have had an low salinity effect from cores without any significant clay content, as a result it was proposed that the dissolution of carbonate/anhydrite minerals, which are oil wet, or act as cement for mixed wet particles, could be the mechanism behind low salinity flood (Pu et.al., 2008,2010; Lebedeva et.al., 2009). Dolomite and anhydrite particles were confirmed present after high salinity flooding by using CT and AFM imaging techniques, after low salinity flooding these particles were no longer seen. The suggested mechanism may be compared to wettability alteration by mineral dissolution in carbonate rocks (Evje et.al., 2010, 2011; Hiorth et.al., 2010). There are however several conflicting results of this theory, the main point is that the suggested mechanism

does not sufficiently explain the requirement of aging in connate water as stated by Tang et.al., 1999a. The role of divalent ions in the connate brine and the salinity threshold seen in some experiments are not either sufficiently explained by the mechanism.

2.9.5.2 Kaolinite dissolution

The existence of permanent (pH-independent) and nonpermanent (pH-dependent) charges are responsible for the surface charge of kaolinite (Schoefield and Samson, 1954). The isomorphic substitution of Si for Al in tetrahedral positions leads to a permanent negative charge within the siloxane layer, responsible for the cation exchange capacity (CEC) of kaolinite. The CEC value is in the range of 1-8 mEq/100g, very small compared to other clay minerals (Newman and Brown, 1987). The acid-base properties of the ionisable surface groups located at the edges or at the gibbsite basal plane are responsible for the positive/negative nature of the surface charge and its pH-dependence. Crystal edge electroneutrality give rise to the transformation of the dangling oxygens into silanol (>SiOH) or aluminol (>AlOH) groups and to the adsorption of water molecules (Sposito, 1984). By deprotonation and formation of $>SiO^-$ surface complexes the silanol groups contribute to the negative charge only (Iler, 1979). Aluminol groups can undergo both protonation and deprotonation, at a low and high pH, respectively. Protonation resulting in the formation of $>AlOH_2^+$, and deprotonation in $>AlO^-$ (Carroll-Webb and Walther, 1988). It is generally accepted that the dissolution of solid phases is controlled by numerous elementary reactions occurring at the solid–water interface. The reaction rate is controlled by the formation of surface-activated complexes as stated by the transition state theory applied to the dissolution process.

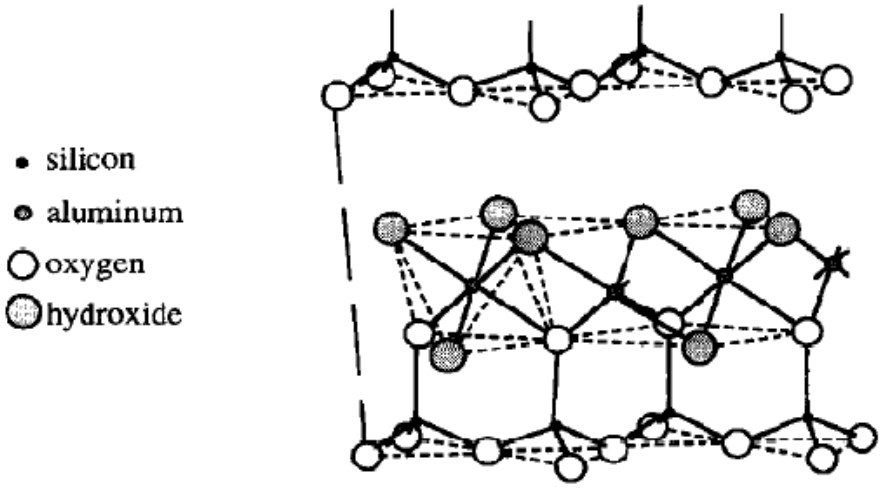

Figure 2.12: Kaolinite structure (Ganor et.al., 1995)

Huertas et.al.,1999, studied the kinetics of the dissolution of kaolinite by following the evolution of dissolved Si and Al concentrations at various pH. Maximal concentrations of dissolved Si and Al at a given time interval were reached at very basic pH, figure 2.13 shows the concentration at several pH levels.

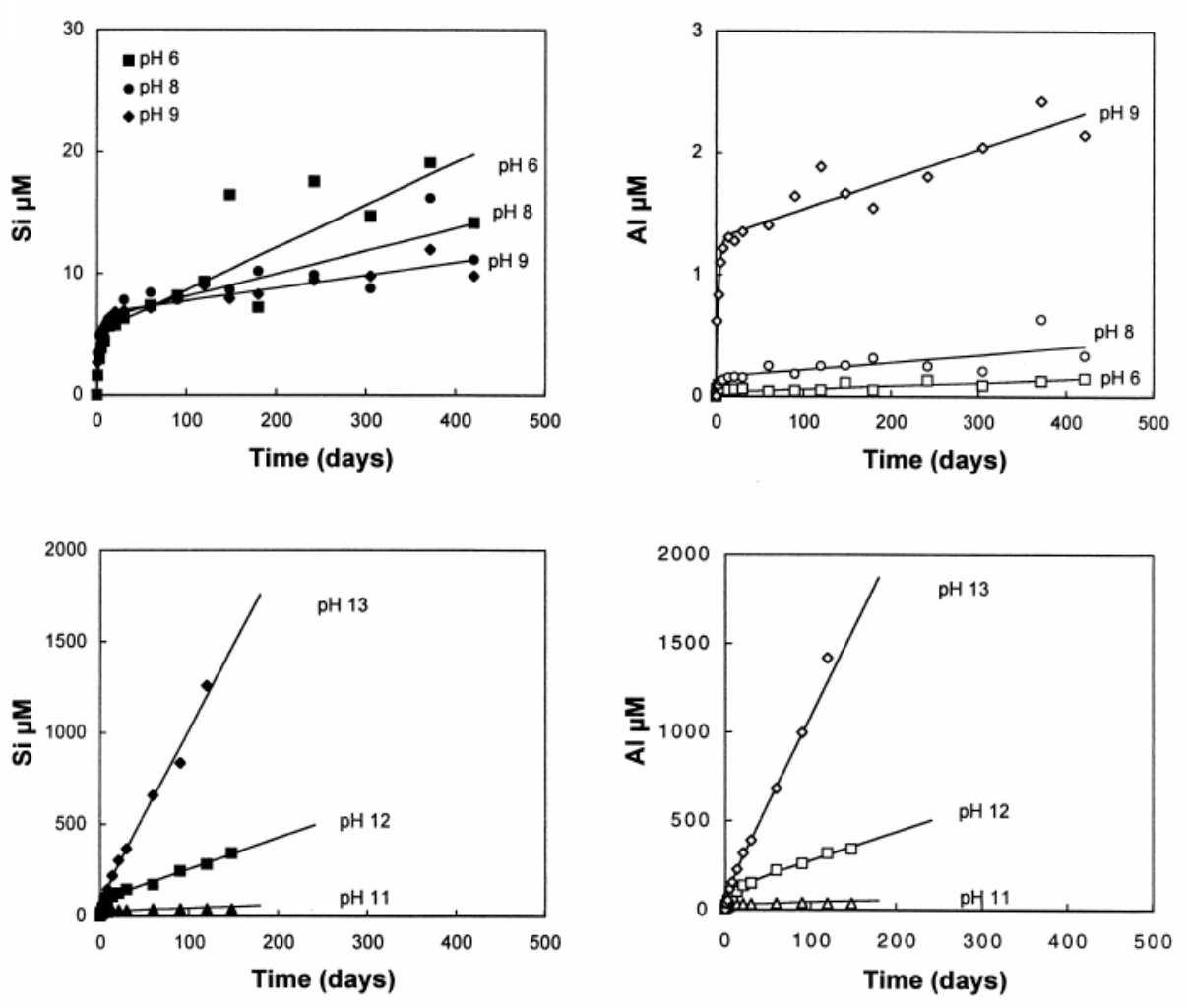

Figure 2.13: Concentration of Si and Al during the dissolution experiments at several pH conditions (Huertas et.al., 1999)

Total dissolution rate is the sum of the short-term reaction and linear dissolution process. Dissolution of fine-grained materials, strained areas on large grains or defects are different processes which may cause the high initial dissolution rate. As all fine particles have been dissolved, the rate will proceed at a constant rate. They reported that the dissolution rate is proportional to the nth order of the activity of protons, water, and hydroxyls in each pH range. Under acidic, neutral, and basic conditions the species attacking the silicate surface are mainly protons, water molecules, and hydroxyls, respectively. Dissolution rate given by pH can then be derived as (Huertas et.al.,1999):

$$r = k_{H^-} a_{H^+}^{n_a} + k_0 + k_{OH^-} a_{OH^-}^{n_b} \quad (2.41)$$

a_{H^+} , a_{OH^-} = proton and hydroxyl activity, respectively
k_{H^-} , k_0 , k_{OH^-} = rate constant under acidic, neutral and basic conditions, respectively
n_a , n_b = corresponding order of reaction

The rate constant showed inflections at pH ≈ 4 and ≈ 10, above and below these values the dissolution rate displayed strong pH dependence. In neutral conditions the rates were much less dependent upon pH.

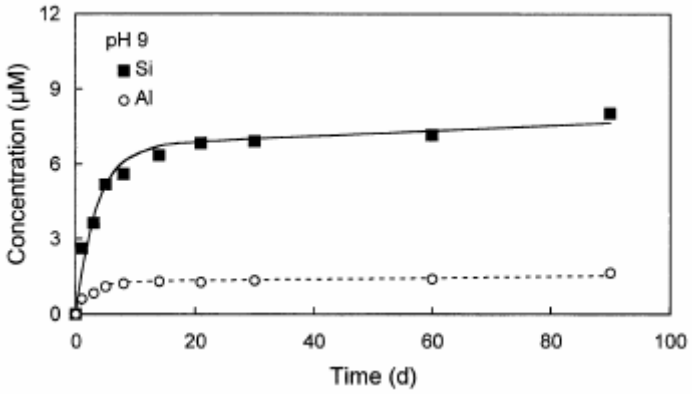

Figure 2.14: Dissolved Si (solid squares) and Al (open circles) at pH = 9. High initial rate followed by a constant rate (Huertas et.al., 1999).

As a silicate or oxide is immersed in an aqueous solution, the protons, hydroxyls, water molecules, ions or organic ligands present in the solution can form surface complexes by reaction with the cations present at the hydrated surface. If protons and hydroxyls are the only species available, the dissolution will be proportional to their respective concentrations adsorbed. Huertas et.al., 1999; 1998, investigated the density of negatively and positively charged sites at the kaolinite surface by acid and base titration, a dependence upon pH were observed, the ionic strength in the range of 0.001 to 1M showed very little influence on the results. The following sites on the kaolinite surface were investigated in the study:

- >Al_2OH : External Al hydroxyls at the basal plane
- >AlOH : Internal Al hydroxyls, aluminol at the edge
- >SiOH : Silanols

Only when the pH is higher than 9 the aluminum sites become negatively charged. High acidity prevent the silanol groups from forming positively charged complexes, and at a pH from 5.5 to 9 they become negatively charged, and in an additional increase in pH they remain saturated. Huertas et.al., 1999, suggested from model calculations that >AlOH is the dominant species at kaolinite surface at a range in pH from approximately 3 to 10. In addition, the model showed that dissolution kinetics of kaolinite is governed by aluminum surface complexes, without direct influence from the >SiO^- sites. Strong and weak acid Al site, >$Al_2OH_2^+$ and >AlO H_2^+, respectively, controls the dissolution mechanism

at acidic conditions. At high pH values it has been argued that the silanol groups are the source of negatively charged surface sites, therefore the $>SiO^-$ must be controlling dissolution rate. However, other results indicate that the deprotonation of the aluminum sites is the rate limiting step, and Al sites form negative surface complexes above pH 9, contributing to the dissolution (Blum and Lasaga, 1991; Huertas et.al., 1999). At neutral conditions dissolution of kaolinite is controlled by the hydration reaction, and neutral species ($>Al_2OH$, >AlOH,>SiOH) do not contribute significantly to the dissolution at pH ranging from 6 to 9. The rate-limiting step in alkaline solutions is the formation of a $>AlO^-$ surface complex and the following detachment of an Al ion, which could lead to an attack of hydroxyls on the open Si framework. At neutral and acidic conditions the rate-limiting is associated with the adsorption of a proton on an Al center, causing a detachment of Al and a following detachment of Si. Elementary the rate is limited by the breaking of the Si-O-Al bridging bonds, supported by the deprotonation and protonation reactions at the kaolinite surface.

A general rate equation can be expressed as the sum of successive terms corresponding to different surface complexes (Huertas et.al.,1999):

$$r = \sum_i k_i [Surface\ complex]_i^{n_i} \quad (2.42)$$

i = various complexes
k_i = rate constant for surface complex, i
n_i =reaction order for surface complex, i

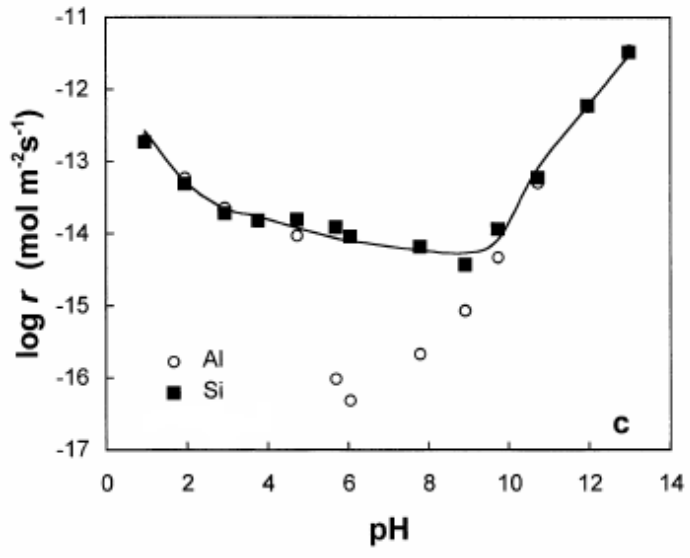

Figure 2.15: Kaolinite dissolution rate, experimental (dots) and theoretical (line). Rate was calculated by the general rate equation for surface complexes (Huertas et.al., 1999).

2.9.6 Influence of flow velocity and water permeability associated with LSW

2.9.6.1 Reduction of Water Permeability due to Physical Plugging

Low Salinity water injection field data are still from the formations in near wellbore region, were the calculated tertiary oil recovery is very high, 20-25% pore volume (Li, 2011). The laboratory reports for increased oil recovery are just as high (Loahardjo et.al., 2007). Li, 2011, performed experimental and theoretical analyses showing that the increased oil recovery from low salinity brine was caused by the mobilization of discontinuous oil as water permeability is reduced due to blockage of the porous network by swelling clay aggregates or migrating clay particles and crystals, this causes a higher negative pressure gradient than that during brine injection at the same flow velocity. The increased oil recovery associated with low salinity flooding in clay-bearing sandstone reservoirs are believed to be dependent upon flow velocity and flow acceleration, as a result the increased recovery from a reservoir will be significantly less than laboratory experiments involving cores at common flow velocity. He also proposed that the low salinity injections had two relevant disadvantages, the reduced water injectivity and degraded mobilization condition, thus, at maximum permitted injection pressure, the oil recovery associated with low salinity water injection cannot be higher than brine injection.

Tertiary oil recovery related to water injection in a reservoir should be based on the experimental dependence of the flow acceleration and velocity. The disconnection of continuous oil phase in secondary oil recovery is connected to snap-off off selloidal interfaces, which is independent of flow velocity at low capillary number, while mobilization of discontinuous oil in tertiary oil recovery associated to water injection is related to pressure gradient, which is dependent on flow velocity at any capillary number higher than the critical.

Li and Wardlaw (1986a,b) proposed a fundamental theory on secondary oil recovery, showing that the disconnection of oil by snap-off of a selloidal interface in a pore is dependent upon the pore-throat aspect ratio (r_P/r_T), wettability, and supply of water. The critical pore–throat aspect ratio for a pore is the ratio above which snap-off will happen in the pore when water is supplied at least to one of its throats.

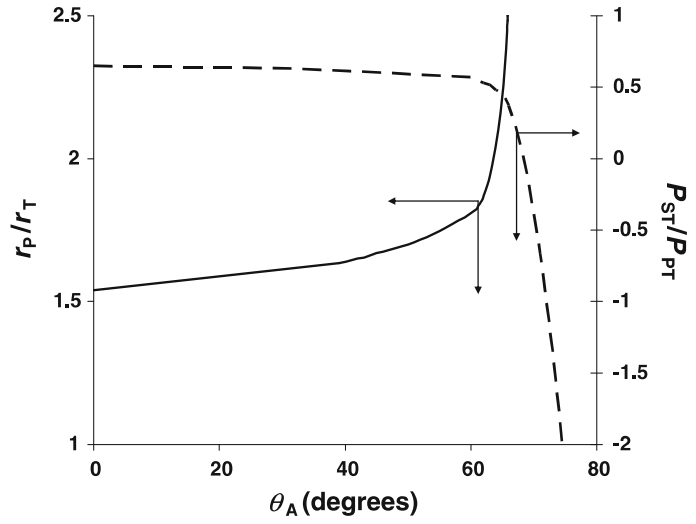

Figure 2.16: Critical pore-throat aspect ratio (r_p/r_t) plotted against advancing contact angle (θ_A). The ratio of snap-off capillary pressure in a throat versus capillary pressure for the advance of a convex interface in the same throat (P_{st} / P_{pt}) are the reciprocal of pore-throat aspect ratio. The broken line represent the critical P_{st} / P_{pt} (Li et.al., 1986a,b).

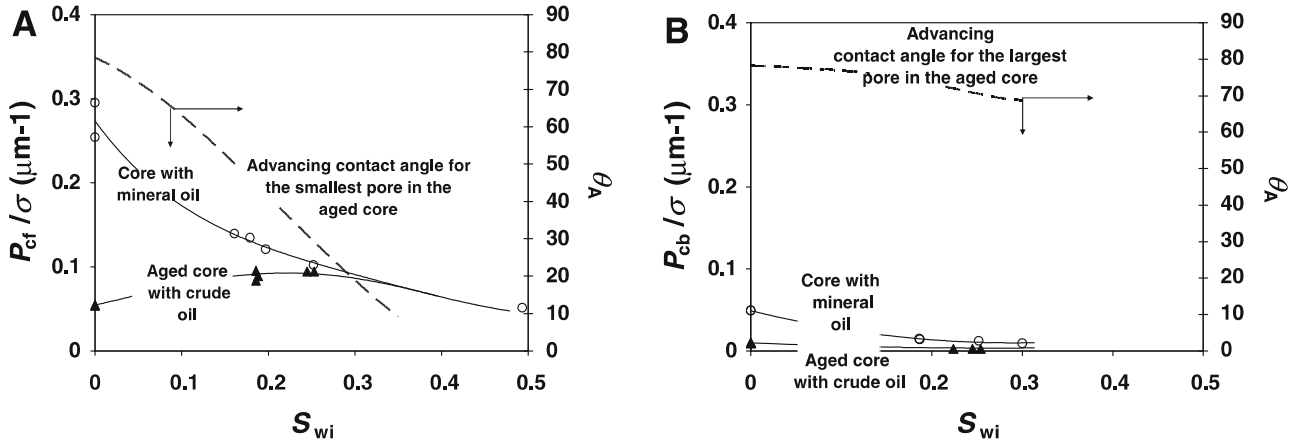

Figure 2.17: Measurements obtained by Li, 2010, of advancing contact angle inside cores, performed on Berea-sandstone with permeability of about 0.9 μm². (A): P_{cf}/σ is the curvature of the interface at the water-invading front. (B): P_{cb}/σ is the curvature of the interface at the core open face. S_{wi} equals initial water saturation, θ_A represents the advancing contact angles.

From two equal cores, the oil recovery will be higher for the core with lower initial water saturation, if the cores have the same initial water saturation, the stronger oil-wet core will have a higher oil recovery. Wettability influence on secondary oil recovery can be explained by the water-invading front during secondary recovery. The continuous oil phase ahead of the front must be disconnected by snap-off to permit water moving forward, and occurrence of snap-off is easier due to the

relatively low critical pore-throat aspect ratio in a more water-wet core. Higher oil recovery at water breakthrough (BT) will be obtained from the more water-wet core, since more oil disconnections can occur at and behind the water-invading front. Snap-off is more difficult due to the relatively high critical pore-throat aspect ratio in a more oil-wet core, and much of the continuous oil phase can be preserved for a longer time to permit continuous oil branches withdrawing from porous channels in a piston like displacement, and higher final oil recovery will be gained from the more oil-wet core (Li, 2011).

The water-invading front is obtained directly from the relationship between the derivative of water fractional flow with respect to saturation at the outlet of the core, and the cumulative injected water volume (V_w) at the moment of water BT (Li, 2010).

$$(2.43) \quad f_f^* = \frac{df}{dS_W} = \frac{1}{V_{wBT}}$$

f_f^* = derivate of water fractional flow with respect to saturation (f^*)
V_{wBT} = cumulative injected water volume (V_W) in PV at BT

Oil phase distributes discontinuously in the pore network during tertiary oil recovery, in the form of drops or blobs which have been trapped in the pore networks due to capillary pressure actions, a phenomenon called Jamin effect (Jamin, 1860). Mechanical work must be provided externally to let trapped drops and blobs move, or surface energy must be reduced internally, or a combination of both. Mobilization of an oil drop or a gas bubble may be related to the dimensionless capillary number (Ca), given by equation 2.47 (Gardescu 1930; Moore and Slobod 1956; Melrose and Brandner 1974), the formula is suitable for very strongly water-wet systems where the water permeability does not apparently change during water injections.

$$(2.44) \quad Ca = \frac{\mu V}{\sigma}$$

μ = viscosity of displacing phase
V = apparent velocity, Darcy velocity of the displacing phase
σ = interfacial tension between the displacing phase and the displaced phase

Critical Ca for onset of mobilization is 7×10^{-6} to 2×10^{-7} for water-wet sandstone cores. (Chatzis and Morrow 1984). For complete oil recovery the *Ca* is about 10^{-2}.

To satisfy the requirements for oil reservoir applications, the capillary number should be redefined, this redefinition will be based on a capillary-trap model as shown in figure 2.18 (Li, 2011).

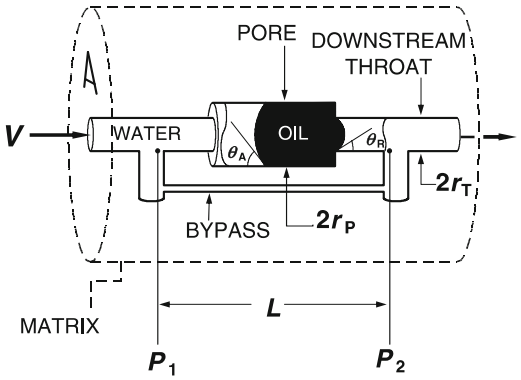

Figure 2.18: Capillary trap elementary model for explaining tertiary oil recovery mechanism, assuming that the investigated oil drop completely blocks the downstream throat. Capillary tubes are circular. V is the flow rate through a unit area (A) of the matrix/porous medium containing the capillary trap. P_1: upstream pressure in water which is exerted on the convex interface in the pore. P_2: Downstream pressure in water which is exerted on the convex interface in the throat. L: length of bypass. θ_A: advancing contact angles. θ_R: Receding contact angles. Li, 2011

Young-Laplace equation for the upstream convex interface is:

$$(2.45) \quad P_{cP} = \frac{2\sigma\cos\theta_A}{r_P} = \frac{2\sigma\cos\theta_R}{r_p\left(\frac{\cos\theta_R}{\cos\theta_A}\right)}$$

P_{cP} = capillary pressure generated by the convex interface in the pore
r_P = radius of the pore
θ_A = Advancing contact angle

Young-Laplace equation for the upstream convex interface is:

$$(2.46) \quad P_{cT} = \frac{2\sigma\cos\theta_R}{r_T}$$

P_{cT} = capillary pressure generated by the convex interface in the downstream throat
r_T = radius of the downstream throat
θ_R = Receding contact angle

$$(2.47) \quad P_{cT} - P_{cP} = \left(\frac{1}{r_T} - \frac{1}{r_p\left(\frac{\cos\theta_R}{\cos\theta_A}\right)}\right)2\sigma\cos\theta_R$$

Critical equilibrium will therefore be:

$$(2.48) \quad P_1 - P_2 = -(P_{cT} - P_{cP}) = \left(\frac{1}{r_p\left(\frac{\cos\theta_R}{\cos\theta_A}\right)} - \frac{1}{r_T}\right)2\sigma\cos\theta_R$$

The generalized Darcy`s law for water phase is needed to investigate the mobilization of an oil drop in the elemental capillary-trap:

$$(2.49) \quad V = \frac{q_W}{A} = -\frac{Kk_{rW}}{\mu_W}\frac{\Delta P_W}{\Delta x} = -\frac{K_W}{\mu_W}\frac{\Delta P_W}{\Delta x}$$

V = apparent velocity
q_W = volumetric flow rate of water
A = cross-sectional area of the core
K = absolute permeability
k_{rW} = relative permeability to the water phase
$K_W = Kk_{rW}$= permeability of the water phase
μ_W = water viscosity
P_W = pressure in water phase
x = distance

Assuming a uniform bypass capillary tube, the pressure gradient in water will be reduced to:

$$(2.50) \quad \frac{\Delta P_W}{\Delta x} = \frac{(P_1 - P_2)}{L}$$

L = Length of bypass

Combining the previous equations results in:

$$(2.51) \quad V = \frac{q_W}{A} = \frac{K_W}{\mu_W}\left(\frac{1}{r_T} - \frac{1}{r_p\left(\frac{\cos\theta_R}{\cos\theta_A}\right)}\right)2\sigma\cos\theta_R\frac{1}{L}$$

$$(2.52) \quad 2\left(\frac{1}{r_T} - \frac{1}{r_p\left(\frac{\cos\theta_R}{\cos\theta_A}\right)}\right)\frac{1}{L} = \frac{\mu_W V}{K_W\sigma\cos\theta_R}$$

The left-hand side shows the resistance against mobilization of residual oil, expressed as reciprocal of permeability (M^{-2}). The geometry of the capillary trap is described by the equation above, R_T and R_P of the main-pass, and L of the bypass, that is the no-flow segment. Assuming same wettability, the resistance against mobilization will be higher for smaller throat diameter, larger pore diameter, or if the length of no-flow segment is shorter than the main pass. Another effect on resistance against mobilization is the contact angle ($\frac{\cos\theta_R}{\cos\theta_A}$). It may be concluded that the initial oil distribution of tertiary oil recovery must have a strong effect on the relation between tertiary recovery and the standard capillary number. Initial and residual water saturation after secondary oil recovery is related to oil distribution, so that the pattern of the oil traps must be different for a different initial oil distribution of tertiary oil recovery.

The right-hand side shows the dynamic value for mobilization of the trapped oil in the capillary trap, thus the standard capillary number (N_C) can be defined as follows:

$$(2.53) \quad N_C = \frac{\mu_W V}{K_W\sigma\cos\theta_R}$$

The standard capillary number (N_c) represent detailed dynamics for mobilization of the trapped oil. The previous dimensionless capillary number (Ca) deal only with behavior of the fluids (V, μ_W, φ), the introduced variables quantitatively define pore structure and oil distribution (K_w), and wettability (θ_R).Lower interfacial tension, stronger oil-wetness, lower water permeability, higher water viscosity, or higher flow velocity always leads to a higher dynamic value of the standard capillary number (N_c). As the oil saturation is reduced or water channels become plugged by for example the clay, the permeability of the water phase (Kw) is reduced.

Studies have revealed that larger oil blobs were disconnected repeatedly during mobilization, indicating that sizes of blobs decreased with subsequent increases in capillary number (Wardlaw et.al., 1985). As a result the anticipated increment of tertiary oil recovery associated with water injection for the same infinitesimal N_C is less for more oil-wet cores, since disconnection by snap-off is harder in more oil-wet cores (Li et.al., 1986a,b).

2.9.6.2 Flow rate and flow acceleration in a reservoir

Partial plugging of pores by LSW injection may lead to a reduction in water permeability. Generalized equation of Darcy`s law may be rearranged to give:

$$K_W = -q_W \frac{\mu_W L_C}{A\Delta P} \quad (2.54)$$

Tertiary oil recovery is strongly related to flow velocity. An essential physics in EOR is that discontinuous oil can always be mobilized if the flow velocity is high enough. The largest reduction in oil saturation occurs in the oil formation near the wellbore regions, were the flow is fastest. If the EOR associated with low salinity injection is only dependent upon the flow velocity and flow acceleration, as suggested by Li,2011, it is very unlikely that the high oil recovery associated with a core at a laboratory is translated to a full field scale. Part or all of the mobilized oil drops will be trapped again as the flow decelerates further away from the injection well, and recovery will not be as high as in the near wellbore region. The mobilized oil cannot pass a zone where the flow velocity is lower than that for the onset of oil mobilization. At some point the oil surface will become unstable and a droplet will detach from the main bulk oil as oil is flowing from one pore into another filled with water through a narrow throat (Mohanty et.al., 1987; Wardlaw, 1980, 1982). Snap-off of oil is a major mechanism causing residual oil in porous media, especially for strongly water-wet systems (Wardlaw, 1980). It has been estimated that 80% of the trapped oil in Berea sandstone cores occurred in snap of geometries (Chatzis et.al., 1983). Main parameters governing snap-off are the aspect ratio of porebody to the pore throat diameter, connectivity of the pore system, pore-wall roughness, oil-water IFT, and the wettability of the porous medium.

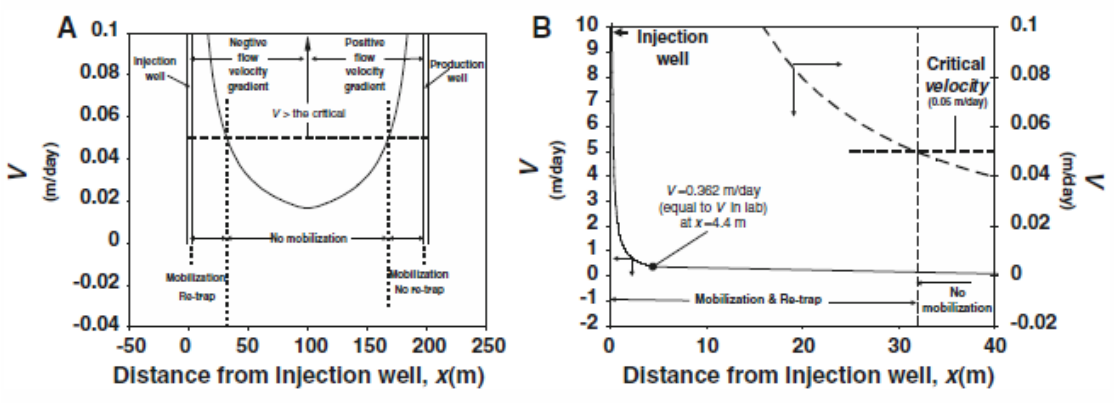

Fig 2.19: Divisions of mobilization and re-trap in a reservoir. A: Produced mobilized oil can only come from the division on the right-hand side due to the conditions required, flow velocity above the critical for oil mobilization and a positive flow velocity gradient. The zone in the middle is a re-trap zone where no mobilized oil can flow through, as the flow velocity is not high enough for onset of mobilization. B: Showing that near the injection wellbore the flow velocity can be two orders of magnitude higher than the critical flow velocity, and reduction in oil saturation in this region is highest due to the highest flow velocity. The figure and numbers are obtained from the work of Li, 2011.

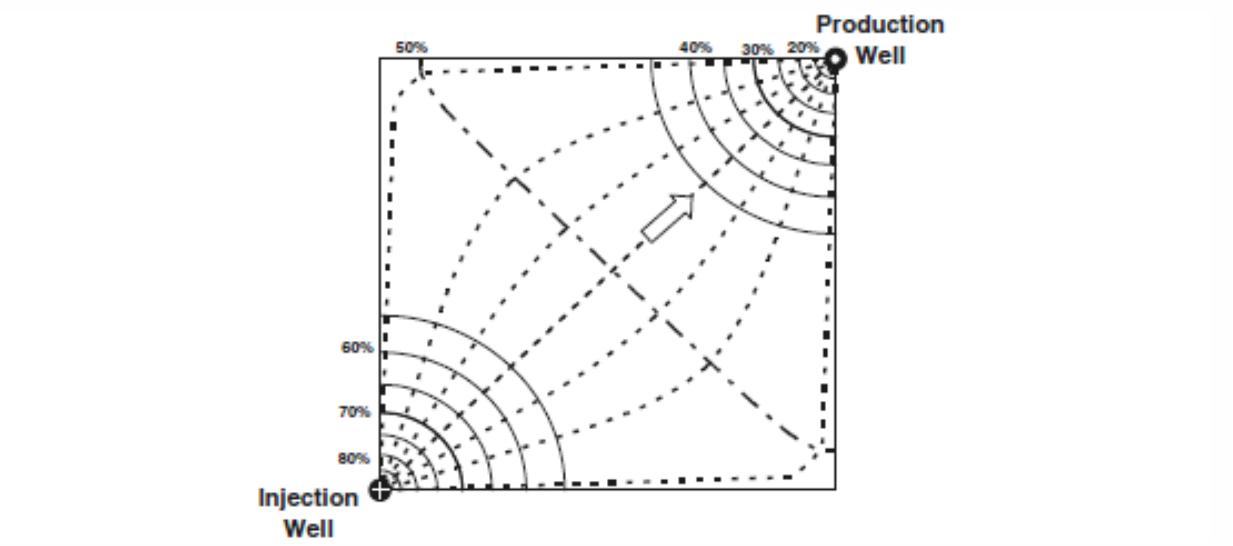

Fig 2.20: Equal-pressure contours and streamlines in a quadrant of a five-spot-network element during one phase flow (Muskat et.al., 1934). Total pressure drop is presented in percentage. Flow direction is indicated by the arrow. The dashed line plus dots represents the equal-pressure contour where the flow velocity is lowest along flow lines. The heavy solid lines show two equal-pressure contours where flow rate is the same, but the sign of the flow velocity gradient at contour 70% (negative) is different from that at contour 30% (positive).

2.9.7 Local pH increase

In the proposed mechanism the following parameters are assumed to be significant in low salinity effects in sandstone (Austad et.al., 2010).

- Type, amount and specific properties of the clay present in the rock
- Initial formation brine properties, such as composition and pH
- Acidic and basic polar components in the crude oil

The mechanism is based on the assumption that increased water wetness of the clay present in the rock is responsible for the increased recovery from low salinity. Both acidic and basic organic materials are adsorbed onto the clay together with inorganic cations, particularly Ca^{2+}, from formation water containing a high concentration of Ca^{2+} (Austad et.al., 2010). In reservoir formation water the pH could be low due to dissolution of sour gases like CO_2 and H_2S. The equilibrium of interactions between the brine and rock may be disturbed by injecting low salinity water with a lower concentration of ions than the initial formation brine, as a result a net desorption of cations, especially Ca^{2+}, may occur. To counteract for the loss of cations, protons (H^+), from the water close to the clay surface can adsorb onto the clay. According to Austad et.al., 2010, there will then be a local pH increase close to the clay surface as shown by the reaction below.

$$CO_2 + H_2O \rightarrow H_2CO_3 \leftrightarrow H^+ + HCO_3^-$$

$$H_2S \rightarrow H^+ + HS^-$$

$$(Clay - Ca^{2+}) + H_2O = (Clay - H^+) + Ca^{2+} + OH^- + Heat$$

This desorption of active cations from the clay surface is the essential reaction to create alkalinity which will start the wettability alteration. As the pH is increased close to the clay surface, a reaction between the adsorbed acidic and basic material will occur. As a result from the suggested theory, active clay minerals are needed to obtain any low salinity effects (Austad et.al., 2010).

$$(Clay - NHR_3^+) + OH^- = Clay + R_3N + H_2O$$

$$(Clay - RCOOH) + OH^- = Clay + RCOO^- + H_2O$$

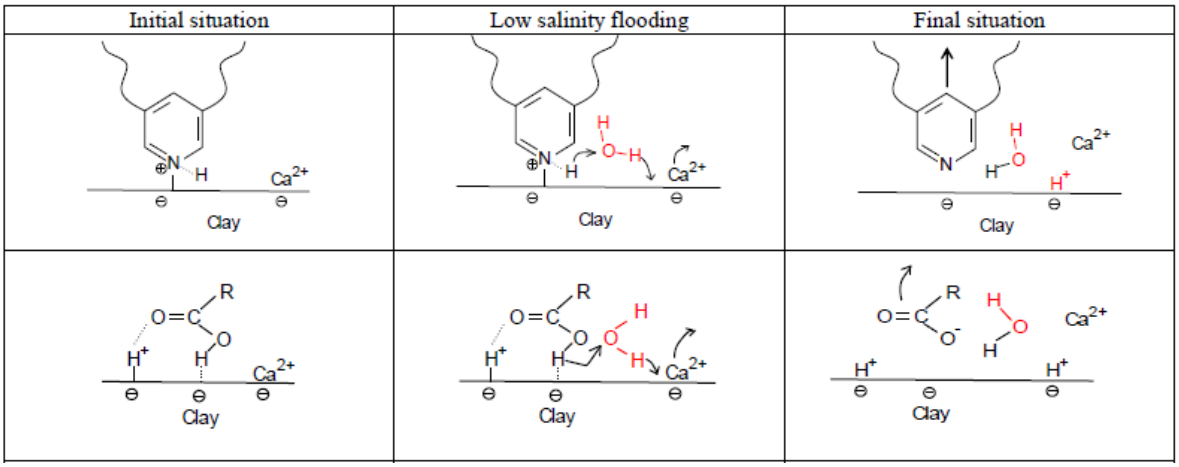

Figure 2.21: A simplified caption of Austad et.al., 2010, suggested mechanism for low salinity effects. Basic component at the top, acidic component at the bottom.

2.9.7.1 Cation adsorption

Initial formation water usually has a much lower concentration of Na^{2+}, Ca^{2+} and Mg^{2+} then H^{+}, which has the strongest attraction towards the clay surface. At reservoir conditions the active cation, Ca^{2+}, are adsorbed onto the clay together with acidic and basic material, assuming formation water with a pH close to 5. For kaolinite and Chlorite the mechanism of ion exchange are mainly associated to the edge surfaces. As for illite/mica and montmorillonite, lattice substitutions are believed to be the main mechanism (Austad et.al., 2010). Different clays has different characteristics and show selectivity for different cations. Montmorillonite shows a small selectivity for Ca^{2+} over Na^{2+}, Kaolinite shows a stronger selectivity for Ca^{2+} (Kleven et.al., 1996). Illite/mica is believed to have selective characteristics similar to montmorillonite.

Cations, basic and acidic organic matter, and H^{+} all compete for the adsorption sites on the clay surface.To obtain any low salinity effects reservoir rock containing kaolinite and chlorite should have formation water with a high concentration of Ca^{2+}, as for reservoir rock containing montmorillonite and/or illite/mica the divalent cations in the initial formation water may not be essential (Austad et.al., 2010).

2.9.7.2 Local pH changes

Desorption of active cations as explained earlier, leads to an increase in pH, and the pH of the effluent is to some degree dependent upon the composition of the injected brine. Austad et.al., 2010, suggested that a local increase in the pH close to the water-clay interface is needed to desorb the organic matter, and this will only happen if desorption of cations occur. Substitution of Ca^{2+} by protons increases the pH close to the clay surface and causes a fast desorption of basic and acidic

material by proton transfer as shown earlier. If divalent cations in the injected brine create complex formation of the sort shown in the equation below, the pH could only have a small increase.

$$Ca^{2+} + OH^{-} = [Ca...OH]^{+}$$

With a pH buffer such as CO_2 there may not be any increase in the effluent. However, the activity described by pH measurements of H^+ in the bulk solution may differ from the activity close to the interface between water and minerals (Baily et.al., 1968). A localized pH increase close to clay surface can still occur, and cause a desorption of organic material from the clay surface in pH buffered systems.

Lager et.al., 2008b, performed an experiment in which the effluent from core floods showed a decrease in the concentration of multivalent cations, specially Mg^{2+}. They initially stated that the change in Mg^{2+} concentration were due to multi ion exchange. However, as suggested by Austad et.al.,2010, the lowered concentration could be from precipitation of $Mg(OH)_2$ as a result from a local pH increase in the injected low salinity water. As $Mg(OH)_2$ is precipitated the local alkalinity will decrease, this could have an influence on the desorption of organic material on the clay surface.

2.9.7.3 Important parameters

Based on the proposed mechanism the success of low salinity flooding and magnitude of increased oil recovery are mostly determined by the type and amount of clay, initial composition of the formation brine and reservoir pH, acidic and basic compounds in the crude oil, and ionic strength and composition of the low salinity brine.

Both polar components and active cations are required to be initially adsorbed onto the clay. Considering low salinity effect, it appears that clay minerals with a high cation exchange capacity appear to be favorable. The content of active polar components in crude oil can be indicatively measured by the acid and base number of the oil, and different wetting conditions are obtained with different acid and base numbers. Oil with low acid number and high base number could allow for basic components to be adsorbed onto the negatively charged silica.

Amount and composition of divalent cations, and pH are determined by the properties of the formation water. An optimal low salinity effect may be achieved by a balanced initial adsorption of active cations, protons and organic material onto the clay surface. The low salinity effects will be low if the adsorption of active ions and organic material is high and low, respectively, as the rock is already water-wet. In this case the desorption could give a higher increase in pH during low salinity flooding. If the concentrations of specific active ions area above a certain level the initial pH may play an important part for optimal adsorption of these active ions (Austad et.al., 2010). The composition

of injected low salinity water is assumed to be of less importance, as long as the concentration of active ions is low enough to cause a significant desorption from the clay surface.

Austad et.al., 2010, summarized the suggested mechanism as follow:

- Initially there is a balanced adsorption of organic material, protons and active cations onto the clay minerals, preferentially at a reservoir pH of about 5.
- Injection of low salinity water will lead to an reaction at the clay surface, where Ca^{2+} is substituted by H^{+}, resulting in desorption of adsorbed cations, which will increase the pH close to the water-clay interface.
- An ordinary acid-base reaction occurs between OH^{-} and the adsorbed acid and protonated base. Desorption of organic material is stimulated, and the water-wetness and oil recovery is increased.
- Different clays have diverse adsorption/desorption windows. The presence of a negative zeta potential material is essential, and the potential for increased recovery from low salinity brine is dependent upon the CEC of the clay.

2.10 Spontaneous Imbibition

Spontaneous imbibition may be defined as the process in which a wetting fluid is drawn into a porous medium by capillary action, and is driven by surface energy. The capillary pressure is determined by interfacial tension and the curvature of the interface. Curvature magnitude is dependent upon the surface forces and pore geometry, and if the curvature is concave with respect to the wetting fluid occupying the porous media, and the interface is allowed to advance, the displacement is spontaneous. Capillary and gravity forces, and the interplay between the two, are the most important displacement forces, especially at cases with neutral wetting states or low interfacial tension.

Recovery by spontaneous imbibition of brine into reservoir rock is particularly important for fractured reservoirs, especially with low permeability, and imbibition has been recognized in several different recovery processes, such as waterflooding of heterogeneous reservoirs, thermal recovery by steam injection through imbibition of condensed water, and WAG. An increasing amount of reservoirs are classified as low permeability, and under water injection the oil recovery from the rock matrix are generally dependent upon the spontaneous imbibition of water, which are a relatively slow process.

2.10.1 Free imbibition

The rate of imbibition is measured with free access of brine to the rock face. In other words, the rock is immersed in brine and the oil recovery is recorded over time as the brine imbibes and displaces the oil. The capillary pressure is often referred to as the dynamic capillary pressure.

2.10.2 Parameters influencing the imbibition process

Several parameters affect the performance of spontaneous imbibition, such as permeability, fluid saturations, wetting state, heterogeneity and fluid properties (Viscosity, density, IFT). Some of the influencing parameters are discussed below.

2.10.2.1 Permeability

Water imbibition has previously been shown to be a fast and effective oil recovery process for low permeable and strongly water-wet chalk (Cuiec et.al., 1994). Therefore spontaneous imbibition is accepted as an important recovery mechanism for low permeability or fractured reservoirs. For a gravity dominated imbibition, assumed to follow Darcy's law, a higher flow rate will result from an increase in permeability.

2.10.2.2 Initial water saturation

The effect of initial water saturation is not easily predicted, due to the variable wetting state of reservoir rock. Morrow and Mason, 2001, states that in reservoir conditions, a high initial water saturation leads to a reduced capillary pressure, but increased mobility of invading water. Viksund et.al., 1998, conducted experiments with strongly water-wet chalk and Berea sandstone. It was reported that with initial water saturation ranging from 0-30%, the final recovery for sandstone changed a little. Zhou et.al., 2000, performed experiment by countercurrent spontaneous imbibition with Berea sandstone, imbibition rate and water wetness were reported to decrease with an decrease in initial water saturation.

2.10.2.3 Boundary condition

Cocurrent flow occurs if the invading water and producing oil flow in the same direction as the water displaces the oil. Countercurrent flow are defined as when the two phases flow in opposite directions, which may be the only possible flow pattern if the matrix or core are completely surrounded by water. At counter-current flow the total velocity is zero inside the core, based on the assumption that advancing water displaces an equal volume of oil from the pore space, which escapes through the inlet by flowing back to the surface of the core.

Depending on the ratio of gravity to capillary forces, water injection rates and boundary condition of the fracture network matrix block, spontaneous imbibition can be cocurrent or countercurrent in

fractured reservoirs (Al-Lawati et.al., 1996; Hamon et.al., 1986). Cocurrent flow may occur if only parts of the matrix are exposed to water, and gravity segregation of oil and water occurs. Experiments performed on low permeable chalk showed that countercurrent flow may be the dominat mechanism, especially for brine-oil displacement from the bottom of the rock blocks (Cuiec et.al., 1994). Spontaneous water-oil imbibition tests in strongly water-wet sandstone at laboratory conditions were conducted at both cocurrent and countercurrent flow patterns by Bourbiaux et.al., 1990. It was reported that for the dominant cocurrent flow case, the brine saturation profile measurement showed that a brine-oil front moved regularly from the lower to the upper end, and as the driving effect of gravity forces decreased as the front nearing the upper face, the slope of the front decreased with time. For the pure countercurrent flow case, as it progressed towards the bottom of the sample the oil/brine front became flat. The two fronts progressed at similar speed from each sample end towards the center in a combination of cocurrent and countercurrent flow case. For spontaneous imbibition a countercurrent flow will be slower than a cocurrent flow, as the movement of both oil and water in opposite directions will reduce the total mobility.

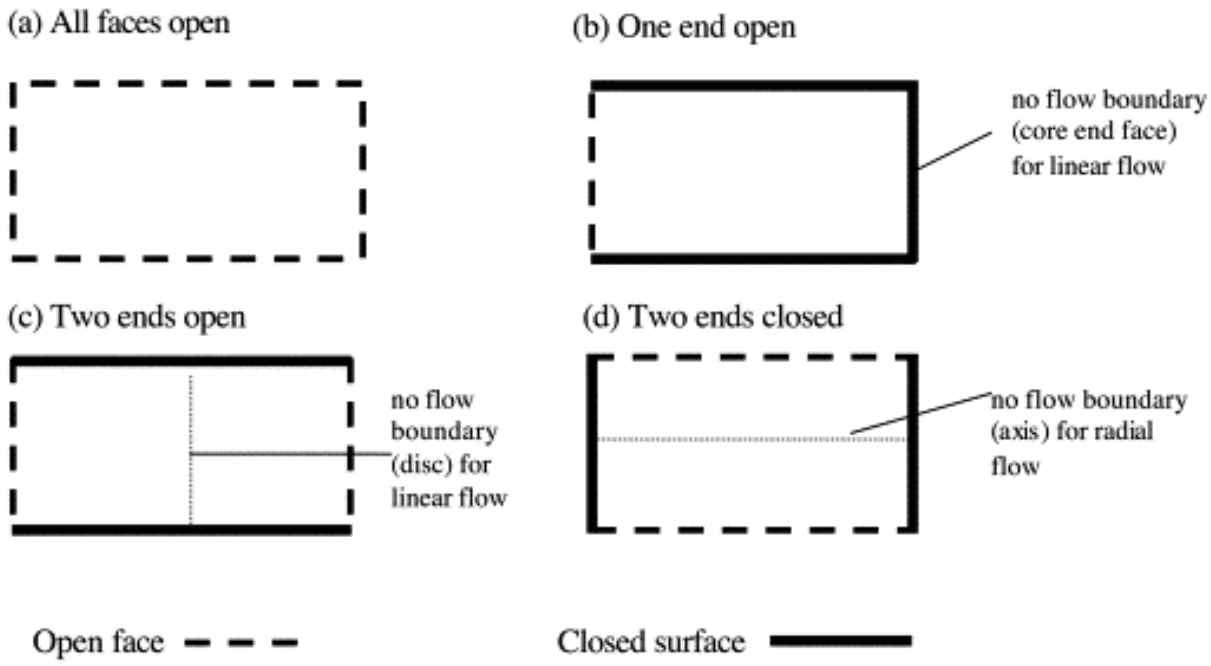

Figure 2.22: Various combinations of boundary conditions used during imbibition (Norman et.al., 2001).

Babadagli et.al., 1999, conducted tests with Berea sandstone samples, it was reported that for countercurrent flow, more time was required in order for the capillary imbibition process to start as less matrix contact area was exposed to the imbibing fluid. For concurrent experiments, the ultimate recovery was approximately the same for all the test, not related to the boundary conditions, the recovery rate was however decreased as more area on the matrix was coated.

2.10.2.4 Wetting state

The wetting state of the rock surface is essential for the spontaneous imbibition, as it effects the fluid distributions, which are related to the relative permeability and capillary pressure, forces that greatly influences the displacement process and performance (Anderson, 1986). Zhou et.al., 2000, performed spontaneous imbibition experiments on Berea sandstone with different wetting states, reporting that the oil recovery passed through a maximum in recovery, as the wetting state decreased from very strongly water-wet. The imbibition rate was also found to be related to the wetting state, with an increased imbibition rate with increasing water-wetness.

2.10.3 Scaling of spontaneous imbibition

The process of SI is of crucial importance to evaluate the wettability of a rock, and is also one of the key production mechanisms in the world's largest remaining oil reservoirs (Jadhunandan and Morrow, 1991; Morrow et. Al., 1994; Morrow and Mason, 2001). To characterize the influence of key parameters on SI, scaling groups need to be used, and are essential to understand SI. Scaling groups are used for an appropriate up scaling of data (Morrow and Mason, 2001), a well as modeling and simulating flow in fractured and heterogeneous reservoirs (Barenblatt et.al., 1960; Warren and Root, 1963). Laboratory measurements are often used in the prediction of oil recovery, and could be scaled up to forecast oil recovery at reservoirs scale. Factors involved are rock properties, liquid viscosities, interfacial tension, core geometry and wettability.

Mattax et.al.,1962, defined a scaling group:

$$t_{DMK} = \frac{t\sqrt{\frac{k}{\phi}}\sigma}{\mu L^2} \tag{2.55}$$

$$\left(\frac{t\sqrt{\frac{k}{\phi}}\sigma}{\mu L^2}\right)_{model} = \left(\frac{t\sqrt{\frac{k}{\phi}}\sigma}{\mu L^2}\right)_{matrix\ block} \tag{2.56}$$

t_{DMK} = dimensionless time
t = time
k = permeability
Φ = porosity
σ = interfacial tension
μ = viscosity
L = length of the core

The scaling group is a form on inverse capillary number, expressing the ratio of capillary force to viscous resistance. If imbibition oil recovery is plotted against the dimensionless scaling parameter above, an equal recovery curve will be achieved for the model and for matrix blocks of the same geometry and rock type. As a result, the imbibition test on small laboratory samples can scale imbibition behavior for same shape and rock type reservoir matrix blocks. The equation above shows that if all other factors are equal, the time before a given water saturation are reached is proportional to the square of the matrix block size, defined by L, a characteristic linear dimension of the block. It is subject to the following six conditions:

1. Gravity effects can be neglected
2. Sample shapes and boundary conditions must be identical
3. Oil/water viscosity ratio is duplicated
4. Initial fluid distribution is duplicated
5. Relative permeability functions must be the same
6. Capillary pressure functions must be related by direct proportionality

These conditions are obviously hard to satisfy. The scaling problem is not easy to solve, as it need to provide a working account of the factors that can affect imbibition through the identification of the dominant variables under various complex conditions that are typical for oil reservoirs. The conditions stated above are only a useful starting point for predicting oil recovery.

$\sqrt{\frac{k}{\phi}}$, is proportional to the microscopic radius, as defined by (Leverett, 1939):

$$r = \sqrt{\frac{8k}{\phi}} \quad (2.57)$$

2.10.3.1 Viscosity ratio

Ma et.al., 1999, systematically tested the effect of oil/brine viscosity ratio on imbibition rate. They found that the oil recovery rate was inversely proportional to the geometric mean of the oil and water viscosities.

$$t_D = t\sqrt{\frac{k}{\phi}}\frac{\sigma}{\sqrt{\mu_o \mu_w}}\frac{1}{L_C^2} \quad (2.58)$$

$$L_C = \sqrt{\frac{V_b}{\sum \frac{A_i}{d_i}}} \quad (2.59)$$

L_C = characteristic length, shape factor
V_b = bulk volume

A_i = different surface areas exposed for spontaneous imbibition
d_i = corresponding distance to the no-flow boundary

The characteristic length, L_C, is defined by the distances to the no-flow boundaries with respect to counter-current flow from all open faces of the rock. Type of shape factor is correlated to the relative contribution of capillary and gravitational forces acting on the fluids. When capillary forces are governing fluid flow, a shape factor describing the surface area of the sample seems to be the best fit for scaling the core dimensions. In the case for low IFT, gravitational forces may be dominating, and the core may be scaled by using just the height of the sample as the characteristic length. Zhang et.al., 1996, conducted various test with different viscosity ratios and boundary conditions. Their result, included those of Mattax and kyle, and Hamon and Vidal are plotted below. The data are correlated by the characteristic length, this implies that for all the tested geometries and boundary conditions the basic imbibition mechanism is counter-current.

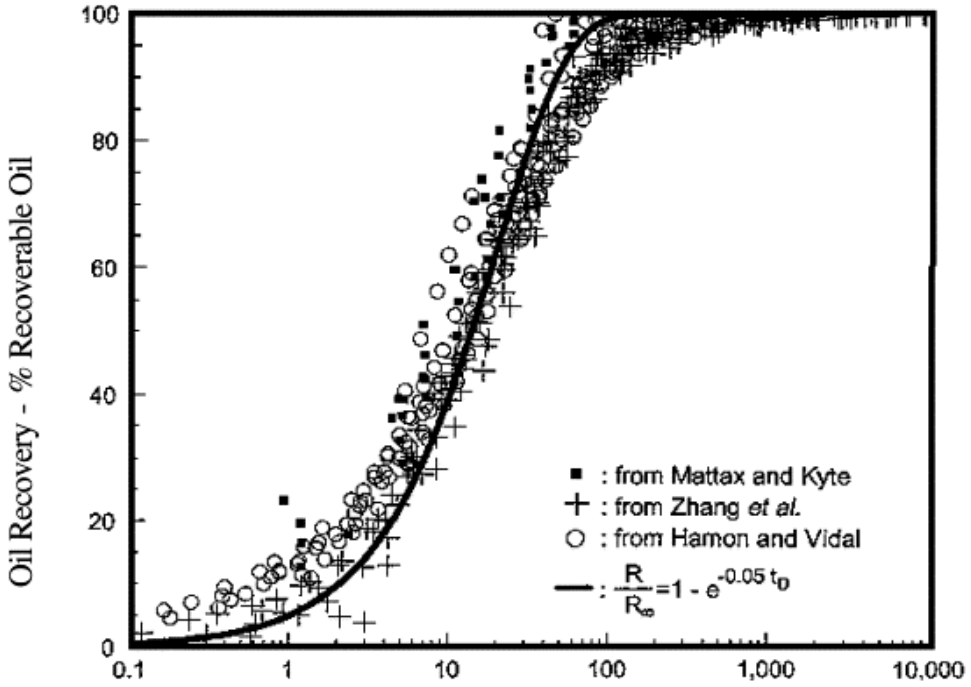

Figure 2.23: Normalized oil recovery plotted against dimensionless time for very strongly water-wet imbibition (Norman et.al., 2001).

2.10.4 Imbibition Rate and Time

Some authors have derived an equation that describes the movement of water into dry soils, and a similarity to the diffusion equation was observed. The computed displacement fronts are significantly diffuse and it is assumed that the diffusion coefficient is proportional to the partial derivative of capillary pressure with respect to water saturation. From this analogy, the predicted volume of water imbibed is proportional to the square root of time, and is confirmed by experimental results for sandstone (Handy, 1960; Garg et.al., 1996). Mattax et. al., 1962 also presented the following relationship between imbibition rate, q(t), and imbibition time, t.

$$q(t) = \frac{C}{\sqrt{t}} \quad (2.60)$$

In some cases the diffusion-type equation can be problematic, an alternative is assuming piston-like displacement, deriving an equation which is also dependent of volume imbibed on the square root of time. Handy, 1960, examines imbibition in the limit that capillary forces dominate over buoyancy and viscous forces, in his analysis the velocity of imbibed phase is proportional to the gradient of capillary pressure with respect to distance, and fronts are assumed to be sharp.

Depending on the assumptions, imbibition can be described by either a frontal-advance equation or diffusion-like equation, whereas the main difference is that in the diffusion equation method it is predicted that the smallest pores fill first, and larger pores later. The frontal advance equation predicts that all pores are connected, and all pores fill simultaneously. The mass of water imbibed is a linear function of the square root of time in both methods, as agreed upon by experiments. However, the expected end result of the diffusive process contradicts the quite abrupt end of imbibition, leading to the assumption that the frontal advance equation is a better fit for describing the true process.

The flow equation may be defined as follows, if imbibition occurs vertically upward.

$$u_W = \frac{k_w}{\mu_w}\left(\frac{p_c}{x} - \Delta\rho g\right) \quad (2.61)$$

p_c = capillary pressure
μ_w = water viscosity
k_w = effective water permeability
u_W = flow rate
$\Delta\rho$ = density difference
g = acceleration due to gravity
x = position of front

Assuming piston-like displacement and constant capillary pressure, p_C.

$$(2.62) \quad u_W = \phi S_W \frac{\partial x}{\partial t}$$

S_W = fractional water content of the pore space
ϕ = porosity
x = distance
t = time

Substituting equation 2.64 into 2.65 yields:

$$(2.63) \quad \frac{\partial x}{\partial t} = \frac{k_W}{\phi \mu_W S_W}\left(\frac{p_C}{x} - \Delta\rho g\right)$$

Integrating the equation above:

$$(2.64) \quad x + \frac{p_c}{\Delta\rho g}\ln\left(1 - \frac{\Delta\rho g x}{p_c}\right) = -\frac{k_W \Delta\rho g}{\phi \mu_W S_W} t$$

Assuming that gravity forces are negligible compared to capillary forces, the equation above reduces to:

$$(2.65) \quad \frac{\Delta\rho g x}{p_c} \ll 1$$

$$(2.65) \quad x^2 = \left(\frac{2 p_C k_w}{\phi S_W \mu_W}\right) t$$

$$(2.66) \quad x^2 = \frac{Q_W}{\phi A_C S_W}$$

$$(2.67) \quad {Q_W}^2 = \left(\frac{2 p_C k_w \phi {A_C}^2 S_W}{\mu_W}\right) t$$

A_C = cross-sectional area of the sample
Q_W = total volume of imbibed water

From the equation above it can be observed that the rate of imbibition is a function of effective water permeability, water saturation, and the capillary pressure. The mass imbibed follows a linear relation to the square root of time, and the slope is proportional to the square root of the product $(p_C k_w S_W)$. These are also the unknown quantities, as the rest are more or less easily measured.

The product of $(p_C k_w S_W)$ may be referred to as the imbibition potential, and it allows the quantification of the rate of imbibition as a function of known values in different rocks (Schembre et.al., 1998).

$$(2.68) \quad (p_C k_w S_W) = \frac{\lambda^2 \mu_W}{2\phi {A_C}^2}$$

$$(2.69) \quad \lambda_{imb} = \frac{Q_W}{\sqrt{t}}$$

It can then be derived that the imbibition recovery, $R_{im}(t)$, are defined as:

$$(2.70) \quad R_{im}(t) = \frac{1}{V_P(1-S_{wi})}\int_0^t q(t)dt = \frac{2C}{V_p S_{oi}}\sqrt{t}$$

C = constant
S_{wi}, S_{oi} = initial water and oil saturation, respectively
V_p = pore volume

2.10.5 Characterization of wettability

A dominant factor in the rate of oil recovery is the degree of water wetness, since rocks that spontaneously imbibe water are at least partially water wet. The effects from capillary pressure driving force and the opposing viscous resistance to flow are essentially the determining parameters for the rate of spontaneous imbibition.

Graue et.al., 1998, suggested that measurements of spontaneous imbibition rates of water for oil/brine/rock systems can be used to characterize wettability in a way that reflects both rate and amount of oil production with an emphasis on early time recovery. The characterization can be improved if other affecting parameters are considered, these parameters include: porosity, rock structure or permeability, oil and water viscosities and interfacial tension.

Babadagli, 1996, used the imbibition recovery curve (eq. 2.70) to quantify wettability characteristics. If all other parameters are constant, the slope C, is only a function of wettability. He introduced a wettability index, $f(\theta)$, ranging from 0 to 1, where the highest slope is equal to 1, representing strongly water wet conditions. The wettability index as introduced does not contain all the parameters affecting imbibition, therefore Shahri et.al., 2012, derived a new index containing all parameters, called the Normalization Index:

$$(2.71) \quad R_{im}(t) = \frac{C^*\frac{K}{\phi}}{V_P(1-S_{wi})\sqrt{\mu_o\mu_w}L_C^2}\left[\frac{\sigma}{\sqrt{\frac{K}{\phi}}} + \frac{\Delta\rho g L_C^2}{L_H}\right]\sqrt{t}$$

L_H = Vertical height of the core
g = gravity constant
$\Delta\rho$ = density difference between water and oil
C^* = modified constant used to calculate the normalization index

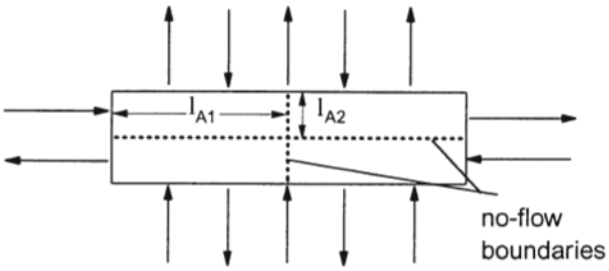

Figure 2.24: Countercurrent imbibition with all faces open. Note the superposition of no-flow boundaries.(Zhang et.al., 1996)

From eq.2.59 and figure 2.24, the characteristic length is given by:

$$L_C = \frac{Ld}{2\sqrt{d^2 + 2L^2}} \quad (2.72)$$

L = length of the core
d = diameter of the core

3. Experimental

This chapter pertains to describe the experimental procedures, apparatus and materials. Two different experiments were conducted in this thesis:

- Coreflooding to investigate oil recovery associated with different brines
- Spontaneous imbibition to study the different effects on the cores after flooding, and different brine effects

The cores were first saturated with oil, and then aged for a minimum of 2 weeks. Flooding was performed with different brines. After the flooding experiments the cores was re-saturated with oil, and then aged for minimum 2 weeks, spontaneous imbibition were then performed at increasing temperatures. In general the following steps were done in one experiment:

- Saturating the core with synthetic sea water (SSW)
- Injecting SSW at three different rates at room temperature to establish absolute permeability
- Oil flooding to saturate the core with oil and establish initial water saturation
- Aging at 50 ^{0}C for a minimum of 2 weeks
- Flooding with the selected brine to study recovery and effluent
- Oil flooding to re-saturate the core with oil before imbibition experiments
- Aging at 50 ^{0}C for a minimum of 2 weeks
- Spontaneous imbibition in Amott cell with selected brine at increasing temperatures (room temperature, 50 ^{0}C and 70 ^{0}C, respectively).

3.1 Experimental Apparatus

3.1.1 Flooding setup

Core flooding setup consisted of an oven to adjust the flooding temperature, a Gilson 305 pump, piston cell, core holder, a computer to register inlet and delta pressure, a measuring burette, and a back pressure valve. A confining pressure of 20 bars was maintained through the tests, to simulate reservoir conditions and give a good seal between the shrinkable sleeve and core. A backpressure of 10 bars was used. The computer was used to register and log pressure parameters in time, the inlet pressure into the core, and the pressure difference across the core due to the pressure loss from the flow was recorded. Produced liquids, both effluent water and produced oil was sampled and recorded at intervals. The pH was measured and logged through the test. During flooding, the aged

core was put in the core holder and connected to the flooding setup. Temperature was increased, confining pressure built up to 20 bars, and different types of fluids were injected into the core by piston cells. A sketch of the flooding set-up is shown below.

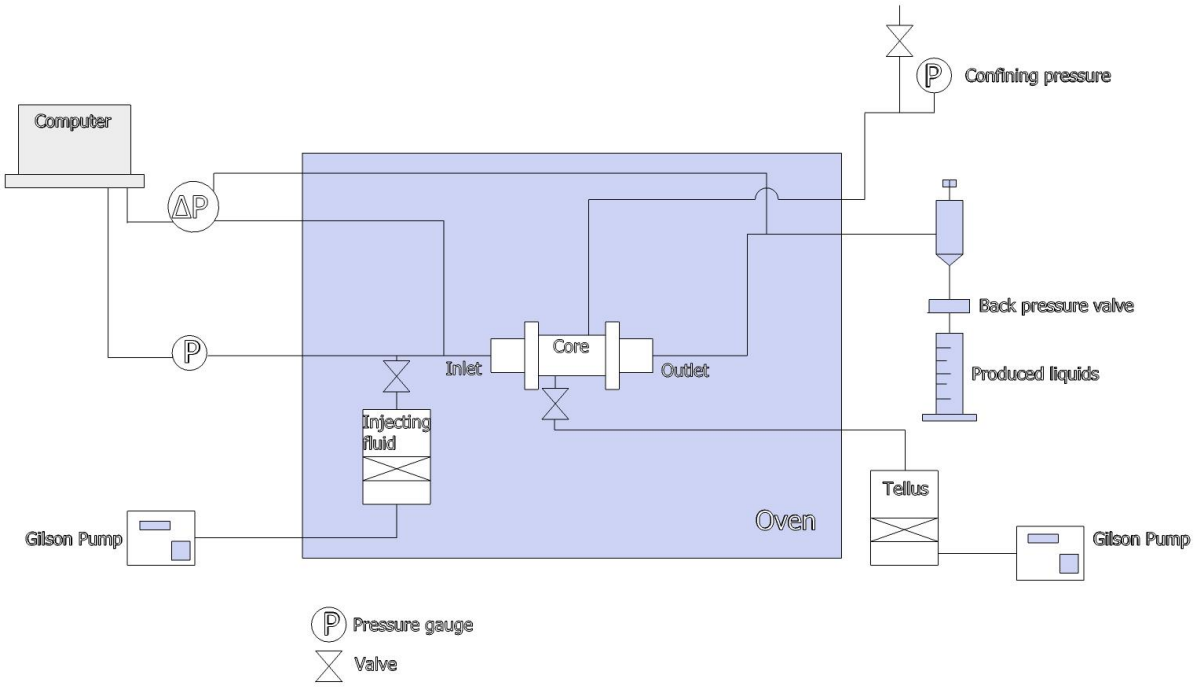

Figure 3.1: Simplified sketch of flooding set-up.

For all floodings, either brine or oil injection, the core was weighed before and after to check for any discrepancy between the measured volumes and calculated saturations. Assuming a 100% fluid saturated core, the volumes of different fluids can be checked by simple calculations based on the density of the fluids. As the core was mounted in the core holder, it was first wrapped with a double layer of Teflon tape, the heat shrinkable sleeve was then fitted by heating. The inlet and outlet of the core holder were blocked as to prevent any fluid loss from the heating.

3.1.2 Volumetric pump

For all injections, and to create the confining pressure, volumetric pumps were used in order to control the flow rate and pressure. The pumps used were Gilson 305, 806 Manometric module.

3.1.3 Vacuum pump

A vacuum was used to remove all the air from the cores and to ease the saturation process for the initial saturation with SSW. The core was simply put in an air tight bowl connected to a vacuum pump which were left running until a sufficient low enough pressure were obtained, usually about 3 hours.

3.1.4 Measuring system

The volume of produced fluids was simply measured by a timer and a measuring burette. The error introduced by the visual reading of the fluid meniscus were taken into account and made as small as possible. The pH was measured continuously as to not let the produced effluent react with the air, which could affect the results, a Mettler Toledo pH meter were used. Calibration was performed with three buffer solutions at pH 4, 7 and 10, precision is about ± 0.02. The samples were then stored in glass bottles until the Ion-configuration could be measured.

3.1.5 Anion and Cation analysis

A Dionex ICS-3000 ion chromatograph was used to measure the anion and cation content of the produced water for selected samples. The samples were first diluted, 1 to 200 times for high salinity produced water, and 1 to 50 times for low salinity. They were then filtered and put in the Ion chromatograph for analysis. The chromatograph was connected to a computer which recorded and calculated the results. After the test was finished, the raw data stored on the computer was processed manually by the program Chromeleon 7, adjusting the results for each sample for all ions to minimize error. The data are given in the appendix.

Figure 3.2: Dionex ICS-3000 Ion Chromatograph.

SSW	Chloride	Carbonate	Sulfate	Sodium	Potassium	Magnesium	Calcium
Average	0,525	0,002	0,024	0,45	0,01	0,045	0,011375
Std.dev	0,002102165	0,000165144	8,92686E-05	0,00420155	0,0005655	0,0001948	0,0043036
Corrected Std.dev	0,002247309	0,000176547	9,54321E-05	0,00449164	0,0006045	0,0002082	0,0046008
%	0,400412368	8,257223153	0,37195232	0,93367705	5,654822	0,4328623	37,833951
Variance	4,4191E-06	2,72727E-08	7,96888E-09	1,7653E-05	3,198E-07	3,794E-08	1,852E-05

Table 3.1: Average concentrations including deviation from the SSW samples used as a base for calculating concentration of effluent samples. All concentrations values are in mole/liter.

3.1.6 Interfacial tension measurement (IFT)

The interfacial tension (IFT) measurements were performed by the volume drop method, using a volume tensiometer (DVT30). The tensiometer was supplied by KRÜSS GmbH, Germany. Repeatability is reported to be ±0.1 mN/m.

3.1.7 Imbibition setup

During the imbibition tests the cores were placed in a volumetric Amott cell and the test were conducted at increasing temperatures, starting with room temperature, and then increased to 50 ^{0}C, and 70 ^{0}C respectively. The Amott cell consist of a tubular glass base, into which the core is placed, and a measuring burette incorporated on top to allow the produced oil to be quantified. The two pieces were sealed together by silicon grease, and the cell was filled with brine through the bottom tube until desired height. Synthetic seawater was used as the initially saturating brine and imbibing fluids, if not otherwise stated. The amount of oil was monitored and recorded versus time with appropriate time intervals.

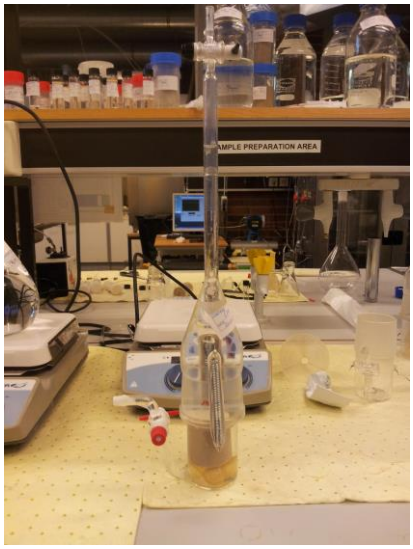

Figure 3.3: Amott cell used for imbibition experiments.

3.2. Materials

3.2.1 Porous media

Outcrop sandstone cores were used in the experiments. The result from the mineral analysis is given below, a complete solid analysis is given in the appendix. The test was performed by Intertek West Lab AS.

Mineral Name	Chemical Formula	Semi Quantitive (%)
Quartz	SiO_2	94
Kaolinite	$Al_2Si_2\ O_5(OH)_4$	1
Muscovite	$(K,Na)(Al,Mg,Fe)_2\ (Si_3.Al,O_{10})\ O10(F,OH)_2$	1
Microline	$KAlSi_3O_8$	1

Table 3.2: Mineral analysis of the sandstone used in the experiments.

Core number	Diameter (cm)	PV (ml)	Length (cm)	Porosity	Permeability (Darcy)	r, leverett	Characteristic length [cm]
#3	3,63	13,77	5,63	0,236	1,0	5,77532E-06	1,168
#4	3,76	13,23	5,03	0,236	0,9	5,47396E-06	1,175
#5	3,75	13,22	5,06	0,236	1,0	5.77398E-06	1,174
#6	3,76	13,29	5,05	0,237	0,95	5,6227E-06	1,176
#7	3,77	12,37	5,05	0,219	0,8	5,39535E-06	1,179
#8	3,77	13,15	5,13	0,229	1,05	6,00467E-06	1,183
#9	3,78	12,91	5,11	0,225	1.0	5,88733E-06	1,184
#10	3,78	12,66	5,09	0,221	1,2	6,58778E-06	1,183
#11	3,76	13,24	5,075	0,235	1,1	6,12625E-06	1,177
#12	3,775	12,94	5,085	0,227	1,0	5,90119E-06	1,182
#13	3,75	15,01	5,69	0,239	0,95	5,5995E-06	1,202

Table 3.3: Properties of the different cores used.

3.2.2 Oil

Normal-decane (n-C_{10}) was used as a hydrocarbon phase, supplied by Chiron AS in HPLC grade (purity >99%). N,N-Dimethyldodecylamine (NN - DMDA) were used as oil soluble additives to mimic amine in the oil. Concentrations of 0.01 mole/liter were used. Physical properties of the oil at different temperatures are given below, the numbers are obtained from the simulation program PVTsim (20.1). It is assumed that the small concentration of NN-DMDA does not have any significant influence on the properties of the oil.

Components	Supplier and purity	Structural formula
N,N-Dimethyldodecylamine (NN - DMDA)	Fulka ≥ 99%	$CH_3(CH_2)_{11}N(CH_3)_2$

Table 3.4: Polar components.

N-Decane / Temperature	Room temperature, 20 ^{0}C	50 ^{0}C	70 ^{0}C
Viscosity (cP)	0,920	0,5802	0,4812
Density (g/ml)	0,730	0,7683	0,7525

Table 3.5: Properties of n-Decane.

3.2.3 Brines

Several different types of brine have been used for both initial saturation fluid, flooding and spontaneous imbibition. The brines are given name by content, as listed below. Table 3.6 give the composition of the different brines. See appendix for complete description of brines.

- **SSW**: Synthetic seawater.
- **LSW**: Low-salinity water, SSW diluted 25 times.
- **Mg**: Brine only containing $MgCl_2$ at seawater concentration ($0.045\mathrm{M}$).
- **SO4**: Brine only containing Na_2SO_4 at seawater concentration ($0.024\mathrm{M}$).

During the preparation of brines, different amounts of reagent grade chemicals were dissolved in distilled water as by compositions, and then stirred by a magnetic bar for at least 3 hours. When the salts were properly dissolved, the brine was filtered through a 0.22 µm Millipore filter to remove unsolvable particles. The brine was stored in clear glass bottles.

Ion Name	**SSW (mole/L)**	**LSW (mole/L)**	**Mg (mole/L)**	**SO4 (mole/L)**
$\mathbf{HCO_3^-}$	0.002	0.00008	-	-
$\mathbf{Cl^-}$	0.525	0.021	0.09	-
$\mathbf{SO_4^{2-}}$	0.0240	0.00096	-	0.0240
$\mathbf{Mg^{2+}}$	0.045	0.0018	0.045	-
$\mathbf{Ca^{2+}}$	0.013	0.00052	-	-
$\mathbf{Na^+}$	0.450	0.018	-	0.048
$\mathbf{K^+}$	0.010	0.0004	-	-
TDS (g/L)	33.39	1.3356	4.2844	3.414
Ion Strength (mole/L)	0.657	0.0263	0.135	0.072

Table 3.6: Composition of brines. All concentrations values are in mole/liter.

Temperature	Room temperature, 23 ^{0}C	50 ^{0}C	70 ^{0}C
Oil (cP)	0,920	0,5802	0,4812
SSW (cP)	0,9971	0,5901	0,4382
LSW (cP)	0,9347	0,5484	0,4052
Mg (cP)	0,9451	0,5556	0,4110
SO4 (cP)	0,9390	0,5514	0,4077

Table 3.7: Calculated and simulated viscosity for the different brines and oil.

Dynamic viscosities of the different brines are calculated from equation 3.1 given by Fabuss et.al., 1969. Accuracy is reported to be $\pm$0.4%, range is within 20<T<150 [^{0}C] and 0<S_p<130 [g/kg], which is more than sufficient for this case.

$$\log\left(\frac{\mu_{sw}}{\mu_w}\right) = 0.04281I + 0.001231I^2 + 0.000131I^3 + (\log(10^3 * \mu_w) * (-0.03724I + 0.018591I^2 - 0.00271I^3) \quad (3.1)$$

$$\mu_w = (4.2844 * 10^{-5}) + \frac{1}{(0.157(T+64.993)^2 - 91.296)} \quad (3.2)$$

μ_w = pure water viscosity

μ_{sw} = viscosity of brine

I = Ionic strength

T = temperature [^{0}C]

Brine	SSW	LSW	SO4	MG
Interfacial tension [mN/m] with N-decane + NN-DMDA	20.1	31.5	31.1	32.2

Table 3.8: Measured interfacial tension at room temperature for the different brines.

3.3 Procedures

3.3.1 Saturation procedure

The cores were first dried at 100 ^{0}C for a minimum of 24 hours before weighing. They were then put in an airtight bowl connected to a vacuum pump, evacuating the air inside the core to a sufficiently low enough pressure. Synthetic seawater was then used to saturate the core 100%, and the core was weighed again.

3.3.2 Absolute permeability

Absolute permeability was measured by placing the 100% SSW saturated core in the flooding setup, and then SSW were injected at three different rates at room temperature. The rate was kept constant for 10 minutes while the delta pressure was recorded, the average from the pressure readings was then used to calculate permeability. Absolute permeability was averaged by the result for each flow rate.

3.3.3 Pore volume calculation

Calculation of the pore volume is based upon weight difference from a dry and 100% saturated state, and the density of the synthetic seawater. The pore volume is expressed by the equation below:

$$PV = \frac{W_S - W_D}{\rho_{SSW}} \quad (3.3)$$

PV = Pore Volume of the core, [cm^3]

W_S = Weight of a 100% saturated core, [g]

W_D = Weight of a dry core, [g]

ρ_{SSW} = Density of the saturation fluid, Synthetic seawater, [$\frac{g}{cm^3}$]

3.3.4 Porosity calculation

Porosity is a measure of a rocks ability to hold fluid. Mathematically, porosity is the open space in a rock divided by the total rock volume, and is normally expressed as a percentage of the total volume of the rock.

$$\Phi = \frac{Vp}{V_B} \times 100\% \quad (3.4)$$

$$V_B = \pi H R^2 \quad (3.5)$$

Φ = Porosity [%]

V_P = Pore volume [Cm^3]

V_B = Total bulk volume [Cm^3]

H = Height of the core [cm]

R = Radius of the core [cm]

3.3.5 Oil Saturation / Establishment of initial water saturation

After the cores were 100% saturated with synthetic seawater, it was placed in the flooding setup previously described to establish initial water saturation, S_{WI}. The cores were flooded with oil at a temperature of 50^{0}C and a flow rate of 0.2 ml/min, which equals about 22 PV/d. The core was flooded with minimum 2PV of oil, and the amounts of water drained were recorded.

3.3.6 Oil recovery calculation

Produced oil was measured and logged at intervals by a measuring burette. Oil recovery is mostly presented in fraction of original oil in place, defined in the equation below.

$$Recovery = R = \frac{V_{prod}}{OOIP} \quad (3.6)$$

$$OOIP = S_{oi}V_P = (1 - S_{wi})V_p \quad (3.7)$$

S_{oi}, S_{wi} = Initial oil saturation and initial water saturation, respectively [fraction]

V_p = Pore volume [ml]

V_{prod} = Produced oil [ml]

Normalized recovery curves are sometimes used to scale and compare the different experiments.

$$R_{norm} = \frac{R}{R_{total}} \quad (3.8)$$

R_{norm} = Normalized recovery

R_{total} = Total recovery at the end or end point

R = Oil recovery

3.3.7 Aging of the core

After the initial water saturation was determined by flooding with oil, it was submerged in oil in a sealed aging cell. The core was then kept at the selected aging temperature of 50 ^{0}C for a period of minimum 14 days.

4. Results and discussion

Water flooding was carried out in this study to observe for any low salinity effects for our rock, brine and oil combination. After flooding, the cores were re-saturated with oil and spontaneous imbibition was performed to see if the different brines had altered the EOR potential and core properties. In addition the imbibition brine was changed to observe for any low salinity effects.

4.1 Corefloods

In this section of the thesis the results from the corefloods are presented. In total, seven corefloods were conducted on different cores, flooding temperature was 70^{o}C for all:

- **Core #4:** Aging and flooding conducted with SSW. 4 PV were injected at a rate of 4 PV/day (0.035 ml/min) and then increased to 16 PV/day (0.14 ml/min).
- **Core #5:** Aged with SSW, flooded with LSW. 4 PV were injected at a rate of 4 PV/day, and then increased to 16 PV/day.
- **Core #6:** Aged with SSW. Flooded with SSW followed by LSW, both for 24 hours at 4 PV/day. The rate was then increased to 16 PV/day for LSW, flooding at least 4 PV. At the end a minimum of 2 PV of SSW was injected to obtain same initial aging brine present in the core.
- **Core #7:** Aged with SSW. Flooded with SSW followed by SO4, both for 24 hours at 4 PV/day. The rate was then increased to 16 PV/day for SO4, flooding at least 4 PV. At the end a minimum of 2 PV of SSW was injected to obtain same initial aging brine present in the core.
  Core #8: Aged with SSW. Flooded with SSW followed by Mg, both for 24 hours at 4 PV/day. The rate was then increased to 16 PV/day for Mg, flooding at least 4 PV. At the end a minimum of 2 PV of SSW was injected to obtain same initial aging brine present in the core.
  Core #10: Aged with SSW. Flooded with Mg followed by LSW, both for 24 hours at 4 PV/day. The rate was then increased to 16 PV/day for LSW, flooding at least 4 PV.
- **Core #12:** Aged with SSW. Flooded with SO4 followed by LSW, both for 24 hours at 4 PV/day. The rate was then increased to 16 PV/day for LSW, flooding at least 4 PV.
- **Core #3 and #9:** Experienced failure of lab equipment which could affect the result, it was therefore decided to redo the tests.
- **Core #11 and #13:** Only spontaneous imbibition performed.

Core number	S_{wi}	OOIP [ml]	Permeability (Darcy)	Temp [^{0}C]	Flooding fluid
#4	0,23	10,2	0,9	70	SSW
#5	0,25	9,8	1,0	70	LSW
#6	0,19	10,7	0,95	70	SSW-LSW-SSW
#7	0,22	9,7	0,8	70	SSW-SO4-SSW
#8	0,18	10,8	1,05	70	SSW- Mg-SSW
#10	0,20	10,1	1,2	70	Mg – LSW
#12	0,23	10,0	1,0	70	SO4 – LSW

Table 4.1: Core properties and flooding parameters for the corefloods performed in this section.

4.1.1 General characteristics of oil recovery curves and ion-chromatography plotting

The following figures present the basics of the plots used to present the data in the next section. Figure 4.1 shows the cumulative oil recovery (fraction) curve and pH measurements plotted against injected pore volumes of brine. The oil recovery is plotted on the y-axis to the left, and pH to the right. The blue curve represents the oil recovery as a fraction of original oil in place. Injection brine pH is measured at the inlet of the core of each flooding and is assumed constant, presented by the green straight lines. Effluent measured pH is shown as the red squares in the figure. An increase or decrease between inlet and outlet pH are therefore presented as the difference between the red squares and green line. Injection brine at the specific injection rate is explained by the blue boxes on top of the chart, separated by the black vertical lines.

Figure 4.2 shows the results of the anion and cation analysis. Since there are large variations in the concentration of the different ions, they are presented as a relative to the initial concentration of LSW. By using a single plot it is easier to observe any changes and the complete picture of all the relevant ions are presented. A relative concentration simply means that if the value of a ion are equal to 1, the concentration of that ion are equal to the initial concentration of LSW. A relative concentration of 25 means that the ion concentration is 25 times higher than initial LSW. Since LSW are 25 times diluted SSW, a relative value of 25 equals initial concentration of SSW. Similar to the recovery figure, injection brine at the specific injection rate is explained by the blue boxes on top of the chart, separated by the black vertical lines. Complete results with concentrations in mole/liter are given in the appendix.

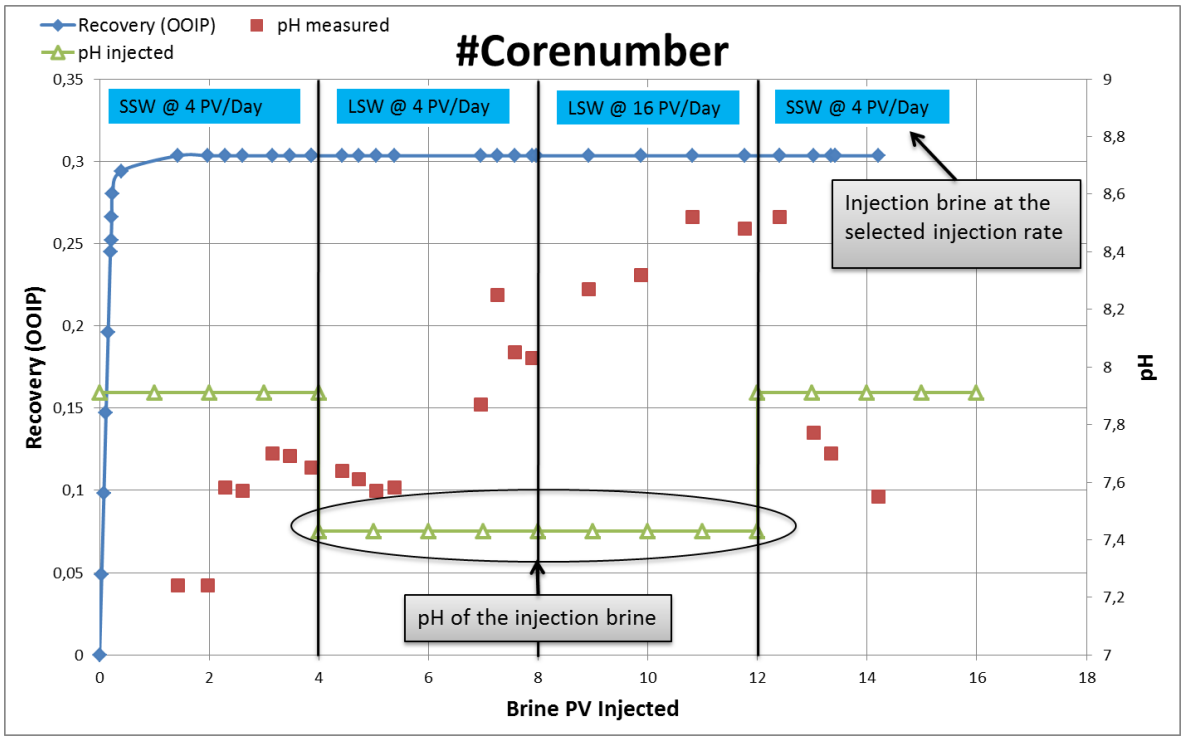

Figure 4.1: General characteristics of oil recovery and pH plot for different injection brines (Linear scale). Recovery (to the left) and pH (to the right) vs. pore volumes of brine injected.

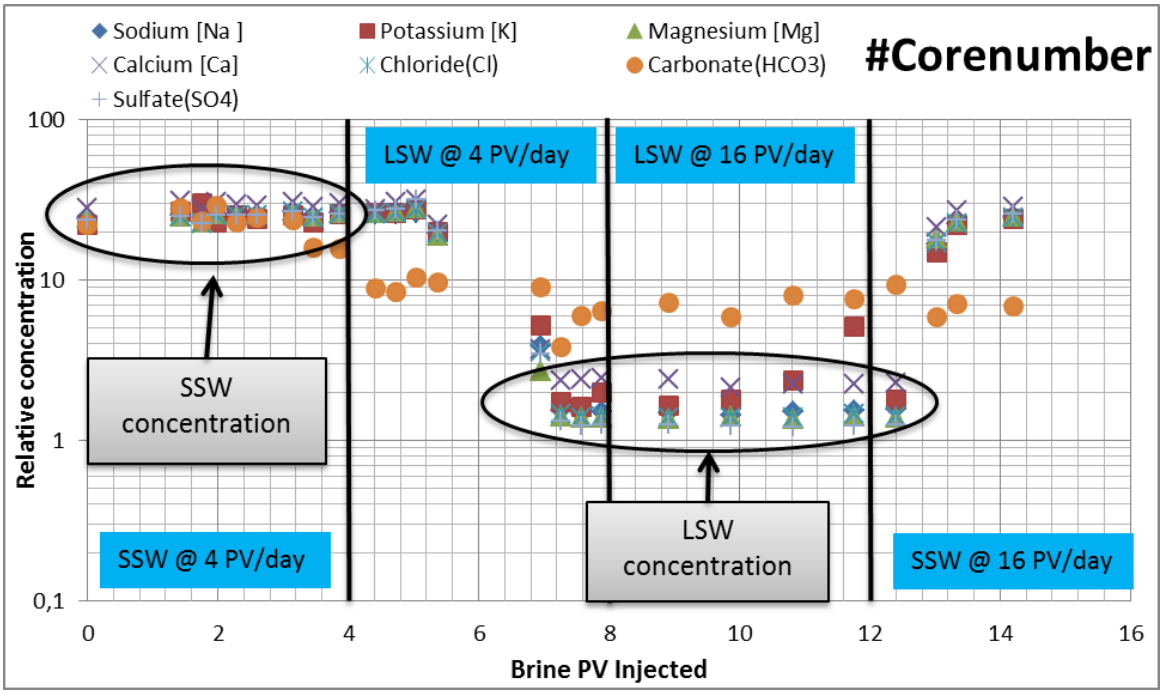

Figure 4.2: General characteristics of the anion and cation analysis. Presented as relative concentrations of LSW vs. pore volumes of brine injected

4.1.2 Core #4 - SSW flooding

Figure 4.3 displays the recovery and pH measurements. During this flooding only SSW was injected, first at a rate of 4 PV/day (0.035 ml/min) and then increased to 16 PV/day (0.14 ml/min) to check for possible end effects. This was done mainly to observe if the increased rate had any effect on the recovery, which is useful for further comparisons of recovery and pH with different brines at the same rate. Also, the core is later used as a base case to compare imbibition to other cores flooded with different low salinity brines. It is observed that the recovery increases linearly and after breakthrough only a small amount of extra recovery is achieved. Final recovery was about 31%.The increased rate did not show any increase in oil recovery, which may be due to the fact that the injection rate and injection rate increase are still small compared to the measured permeability of the core, and oil cannot pass a zone where the flow velocity is lower than that for the onset of oil mobilization. A larger increase in injection rate would most likely result in a more significant increase in the recovery, however, for comparison to other published work and studies the rates were decided to be kept at 4 and 16 PV/day which seems to be the most accepted and used rates. In addition a maximum pressure in the injection well limits injections in oil fields, and a larger increase of the injection rate could not have any real value other than research purposes.

The pH of the injected SSW was measured to 7.9 units, and the effluent was measured to about 7.75. The decrease in pH might be an indication of some brine-rock interaction occurring, the decrease are however small. The slightly lowered pH during injection of SSW is consistent with other flooding experiments performed on similar sandstone (RezaeiDoust, 2011; Aruoture, 2013).

Figure 4.4 presents the pressure drop, it can be observed that the pressure drop increases with recovery, and then remains fairly constant at about 10 mbar. After about 2.5 PV the pressure drop can be seen to decrease, but with some fluctuations in the readings. At an increased rate the pressure increases again.

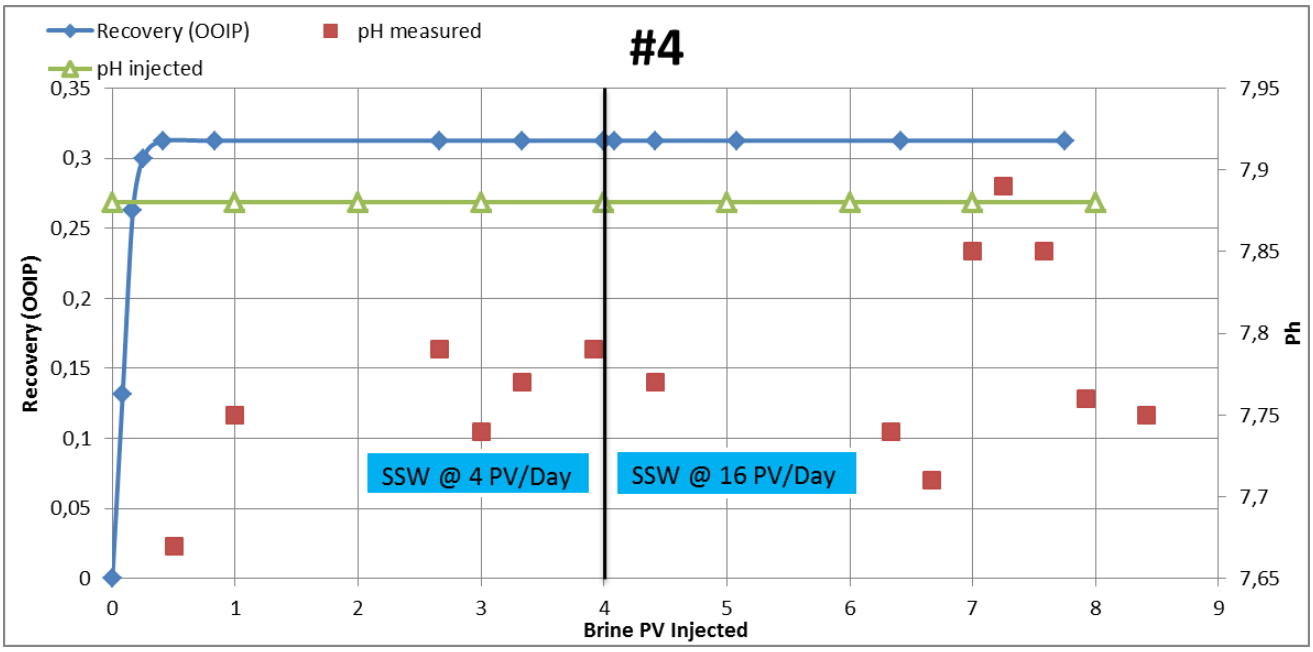

Figure 4.3: Oil recovery and pH plot for SSW injection at different rates (Linear scale). Recovery (to the left) and pH (to the right) vs. pore volumes of brine injected.

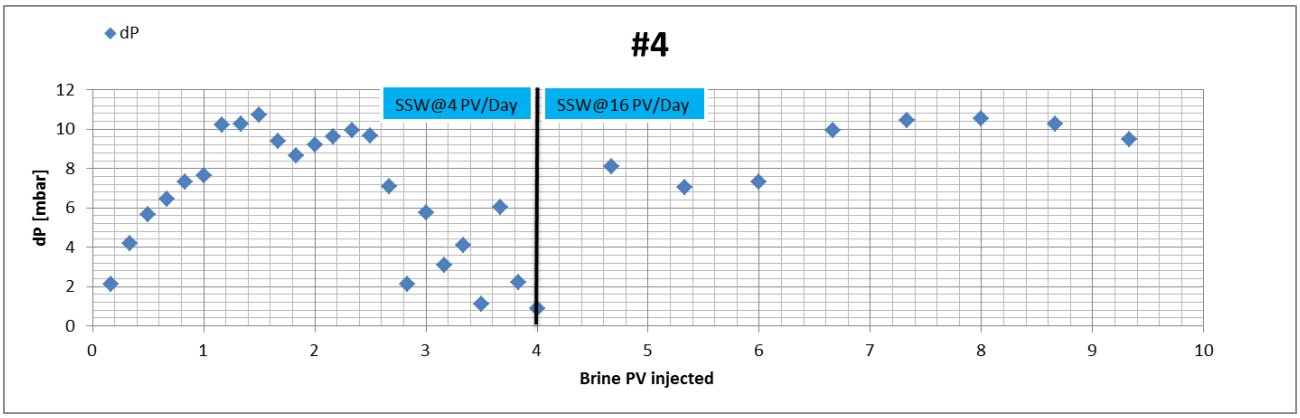

Figure 4.4: Pressure drop in milli-bar for SSW brine injection, plotted against injected pore volume of brine.

4.1.3 Core #5 - LSW flooding

4.1.3.1 Oil recovery and pH effects

In this flooding a core with similar properties as the previous experiment, and same flooding parameters was used. However, the brine injected was LSW, which is SSW diluted 25 times, the complete composition is listed in the experimental section or appendix. The flooding was performed to be able to directly compare SSW and LSW from S_{wi}. Figure 4.5 shows the recovery and pH measurements plotted against injected PV. It can be observed that the recovery increases linearly, and as the previous case, little oil is produced after breakthrough. Final recovery was 22%, a lower

value compared to SSW (31%) as initial flooding fluid, but it can be noted that the initial water saturation of this core was a little higher, decreasing the recovery potential. Another explanation could be the release and migration of fines, possibly plugging pore throats, increasing the residual oil saturation.

During the injection of low salinity brine a significant increase in the pH was measured, with a delta increase of about 1 unit. The pH of the injecting brine was measured to be about 7.4 units, and the effluent measured had an increasing trend, at about 8.4 units at the end of the low rate period. Increasing the injecting rate lead to a further increase in effluent pH, to about 8.6 units. Increase in the pH during injection of low salinity is observed in some, but not all experiments. As mentioned earlier in this thesis, the pH increase is explained as a possible mechanism for low salinity flooding (Austad et.al., 2010; McGuire et.al., 2005). However, low salinity flooding with an significant increase in recovery have been performed without any increase in pH (Lager et.al., 2006). Other researchers have observed an increase in the effluent pH of 1-3 units for non-buffered systems (Austad et.al., 2010; Cissokho et.al., 2009; McGuire et.al., 2005; RezaeiDoust et.al., 2009; Aruoture, 2013).

The increase in pH is most likely due to brine-rock interactions, which are ion exchange and dissolution. Sandstone usually contains a small amount of carbonate in the form of cementing material, and the dissolution of carbonate could explain the increase in pH.

$$CaCO_3 + H_2O \leftrightarrows Ca^{2+} + HCO_3^- + OH^-$$

Similarly the cation exchange mechanism between the brine and mineral surface could also be a reasonable explanation of the increased pH, as both dissolution and cation exchange reactions are accelerated as the low salinity brine are injected.

$$Ca^{2+} - Clay + H_2O \leftrightarrows H^+ - Clay + Ca^{2+} + OH^-$$

The increased concentration of carbonate and calcium in the effluent supports this theory. However, it is observed that the relative increase of carbonate is much higher than calcium. Multi-component ionic exchange has previously been suggested as a possible mechanism (Lager et.al., 2006; Ligthelm et.al., 2009), see previous sections for a complete explanation of the mechanism. If divalent cations were adsorbed by the rock matrix, the concentration of Ca^{2+} and Mg^{2+} should be strongly reduced. This could explain why the concentration increase of Ca^{2+} is relatively small compared to the carbonate. However, the concentration of Mg^{2+} do not change significantly during the flooding, as reported by Lager et.al., 2006. The high levels of potassium (K^+) indicate dissolution of kaolinite, which will be discussed in the next section.

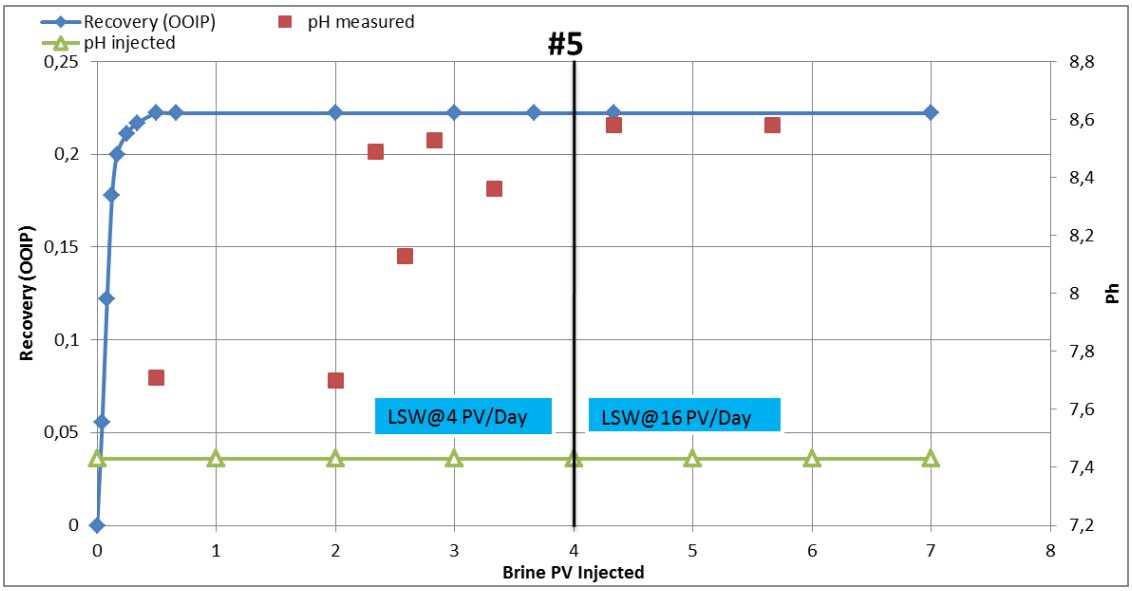

Figure 4.5: Oil recovery and pH plot for LSW injection at different rates (Linear scale). Recovery (to the left) and pH (to the right) vs. pore volumes of brine injected.

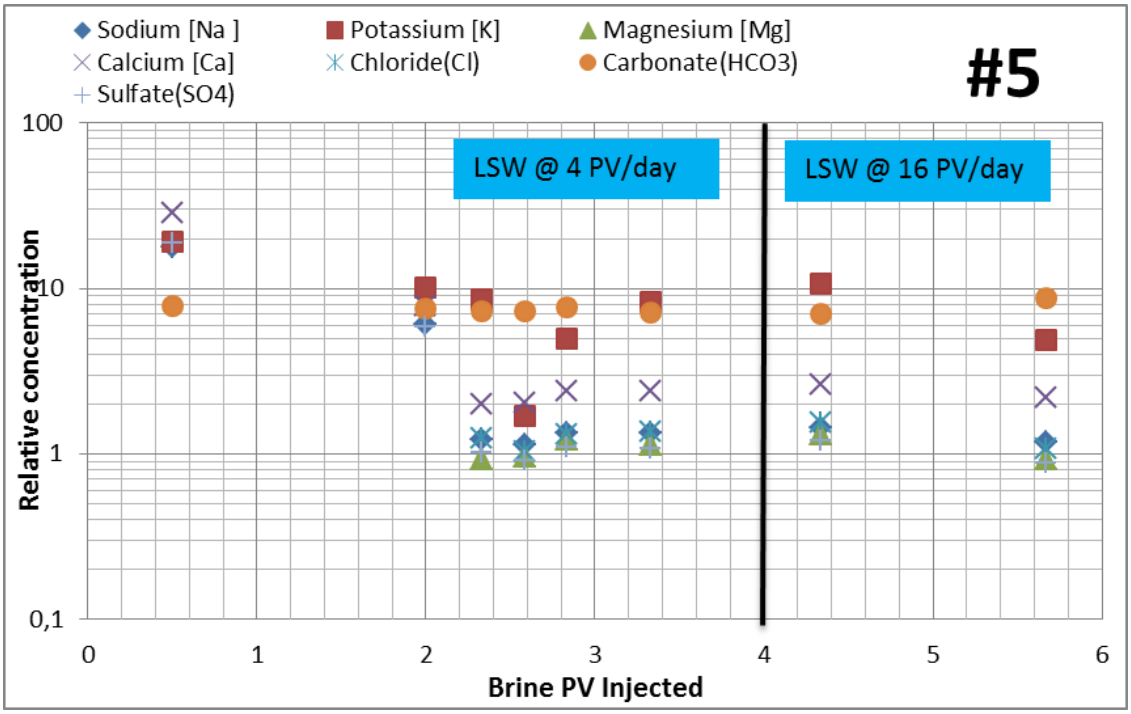

Figure 4.6: Semi-log plot of the cation and anion concentrations in the effluent from LSW flooding. Values are presented as relative concentrations plotted against injected PV. See appendix for data.

4.1.3.2 Pressure drop

Compared to SSW as the initial flooding brine it can be observed from figure 4.7 that the pressure drop measured are much higher for LSW as initial flooding brine. The core properties are basically identical, and it can be concluded that the increase in pressure drop compared to SSW are significant. Injection of high salinity brine leaves the clay and wetting state more or less undisturbed (Lager et.al., 2006), however, as low salinity brine is injected a partial mobilization of mixed wet particles could occur. Tang and Morrow, 1999a, reported a sharp increase in pressure drop across the core as low salinity brine was injected, often accompanied by a small amount of solid particles in the effluent. Clay particles are attracted to the rock surface by a balance between colloidal (van der Waals attractive forces, electrostatic forces), capillary and mechanical forces. Low salinity brine causes the electrical double layer to expand, and possibly stripping some of the clay particles. Migrating fines blocking the smaller pores could explain the increase in pressure drop. The change in wetting patters towards more water-wet and a decrease in trapping of oil in the presence of clay particles are useful to increase the oil recovery. Mineral dissolution, which seems to be the case with LSW, as previously explained, can explain the increase in pressure by the release of fine particles.

Li, 2011, proposed that the increased oil recovery observed with the injection of low salinity brine is associated with a negative pressure gradient higher than that during the high salinity brine injection at the same flow velocity, causing mobilization of discontinuous oil and increased sweep efficiency. Swelling clay aggregates, or migrating clay particles and crystals leads to reduced water permeability due to blockage of porous network. Increased oil recovery from injection of low salinity brine is therefore dependent on flow velocity and flow acceleration. The first experiment with SSW as initial flooding brine proved that an increase in the injection rate did not increase the oil recovery within the error limit, thus the increased negative pressure gradient from low salinity injections will not have any effect either. Rearranging the equation for the generalized Darcy's law for the water phase gives a formula for the water permeability (K_w).

$$V = \frac{q_W}{A} = -\frac{Kk_{rW}}{\mu_W}\frac{\Delta P_W}{\Delta x} = -\frac{K_W}{\mu_W}\frac{\Delta P_W}{\Delta x} \tag{4.1}$$

$$K_w = -q_w \frac{\mu_w L_c}{A\Delta P} \tag{4.2}$$

Water viscosity and water injection flow rate is controlled constant, the increase of negative pressure gradient in water can therefore be resulted by the reduction of water permeability during the injection of low salinity water. Li proposed that there are two factors that control the reduction of water permeability in cores with the same lithology, which is uncoated clay and diluted salinity of the

injected water, both determine the reduction in water permeability by clay plugging. Proposing that the hypothesis that increased oil recovery is due to the release of adhering oil drops on clay fines at the pore walls is contradictory to the fundamental concept that residual oil is trapped due to capillary pressure actions. It can be noted that the simulations performed in the next section also shows a reduction in relative water permeability for low salinity injections compared to high salinity synthetic seawater.

As the injection rate is increased the pressure drop does not increase notable. This might be a result of clay activities and/or redistribution of phases. It is worth mentioning that a reduction in the pressure drop might also indicate a less water-wet situation, and it is interesting that the pH are further increased when the injection rate are increased, which could indicate that the reactions are accelerated due to the increased exposure to injection fluid. However, if the increased pressure is caused by pore plugging and swelling of clay, the increased rate may lead to some release of particles, increasing the permeability.

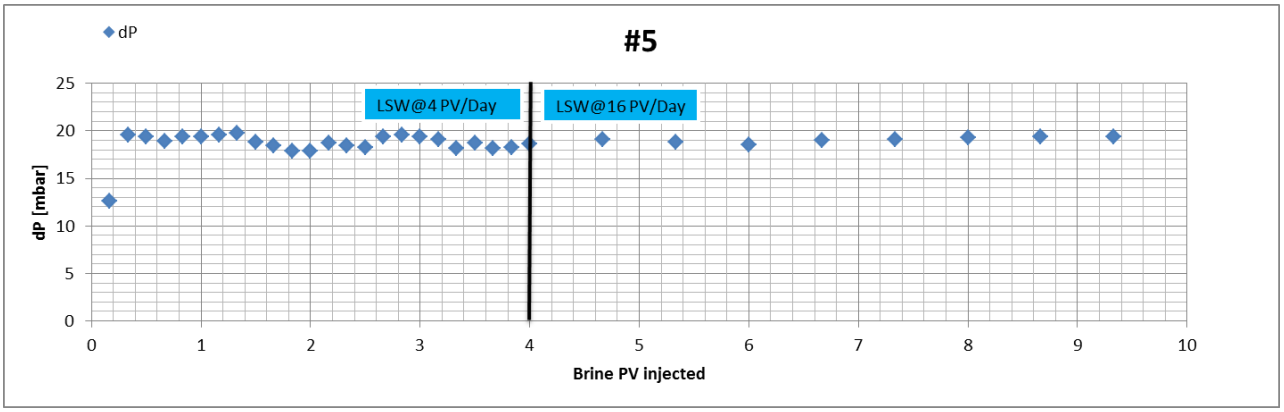

Figure 4.7: Pressure drop in milli-bar for LSW brine injection, plotted against injected pore volume of brine.

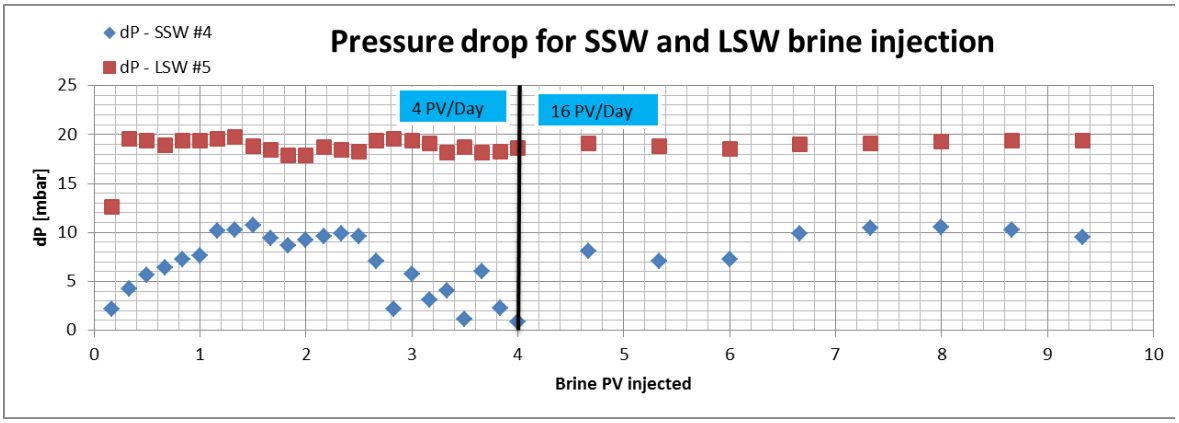

Figure 4.8: Comparison of pressure drop for SSW (blue) and LSW (red) brine injection at low and high rate. Pressure drop in milli-bar, plotted against injected pore volume of brine.

4.1.4 Core #6 – SSW/LSW flooding

Using the same brine compositions and a core with similar properties a more conventional flooding was performed. Flooding with SSW from S_{wi}, and then switching to LSW as a secondary injection. As the injection fluid is changed, a small shut-in period is carried out.

4.1.4.1 Oil recovery and pH effects

From initial water saturation the core was flooded with SSW until no more oil was produced, or for at least 4 PV. The injection fluid was then changed to LSW (25 diluted seawater). Injection rate was constant at 4 PV/day for both fluids, until no more oil was produced from the LSW, the rate was then increased to 16 PV/day to check for any end effects. At the end of the flooding the injection fluid was switched back to SSW again, and at least 2 PV were injected to prepare the core for a new round of oil injection and aging.

Figure 4.9 shows the oil recovery versus injected PV, together with injected and measured pH. As the SSW was injected, there was a piston like displacement of oil, and after breakthrough little oil was produced, similar to the previous floodings. Final recovery was 30%. The pH of the injected SSW was measured to be 7.9 units, pH of the effluent were measured to around 7.6 units during SSW injection. Ion concentration of the effluent was more or less stable during this first stage.

After 4 PV the injection fluid were changed to LSW. The oil production did not increase beyond the error limit of the experimental setup, meaning that no significant oil recovery was observed. The lack of response was surprising as it was believed that the low salinity would have an effect on sandstone containing clay, there are however several authors who also reported mixed results for low salinity field and corefloods (Alotaibi et.al., 2010; Sandengen et.al., 2011; Skrettingland et.al., 2010; Thyne et.al., 2011; Zhang & Morrow, 2006). A response in pH was however observed, which increased by about 0.8 units, as in the previous flooding with LSW as the single flooding brine.

From figure 4.10 it can be observed that the lowered ion concentrations had a response time as the low salinity brine where introduced. What is interesting is that the HCO_3^- seems to respond faster, as the concentration quickly dips with the introduction of low salinity brine. However, the concentration of carbonate remains quite high during the whole flooding period. Similar to the previous experiment, the concentration of Ca^{2+} showed a slight increase (1.27 mM/l), but not as high as the HCO_3^-(0.48 mM/l). As previously stated it can be concluded that the increase in pH is most likely due to brine-rock interactions, which are ion exchange and dissolution of minerals. Magnesium and calcium remains quite constant after the initial dip in concentration, indicating that no multi-component ionic exchange is occurring.

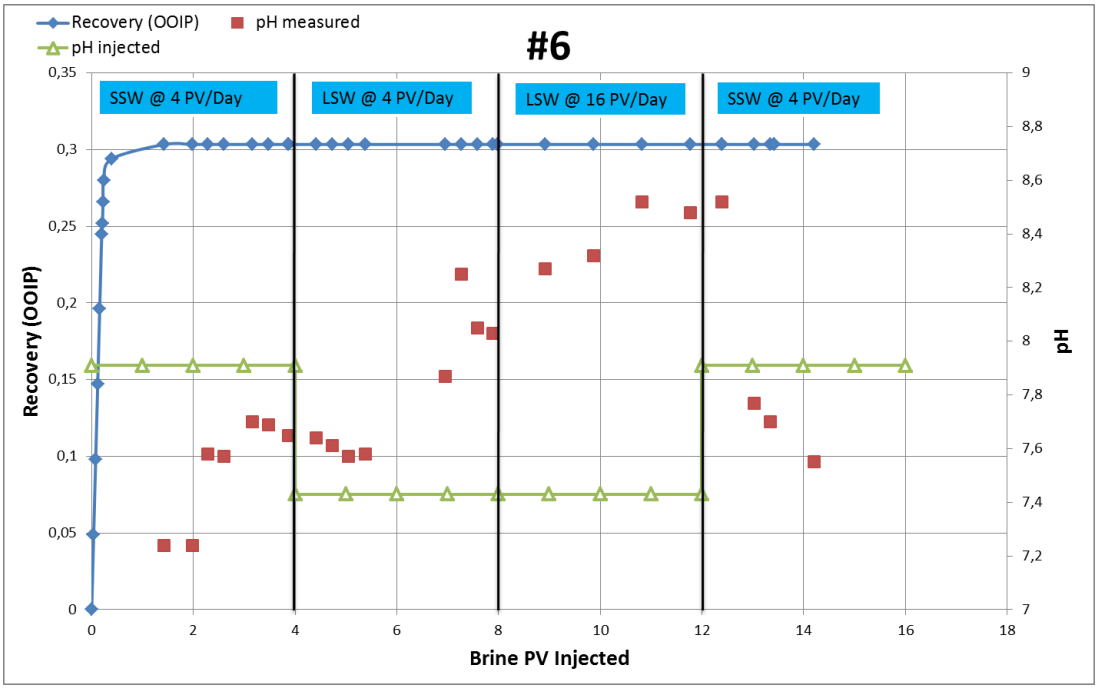

Figure 4.9: Oil recovery and pH plot for SSW injection followed by LSW at different rates (Linear scale). Recovery (to the left) and pH (to the right) vs. pore volumes of brine injected.

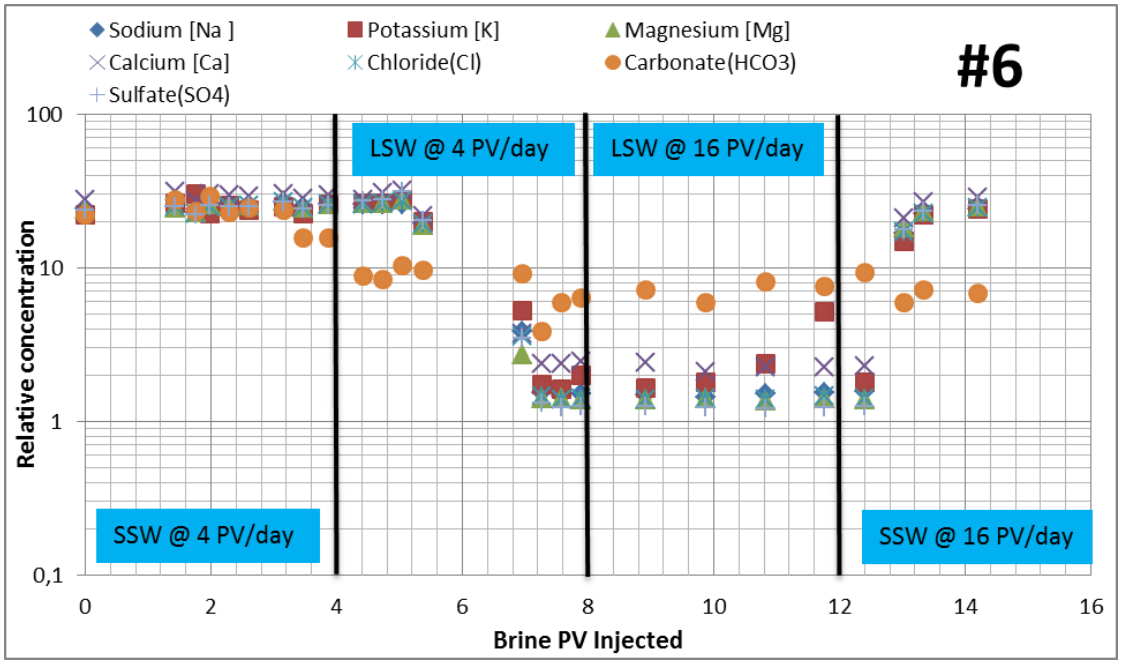

Figure 4.10: Semi-log plot of the cation and anion concentrations in the effluent from SSW and LSW brine flooding. Values are presented as relative concentrations plotted against injected PV. See appendix for data.

Austad et.al., 2010, proposed a chemical mechanism based on desorption by acid/base reaction, this mechanism is also explained in the theory section of this paper. Austad proposed that the most important factors for a successful low salinity flooding in matter of increased oil recovery are the type and amount of clay, composition of initial brine present, initial equilibrium pH and the presence of acidic and basic compounds in the oil, as well as ionic strength and composition of the low salinity brine. Basically, the proposed mechanism suggest that flooding with a brine containing low concentration of surface active inorganic cations, the chemical equilibrium between clay surface, polar oil components and initial brine are disturbed, causing a desorption of cations from the clay surface. Cations in the brine could then compete for the unoccupied negative site on the clay surface, H^+ could adsorb since it has the strongest affinity toward the clay surface. If the H^+ ions are adsorbed, the pH would increase close to the clay surface, and is believed to be the main reason for desorption of organic material from the clay surface.

$$(NHR_3^+ - Clay) + OH^- \leftrightarrows Clay + R_3N + H_2O$$

$$(RCOOH - Clay) + OH^- \leftrightarrows Clay + RCOO^- + H_2O$$

The fact that the injection of low salinity brine did not show any increased recovery, or that the Ca^{2+} did not increase as much as expected might be due that other important parameters for the proposed mechanism are not present in these experiments. The adsorption of polar components onto the clay surface is believed to be dependent of the pH of initial brine / formation water, a pH of 6-7 units are relatively large, and might reduce the clays ability to adsorb organic material. The pH of the SSW used as initial brine in these experiments was measured to be around 7.8 units, which could reduce the low salinity flooding potential that are dependent on the initial wetting state of the core. The small recovery increase after BT might be an indication of the water-wetness of the rock surface. In addition a negative zeta potential material present in the core is essential, and the increased recovery potential of low salinity brine is believed to be dependent on the CEC of the clay present. The CEC will benefit the process in the order of kaolinite<illite<montmorillonite (RezaeiDoust, 2011).

However, another explanation are given by Huertas et.al., 1999. They studied the kinetics of the dissolution of kaolinite by following the evolution of dissolved Si and Al concentrations at various pH. The dissolution rate constant showed inflections at pH ≈ 4 and ≈ 10, above and below these values the dissolution rate displays strong pH dependence. In neutral conditions the rates are much less dependent upon pH. It can be observed that the concentration of potassium (K^+) in the effluent is slightly increased, at an average of 0.94 mMole/l, compared to the injection brine at 0.4 mMole/l. The increased concentration is most likely due to the dissolution of minerals. Solid analysis of the

sandstone used in the experiments shows that Muscovite and Microline are present, both containing potassium. The increase in the dissolution rate can be caused by the increased pH.

The amounts of kaolinite present in the cores used in this study are relatively small, which can explain why there is indications of an increased dissolution rate, but no increase in the recovery. In addition, from the flooding of SSW in Core #4 it was shown that an increase of injection rate did not produce any measurable increase of oil, indicating that the oil is trapped. Due to the high permeability of the core the brine has already created a flow path, which seems to be sufficient to accommodate even the high flow rate. Any potentially released oil may therefore still be trapped, and a higher flow rate may be needed to be able to produce the oil.

After a total of 8 PV was injected the rate was increased to 16 PV/day. No increase in the recovery was observed. The increased rate had an effect on the pH, which increased further by about 0.3 units, a total increase compared to the injection brine of 1.1 unit. This indicates that the reactions occurring in the core are accelerated by the increased rate, there are however no extra oil production as a result. Another interesting observation is the increase in the concentration of potassium, K^+, as the injection rate is increased. Other ions remain unchanged, including carbonate and calcium. The increased concentration of potassium can be explained by clay activities, mainly the dissolution of kaolinite, and it can be observed that the increased concentration are strongly related to the increase in pH, a good indication of the dissolution rate dependence upon pH.

Another explanation is that some of this released clay is trapped in the pores, reducing the permeability. As the injection rate is increased some of this clay may be released, explaining why the concentration of potassium increases, and the pressure drop remains more or less constant.

At the end of the experiment, after a total of 12 injected PV, the brine is changed once more back to SSW. The pH quickly decreased to its previous value at the first stage of the flooding. All ions except carbonate, HCO_3^-, increased to approximately the value of the injected brine.

4.1.4.2 Pressure drop

Unfortunately, because of maintenance and repairs on the electrical system at the university, some data were lost. This includes the pressure data for this and the next flooding. I can only speculate, but after the power outage the pressure gauge and computer were no longer synchronized and the pressure readings were not usable. Due to the fact that this problem occurred only days before Easter, the technicians with knowledge of how to fix the problem were not available. However, some data were simply recorded manually during the flooding. The readings from the display are unfortunately not as precise as when the computer records accurate values.

Similar to the first flooding with SSW the pressure was observed to be increasing during the first hours, until it stabilized at about 10 mbar. After switching to low salinity brine there was a short response time, the pressure drop then increased steadily, and stabilizing at about 20 mbar. It can be concluded that the pressure drop did increase after the low salinity was injected. As discussed in the previous section, the increased pressure might be a result of the expansion of the electrical double layer, and possibly stripping some of the clay particles, and reduction of water permeability.

4.1.4.3 Diffusion

For a non-steady state, where the concentration within the diffusion volume changes with respect to time, Fick's second law may be used, eq. 2.12 section 2.4.5:

$$\frac{\partial c}{\partial t} = D_r \frac{\partial^2 c}{\partial x^2} \tag{2.12}$$

It can be shown that an exact solution to the diffusion equation in Fourier space is

$$\hat{C}_{diffused} = \hat{C}_{sharp} \exp(-\alpha \left|\vec{K}\right|^2) \tag{4.3}$$

From the experiments it can be shown that the diffusion follows the equation given below

$$C_{diff}(x) = C_{start}(0) e^{-\beta x} \tag{4.4}$$

β = constant
x = Pore volumes injected
C_{diff}, C_{start} = diffused concentration and initial concentration, respectively

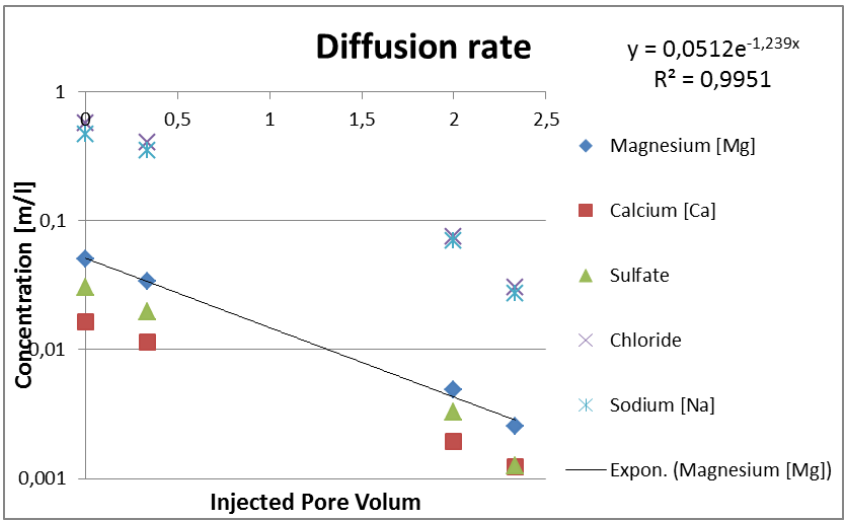

Figure 4.11: Concentration of ions by injected pore volume of LSW (Semi-log scale). Equation given in the chart is for Magnesium.

Figure 4.11 represents the decreasing concentration of some of the ions from the flooding, starting with SSW concentration and the end point as the concentration stabilize. From the figure it can be seen that the mixing zone are approximately 2.3 PV, and the decrease is exponential for all ions tested, except for carbonate. The diffusion equation for each ion is given below.

$$C_{Mg}(x) = 0{,}0512e^{-1{,}239x}, R^2 = 0{,}9951$$

$$C_{Ca}(x) = 0{,}0165e^{-1{,}095x}, R^2 = 0{,}9993$$

$$C_{Cl}(x) = 0{,}5991e^{-1{,}175x}, R^2 = 0{,}978$$

$$C_{Na}(x) = 0{,}499e^{-1{,}133x}, R^2 = 0{,}9708$$

$$C_{SO4}(x) = 0{,}0307e^{-1{,}263x}, R^2 = 0{,}9777$$

$$C_{K}(x) = 0{,}0115e^{-1{,}057x}, R^2 = 0{,}9418$$

The concentration of the measured ions never quite reach LSW levels, this is however expected as the diffusion would slow down significantly at such low concentrations levels. A lot more than 4 PV would need to be injected before the effluent is equal to injected brine.

4.1.5 Core #7 – SSW/SO4 flooding

This core was flooded with SSW from S_{wi}, and then switching to SO4 brine as a secondary injection, see experimental section for complete composition. As the injection fluid is changed, a small shut-in period is carried out.

4.1.5.1 Oil recovery and pH effects

Following a similar procedure, from initial water saturation the core was flooded with SSW until no more oil was produced, or for at least 4 PV. The injection fluid was then changed to SO4 brine, consisting of sodium sulfate (Na_2SO_4) at synthetic seawater concentration (0.024 mole/l). Injection rate was constant at 4 PV/day for both fluids, until no more oil was produced from the SO4 brine, the rate was then increased to 16 PV/day. At the end of the flooding the injection fluid was switched back to SSW again, and at least 2 PV were injected to prepare the core for a new round of oil injection and aging.

Figure 4.12 shows the oil recovery versus injected PV, together with injected and measured pH. The end recovery and curve was similar to the previous SSW floodings, with a linear recovery until breakthrough and little oil production thereafter. Final recovery was about 30%. The pH followed the same trend as the previous flooding, with a small decrease from the injected SSW at about 0.3 pH units. As the SO4 brine was injected the pH started to increase, from a measured pH at about 6.5

units of the injection brine, to a pH of about 9.1 units in the produced effluent at the low injection rate. That is an increase of about 2.6 units, and the increase in pH is larger than for the LSW injection, with an increase of 0.7 units. It is interesting to observe that the monitored pH in the effluent increased exponentially, an increase which can be explained based on the presence of HCO_3^-. In addition, as the injection rate were increased there was an even larger increase of the pH, to a maximum measured pH of about 9.7 units, an increase of 3.2 units.

Huertas et.al., 1999, reported that the dissolution rate of kaolinite displays strong pH dependence, and Al sites form negative surface complexes above pH 9. The effluent showed an average concentration of 3.1 mMole/l for potassium (K^+), which is not in the injected water composition. The ion analysis also indicated the presence of average of 0.5 mMole/l of bicarbonate (HCO_3^-). SO4 injection brine has a higher ionic strength compared to LSW, at 0.072 mole/l and 0.0263 mole/l respectively, indicating that the dissolution of clay and increase in pH have other mechanism in play, not only electrostatic forces.

The relatively low clay fraction in the sandstone cores used is a reasonable explanation to why there was no increased oil production, even though the dissolution was high.

McGuire et.al. (2005) suggested that the increased pH leads to some saponification action, which results in the low salinity action. McGuire also attributed the pH increase to combinations of ion exchange and dissolution that occurs at low salinity conditions, the insitu generated alkaline may then act to improve recovery. The drawback is that not all lab experiments with successful low salinity effect have observed an increase in pH, and in this case there was a large increase in pH, but no increase in recovery. In addition, the presence of a buffer such as CO_2 may prevent any pH increase in field reservoirs.

Figure 4.13 present the results from the ion chromatograph, bear in mind that the results are still presented as a relative to 25 times diluted seawater to be able to better compare the floodings. Complete results in molar concentrations are presented in the appendix. From the analysis it can be observed that the concentrations of magnesium and chloride are quite low, however, for the pure injection brine these are zero. The calcium are approximately the same concentration as LSW (0.52 mM/l), which is a magnitude lower than the values obtained in the previous flooding with LSW, however, when taken into account that the injection brine initially contains no calcium the relative increase are about the same when compared to the injection of LSW. Carbonate remains on the same level, a small increase when compared to the LSW flooding taking into account the initial injection brine concentration. The increase in potassium is substantially larger.

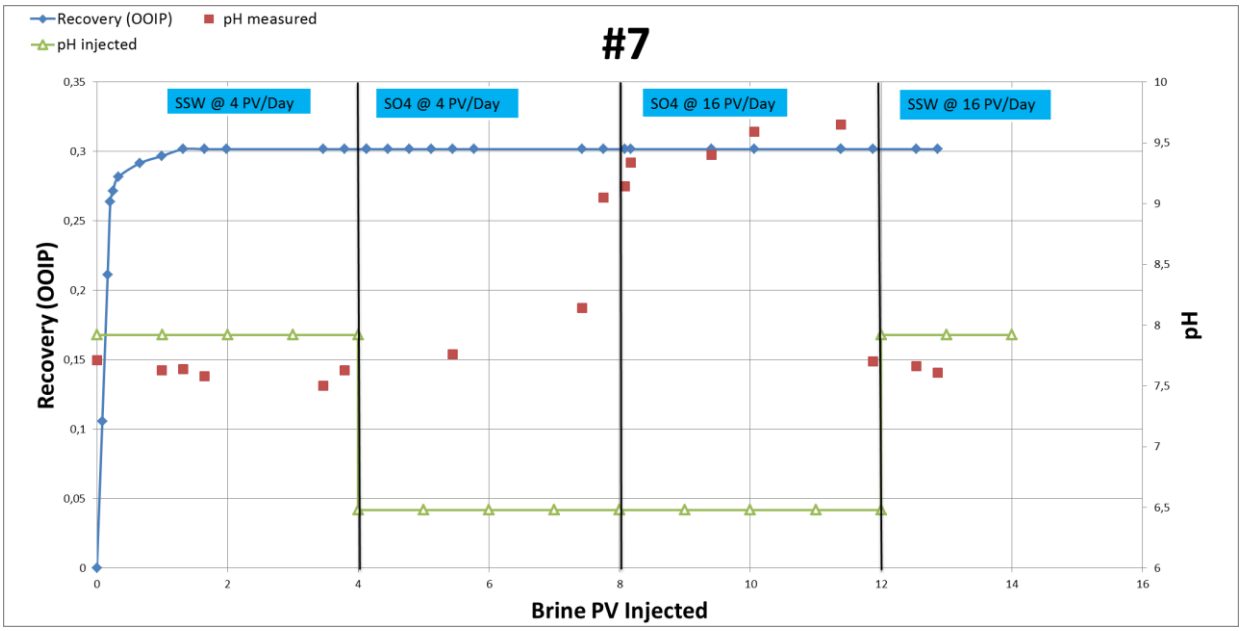

Figure 4.12: Oil recovery and pH plot for SSW injection followed by SO4 brine at different rates (Linear scale). Recovery (to the left) and pH (to the right) vs. pore volumes of brine injected.

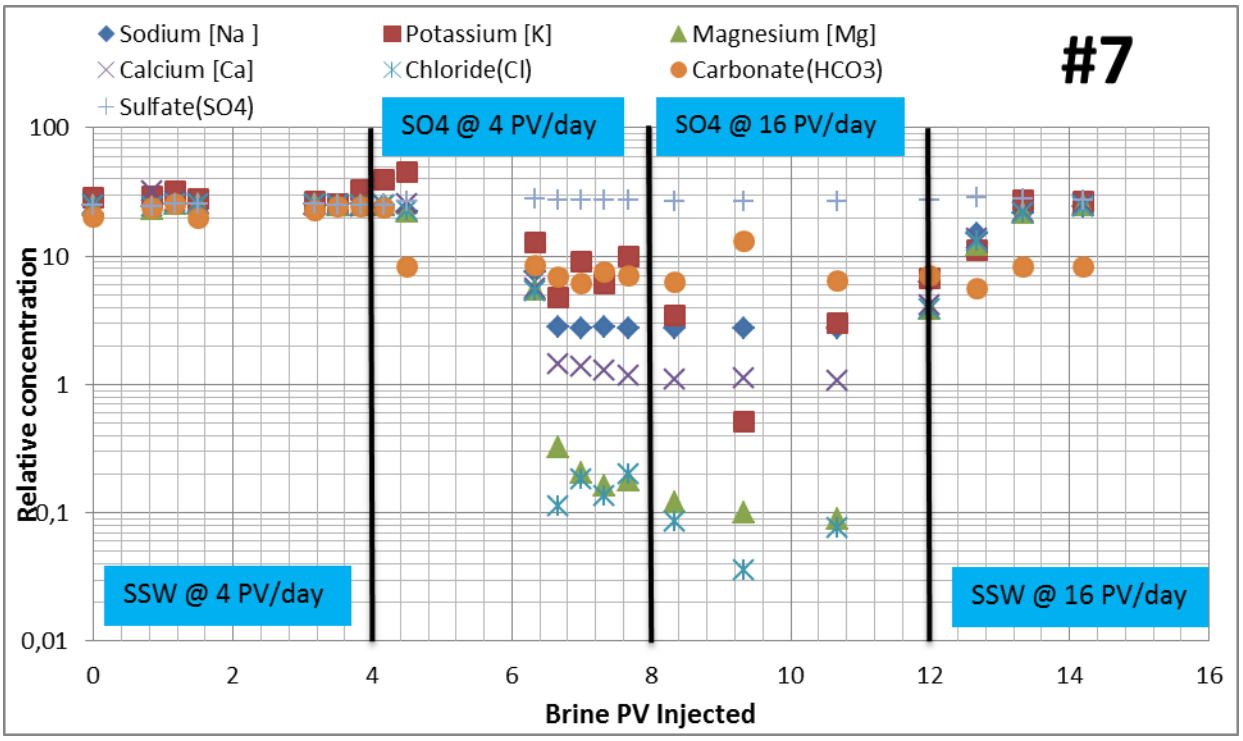

Figure 4.13: Semi-log plot of the cation and anion concentrations in the effluent from SSW and SO4 brine flooding. Values are presented as relative concentrations of LSW, plotted against injected PV. See appendix for data.

4.1.6 Core #8 – SSW/Mg flooding

Following a similar procedure, from initial water saturation the core was flooded with SSW until no more oil was produced, or for at least 4 PV. Secondary injection fluid was then changed to Mg brine, consisting of magnesium chloride ($MgCl_2$) at synthetic seawater concentration (0.045 mole/l). Injection rate was constant at 4 PV/day for both fluids, until no more oil was produced or for at least 4 PV, the rate was then increased to 16 PV/day to check for any end effects. At the end of the flooding the injection fluid was switched back to SSW again, and at least 2 PV were injected to prepare the core for a new round of oil injection and aging. The end recovery and curve was similar to the previous floodings, with a linear recovery until breakthrough and little oil production thereafter, recovery was however a little lower with this core at 27%. A decrease in the pH of about 0.2-0.3 units was measured for the effluent during SSW injection.

As the Mg brine was injected no extra oil recovery was observed. The pH of the effluent increased about 1.25 units compared to the injection brine, a relatively large increase, but due to the fact that the injection brine has a low pH at 6.8 units the effluent only reached a pH of 8 units. Compared to the LSW and SO4 brine injection that reached a pH of 8.5 and 9.65 units, respectively, the pH was relatively low. Ionic strength of the injected low salinity brine was however higher in this case at 0.135 mole/l, which might reduce the brine-rock interactions taking place. At low ionic strength the electrostatic forces between clay particles are usually high, resulting in deflocculating. From figure 4.14 it can be observed that the potassium concentration of the effluent are significantly lower, but carbonate remains on a steady high level at approximately 0.54 mMole/l. Calcium concentrations was on the same level as the SO4 flooding (0.38 mMole/l), which is an indication that the low levels of calcium cannot be explained by reaction with sulfate, since there are very low concentrations of sulfate present in both the injection brine and effluent. It is however important to consider that the core is initially saturated with SSW, and the two brines will not displace each other, but they will diffuse and mix. It can therefore be expected that it takes a considerable long time before the effluent reaches injection brine concentrations. As the injection rate was increased to 16 PV/day, there was no change in pH or concentration of potassium. This could indicate that the reactions occurring by the injection of Mg brine are slow, and not limited by the injection rate.

Low concentration of potassium (0.06 mMole/l) indicates that the brine-rock interactions are small. Injection brine has a higher ionic strength, and the magnesium concentrations are at SSW levels, both of these parameters could limit the reactions occurring. A higher concentration of divalent ions, such as Ca^{2+} and Mg^{2+}, have been reported to reduce the low salinity effect (Jerauld et.al., 2008).

However, the pH was at a level where the dissolution rate of kaolinite is low, hence the low concentration of potassium. Unlike the case of the $NaSO_4$, where the pH seems to be above the inflection point, and the dissolution rate is pH dependent.The pressure is observed to be slowly increasing, which indicate some release of fines.

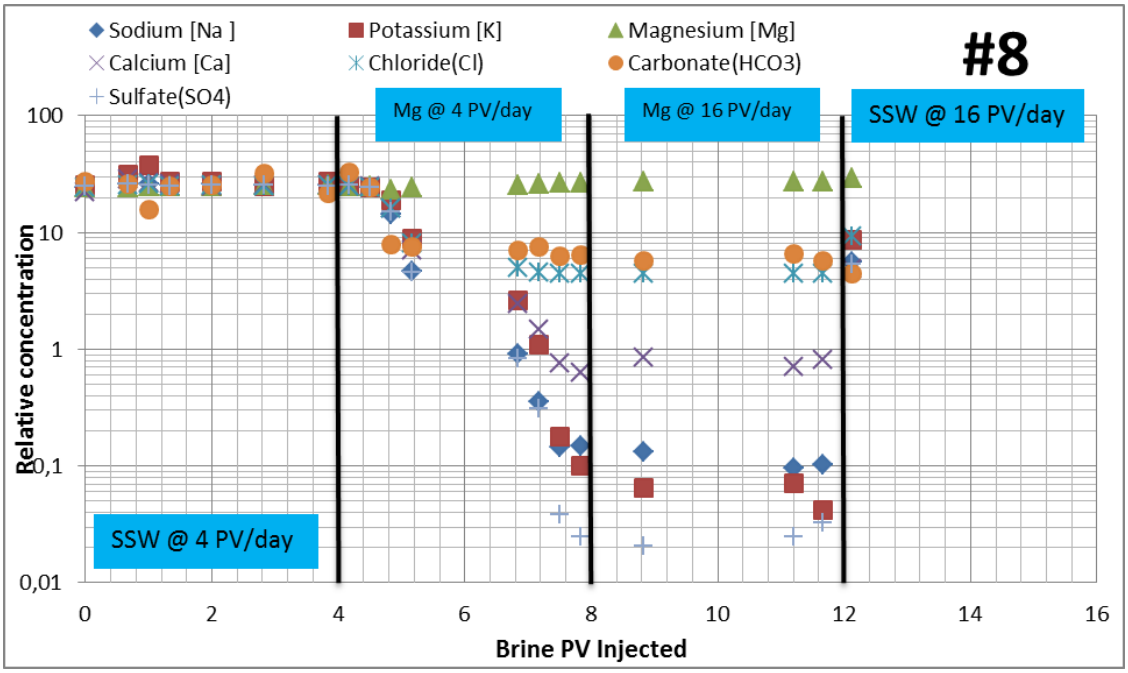

Figure 4.14: Semi-log plot of the cation and anion concentrations in the effluent from SSW and LSW.Mg brine flooding. Values are presented as relative concentrations plotted against injected PV. See appendix for data.

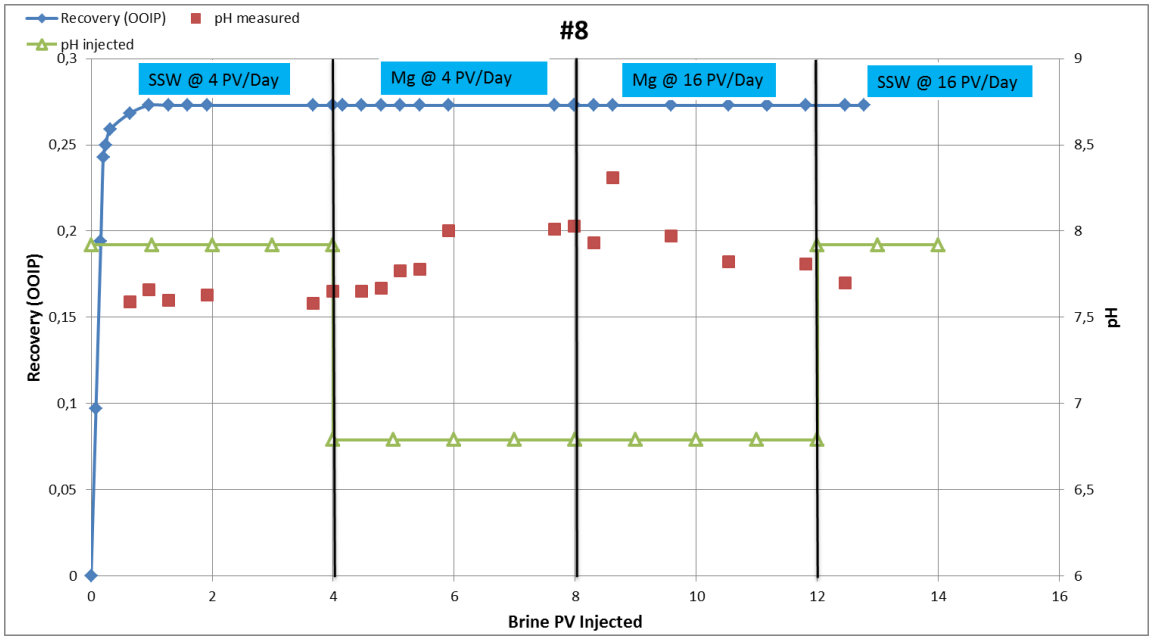

Figure 4.15: Oil recovery and pH plot for SSW injection followed by Mg brine at different rates (Linear scale). Recovery (to the left) and pH (to the right) vs. pore volumes of brine injected.

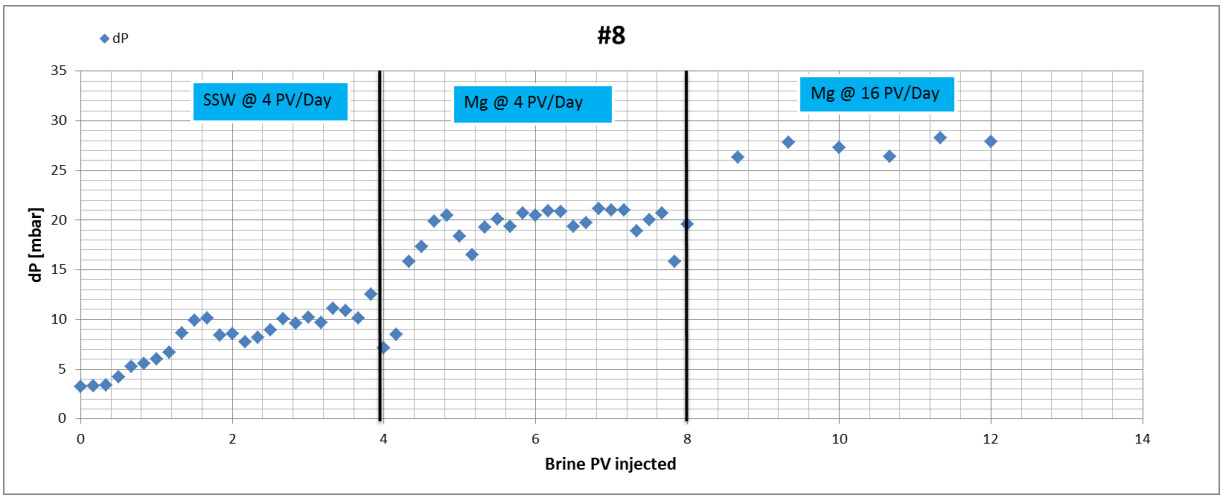

Figure 4.16: Pressure drop in milli-bar for SSW followed by LSW.Mg brine injection, plotted against injected pore volume of brine.

4.1.7 Core #10 – Mg/LSW flooding

From initial water saturation the core was flooded with Mg brine until no more oil was produced or for at least 4 PV at an injection rate of 4 PV/day. Injection brine was then changed to LSW, at an injection rate of 4 PV/day until no more oil was produced or 4 PV was injected, injection rate was then increased to 16 PV/day to check for any possible end effects. The experiment was then ended.

The first part of figure 4.17 show the recovery and pH measured obtained for the injection of Mg brine. A linear recovery until breakthrough is observed, and little oil production thereafter. Final recovery was 24%, a small increase compared to LSW (22%) as initial flooding brine. This is however not above the error introduced by reading of the volumes. Because of the higher ionic strength of Mg brine (0.135 mole/l) compared to LSW brine (0.0263 mole/l), and low pH levels, possibly reducing the level of brine-rock interactions, a performance closer to SSW would not be unreasonable.

Measured pH of the injection brine was about 6.8 units, and the largest increase was measured to 1.1 units. This is a similar result to the previous flooding, were Mg brine was injected as a secondary fluid. As the injection brine is switched to LSW the pH remains on the same level for approximately 4 PV before a decrease is observed, the pH decreases to injection levels at 7.5 units, the remaining oil saturation is unchanged. The slow response in pH may be explained by the presence of HCO_3^-, which has the capacity to act as a buffer.

Figure 4.18 shows the pressure drop during the flooding of different brines. Pressure is increasing during production, before stabilizing at the end. It can be observed that the pressure drop increases with an increasing pH, indicating some brine-rock interaction occurring. The slowly increasing pressure could be explained by fine detachment, which seems to be accelerated by the LSW.

Indicating that the pH is high enough to cause reaction with high surface particles on the clay, however, pH is not sufficiently increased to dissolve the released fines, causing a blocking of the pore.

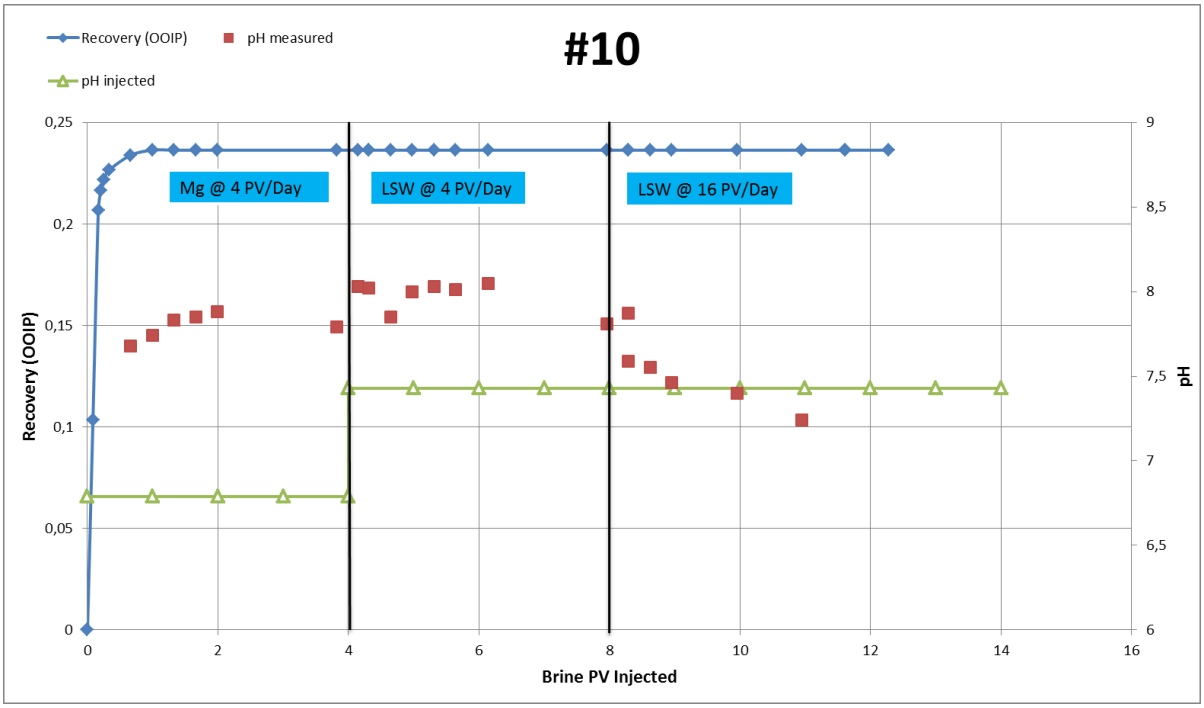

Figure 4.17: Oil recovery and pH plot for Mg injection followed by LSW brine at different rates (Linear scale). Recovery (to the left) and pH (to the right) vs. pore volumes of brine injected.

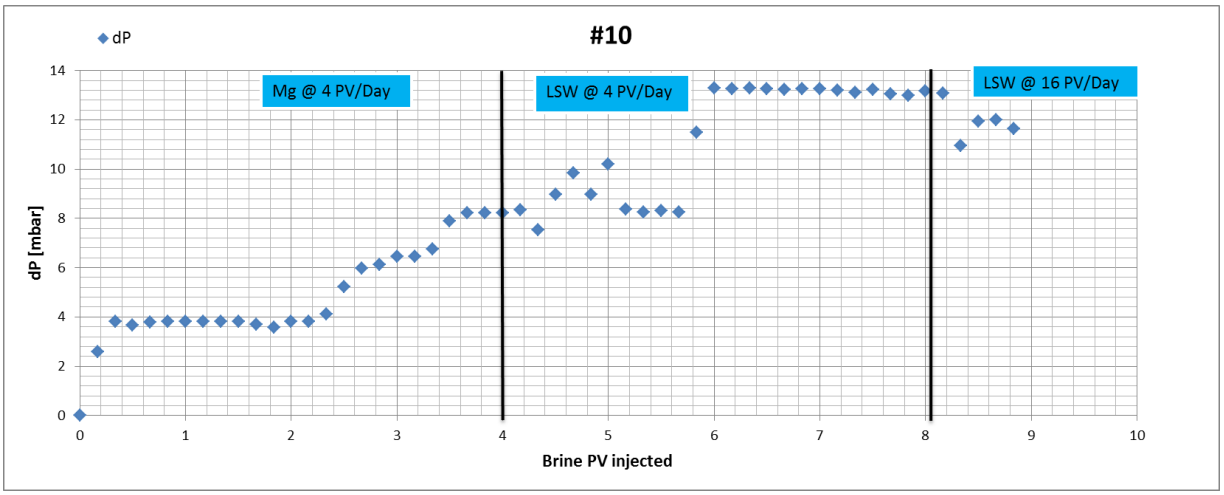

Figure 4.18: Pressure drop in milli-bar for Mg brine followed by LSW brine injection, plotted against injected pore volume of brine.

4.1.8 Core #12 – SO4/LSW flooding

From initial water saturation the core was flooded with SO4 until no more oil was produced or for at least 4 PV at an injection rate of 4 PV/day. The injection brine was then changed to LSW, at an injection rate of 4 PV/day until no more oil was produced or 4 PV was injected, injection rate was then increased to 16 PV/day to check for any possible end effects. The experiment was then ended.

Final recovery was 23%, with most of the oil recovered before water breakthrough. Increase in pH are however larger, with a delta pH of 2.9 units. The pH remains high as the injection brine is switched to LSW, but after approximately 3.5 PV of LSW are injected the pH rapidly decreases to injection levels at 7.5 units. As previously mentioned, the slow response in pH may be explained by the presence of HCO_3^-. Pressure drop can be observed to be increasing and decreasing, likely caused by detachment and migrating fines. Due to the high pH any released fines (kaolinite) will likely dissolve and brake down, and the blocking of a pore may only be temporary. Switching to LSW brine decreases the pH to a level not sufficient to dissolve the particles, and pressure increases to a steady high level.

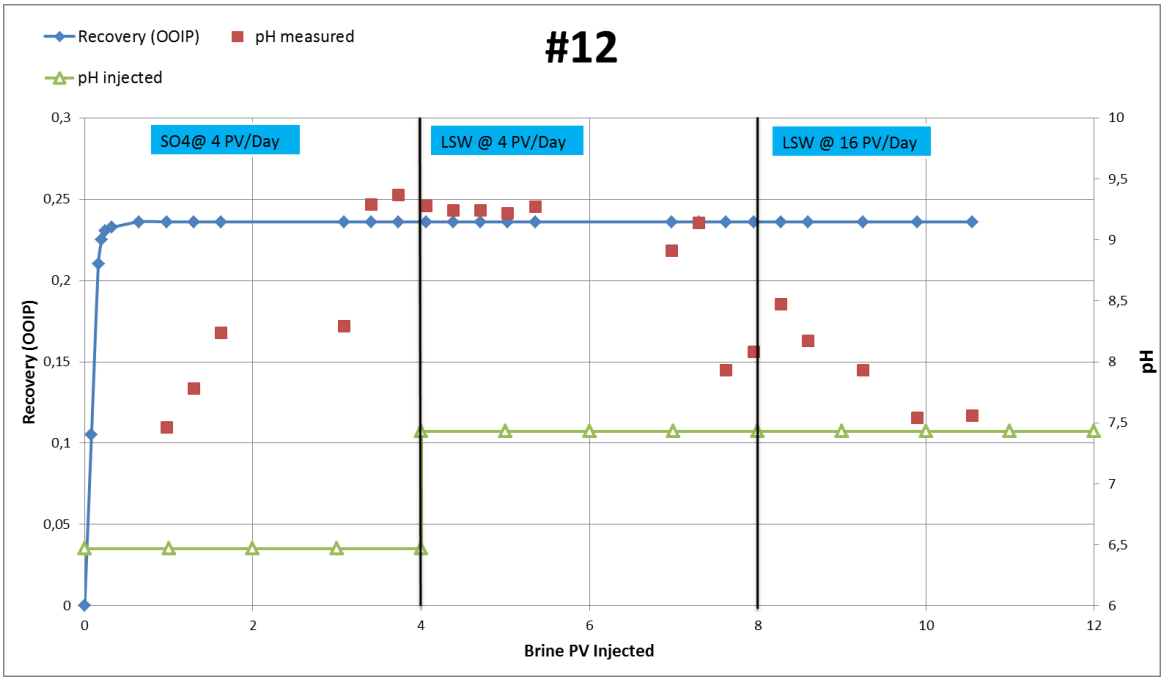

Figure 4.19: Oil recovery and pH plot for SO4 injection followed by LSW brine at different rates (Linear scale). Recovery (to the left) and pH (to the right) vs. pore volumes of brine injected.

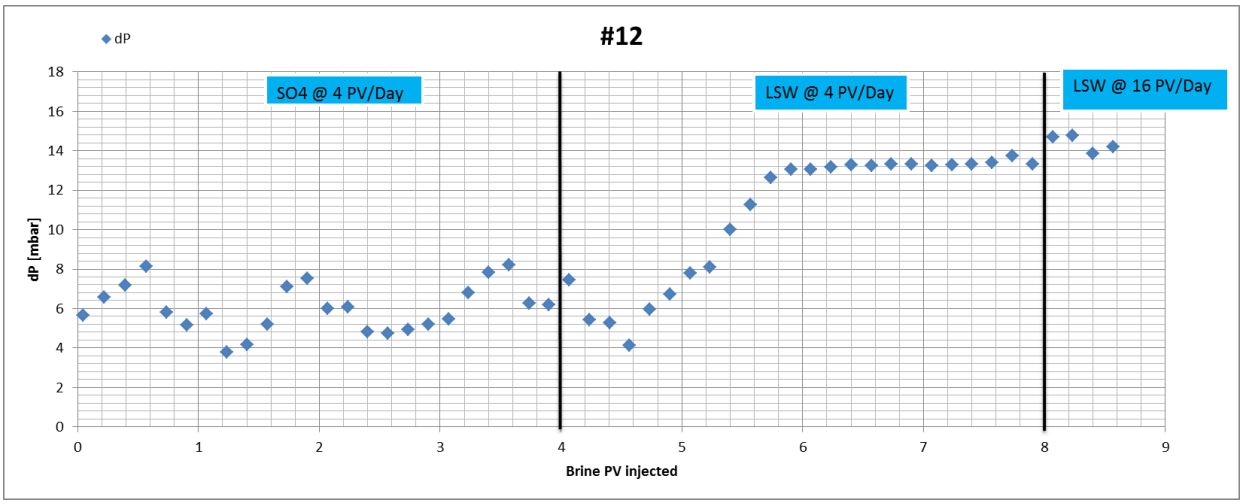

Figure 4.20: Pressure drop in milli-bar for SO4 brine followed by LSW brine injection, plotted against injected pore volume of brine.

4.2 Imbibition

Spontaneous imbibition (SI) with SSW was performed on the flooded cores to check if the different brines had altered the core properties in any way. The objective was to understand the mechanism behind the effects of different brines on oil recovery. After the first set of flooding experiments was conducted, the cores were re-saturated with oil and aged for a minimum of 2 weeks. Spontaneous imbibition was then performed in Amott-cells with SSW at increasing temperatures. The exception is core number 11 and 12, were different brines were used as initial imbibing fluid, and no flooding was performed.

Core #	Flooding brine Sequence	Swi	OOIP [ml]	Boundary Conditions	Temperature [^{o}C]	Initial Imbibing fluid	Second Imb. fluid
#4	SSW	0,23	10,2	Open	23, 50,70	SSW	LSW
#5	LSW	0,26	9,8	Open	23, 50,70	SSW	LSW
#6	SSW-LSW-SSW	0,19	10,7	Open	23, 50,70	SSW	LSW
#7	SSW-SO4-SSW	0,24	9,4	Open	23, 50,70	SSW	SO4
#8	SSW-Mg-SSW	0,21	10,4	Open	23, 50,70	SSW	Mg
#10	Mg – LSW	0,24	9,6	Open	23, 50,70	SSW	Mg
#11	-	0,20	10,6	Open	23, 50,70	Mg	-
#12	SO4 - LSW	0,25	9,7	Open	23, 50,70	SSW	SO4
#13	-	0,24	11,4	Open	23, 50,70	SO4	-

Table 4.2: Core properties and parameters for the spontaneous imbibition performed in this section.

4.2.1 Results

Results for each core are presented in this section, the results is discussed in the next section.

4.2.1.1 Core #4

After establishing initial water saturation and aging for 2 weeks, core number 4 was flooded with SSW. At the end of the flooding experiment oil was injected until S_{wi} was reached, the core was then aged for another 2 weeks. Spontaneous imbibition was then performed with SSW as imbibing fluid. The core was only flooded with initial aging brine, it is assumed that the brine has little effects on the core except displacement of oil, and are therefore used as a baseline to compare the effects of the different low salinity brines.

At room temperature 22.6% of originally oil in place (OOIP) was recovered at about 1 hour, increasing to 23.1% after 48 hours. Main bulk of recovery was relatively fast compared to the flooded cores, and it was observed that the recovery followed to some extent the relationship between imbibition rate and time as presented by Mattax et.al., 1962, see eq. 2.70 at section 2.10.4.

Rate difference could be associated with different wetting states and/or a change in pore structure, in addition to the fact that the core parameter differs slightly for each core. After the imbibition had stabilized and no more recovery was obtained, the temperature was increased to 50 ^{0}C. Recovery was observed to increase to 26.5% after about 9 hours, a relatively small delta increase of 3.9%. A further increase to 30% was obtained when increasing the temperature to 70 ^{0}C, the recovery rate was however small, as the recovery increased by 3.5% over a period of 3 days. After the imbibition had stabilized, the brine was switched to LSW, still at 70 ^{0}C. The LSW brine increased the recovery by 1.5% after a period of 24 hours, most likely caused by an increase in the interfacial tension (IFT).

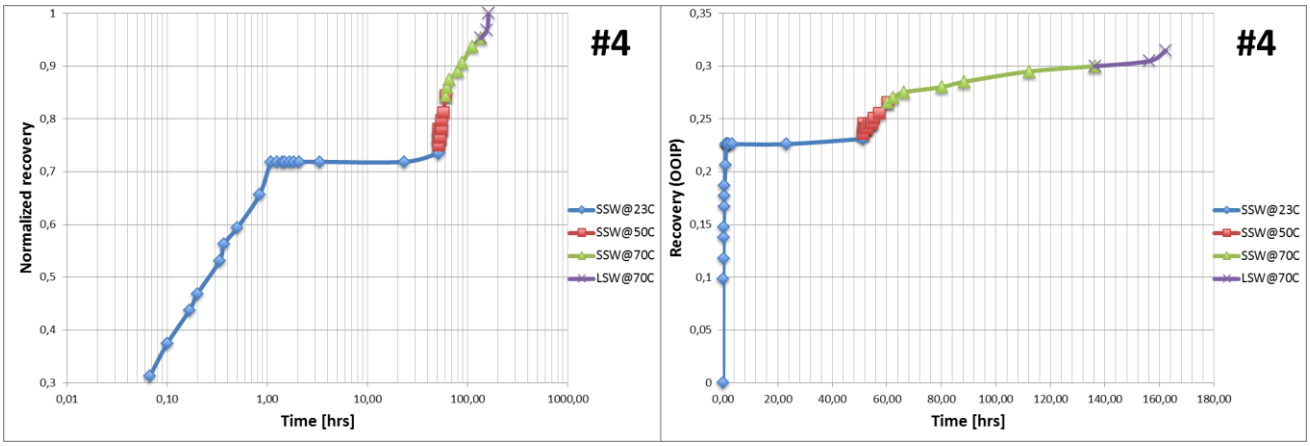

Figure 4.21: SI on core number 4 with SSW as initial imbibition fluid at increasing temperature. To the left: Semi-log plot of normalized recovery vs. time. To the right: Linear scale plot of recovery [fraction] vs. time in hours. Previous flooding sequence: SSW.

4.2.1.2 Core #5

Core number 5 was flooded with LSW before re-injection of oil, aging and then the spontaneous imbibition was performed. At room temperature a recovery of 26.4% was obtained after 1 hour, a small gain compared to core #4 (22.6%), flooded with SSW, initial water saturation was however a little higher in core #5, increasing the recovery. The recovery curve was observed to behave differently, as it continued to increase after the main recovery period, in contrast to SSW flooded core. After 3.5 hours the recovery had slowly increased to 29.5 %, finally stabilizing at 31.5% after 2 days. The increase in recovery by 5.1% after the main recovery period can be considered significant.

At 50 ^{0}C a further increase to 34% was observed after 9 hours. Following the same regime as at room temperature, recovery increased to 34.6% after 24 hours at 50 ^{0}C. Delta increase is at 3.1%, which is not a significant change compared to the SSW flooded core at the same temperature change.

Recovery slowly increased to 38.7% after a long period of 5 days at 70 ^{0}C. Total difference in recovery was about 8.7% between the LSW and SSW flooded core, even though the same imbibing brine was used. After the imbibition had stabilized, the brine was switched to LSW at 70 ^{0}C. The LSW brine increased the recovery by 1.0% after 24 hours, this is however not within the error limit introduced by reading of the values of the amott cell.

The relatively small difference in recovery gain at a temperature increase between the cores might indicate that the main driving mechanism is fluid expansion and a lowered interfacial tension. Increased recovery for this core is mainly due to the differences at room temperature, where the core flooded with LSW had a significant longer recovery period.

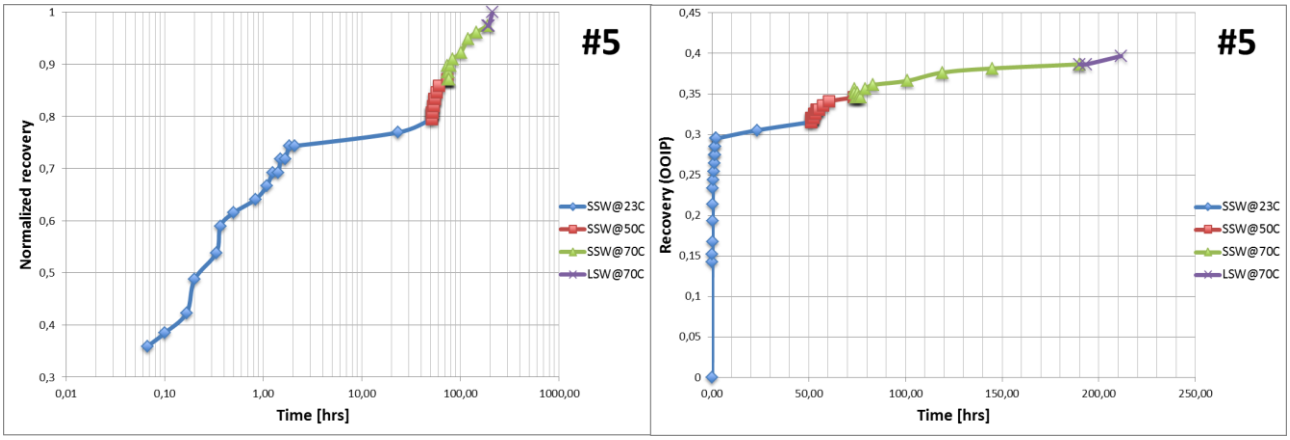

Figure 4.22: SI on core number 5 with SSW as initial imbibition fluid at increasing temperature. To the left: Semi-log plot of normalized recovery vs. time. To the right: Linear scale plot of recovery [fraction] vs. time in hours. Previous flooding sequence: LSW.

4.2.1.3 Core #6

Core number 6 was flooded with both SSW and LSW before re-injection of oil, aging and then the spontaneous imbibition was performed.

At room temperature a recovery of 26.5% was obtained after 1 hour, with a further increase to 29.9% after 4 hours. 24 hours later the recovery had increased to 31.7%, where the imbibition stabilized and no further recovery was observed. At 50 ^{0}C the recovery increased to 35.5% after 3 days. A further increase to 39.1% was achieved at 70 ^{0}C. Switching to LSW brine at 70 ^{0}C increased the recovery by 1.4% within 48 hours.

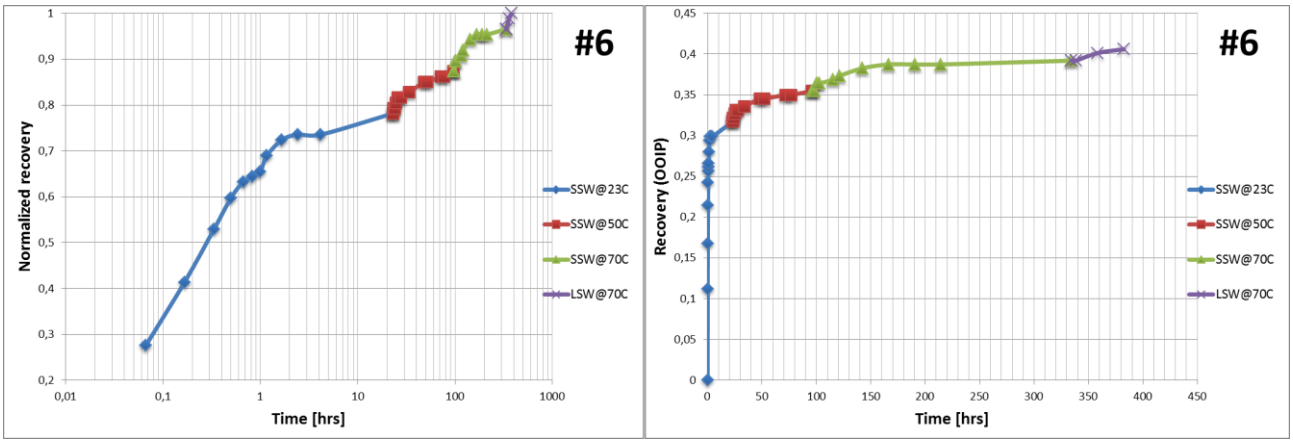

Figure 4.23: SI on core number 6 with SSW as initial imbibition fluid at increasing temperature. To the left: Semi-log plot of normalized recovery vs. time. To the right: Linear scale plot of recovery [fraction] vs. time in hours. Previous flooding sequence: SSW-LSW-SSW.

4.2.1.4 Core #7

Core number 7 was flooded with both SSW and SO4 before re-injection of oil, aging and then the spontaneous imbibition was performed. At room temperature the recovery increased rapidly to 22.4% after about 40 minutes (0.66 hours), no increase in the recovery was observed after the first hour. Recovery increased to 25.6% at 50 ^{0}C after 1 hour, with a small increase to 26.1% after 3 days. Total delta increase was at 3.7%, similar to the previous cores, but the increase occurred within a shorter time frame.At 70 ^{0}C a slow process was observed with an increase to 27.1% after 7 hours, and a total recovery at 29.3% after 6 days, following a similar trend as the SSW flooded core. Switching to SO4 brine at 70 ^{0}C increased the recovery by 0.5% within 24 hours.

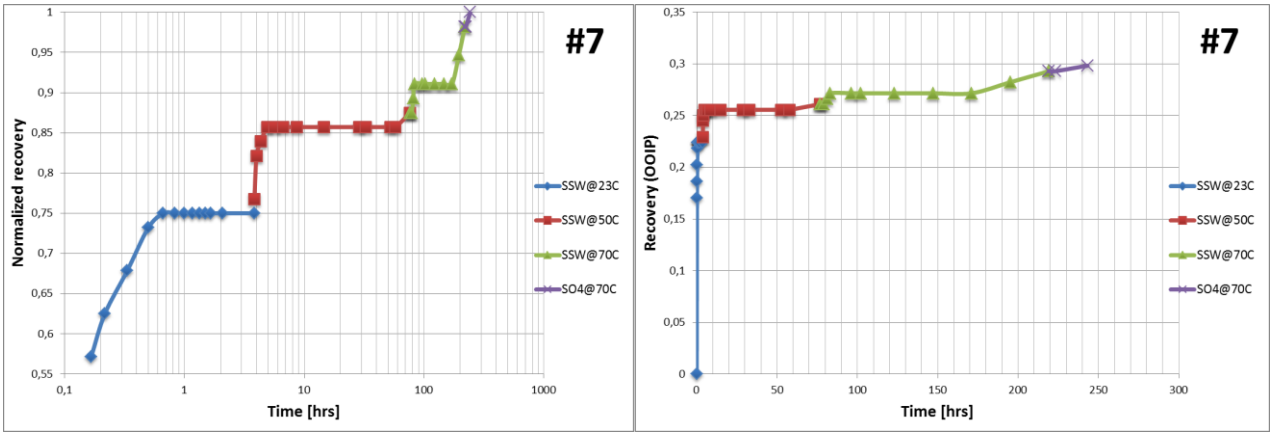

Figure 4.24: SI on core number 7 with SSW as initial imbibition fluid at increasing temperature. To the left: Semi-log plot of normalized recovery vs. time. To the right: Linear scale plot of recovery [fraction] vs. time in hours. . Previous flooding sequence: SSW-SO4-SSW.

4.2.1.4 Core #8

Core number 8 was flooded with both SSW and Mg brine before re-injection of oil, aging and then the spontaneous imbibition was performed. The SI and recovery curve was observed to differ from other cores with different flooding brine. Recovery and the imbibition process was slow, at room temperature a total of 18.3% was recovered, with the main recovery stage lasting for 3.5 hours with a recovery of 16.8%. Even though the imbibition of SSW lasted for a longer period of time, as with the LSW flooded core #5 and #6, the displacement and recovery rate was significantly lower.

A similar result was obtained at 50 ^{0}C, with a slow and steady increase to 22.1% recovery within 2 days. The recovery rate at this temperature had a much longer tail when comparing the cores, indicating that the process was more time consuming. A similar curve was observed when increase the temperature to 70 ^{0}C, with an increased recovery to 25.9% within a period of 7 days. Switching to Mg brine at 70 ^{0}C increased the recovery by 1.0% within 24 hours.

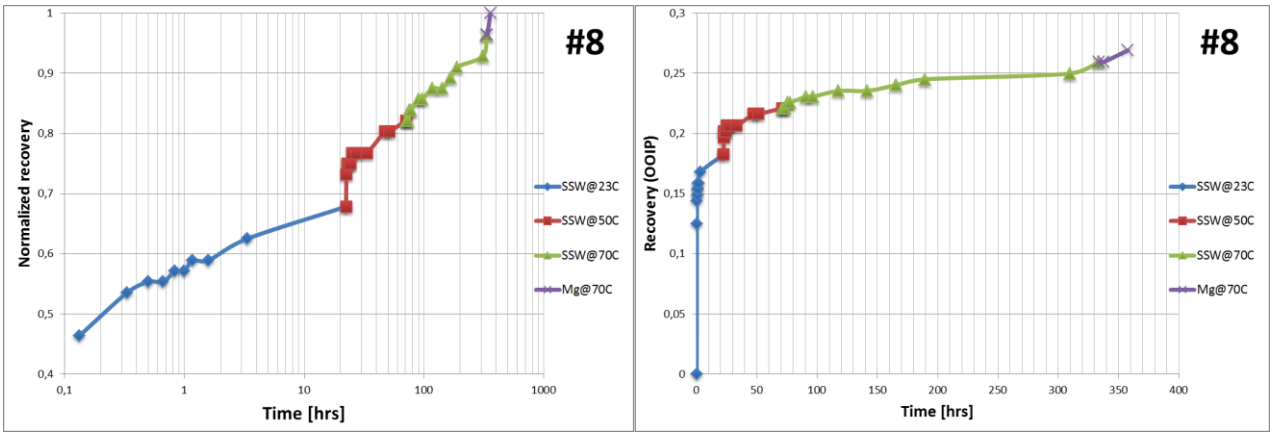

Figure 4.25: SI on core number 8 with SSW as initial imbibition fluid at increasing temperature. To the left: Semi-log plot of normalized recovery vs. time. To the right: Linear scale plot of recovery [fraction] vs. time in hours. . Previous flooding sequence: SSW-Mg-SSW.

4.2.1.5 Core #10

Core number 10 was flooded with Mg brine followed by LSW. Initial imbibing fluid was SSW at increasing temperatures. It seems that the imbibition follows a similar pattern as Mg flooded core (#8), with an even lower recovery (15.6%) at room temperature. However, final recovery at 70 ^{0}C was 24.9%, only 1% lower than #8, as the recovery increased in larger steps at increased temperatures, especially at 70 ^{0}C. Switching to Mg brine at 70 ^{0}C increased the recovery by 1.6% within 48 hours.

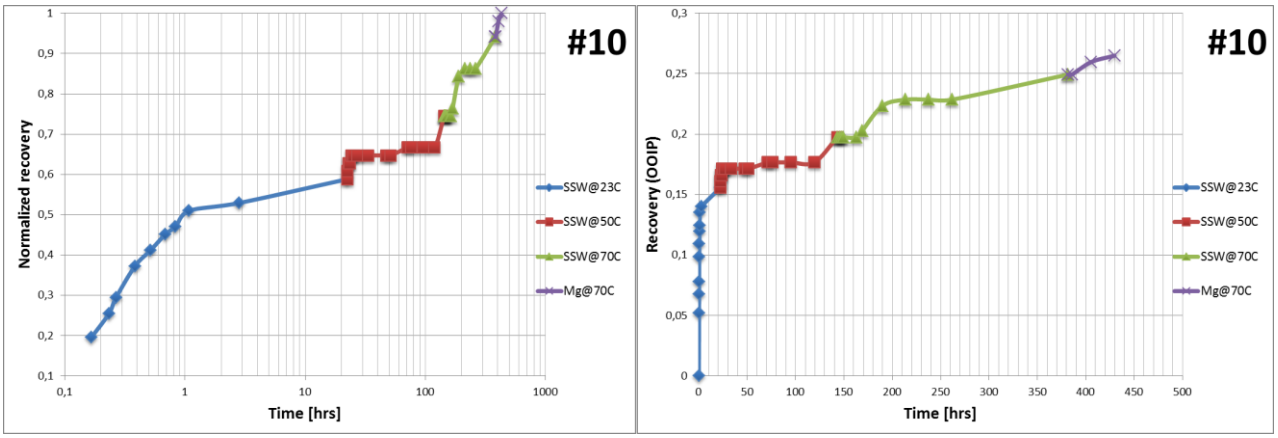

Figure 4.26: SI on core number 10 with SSW as initial imbibition fluid at increasing temperature. To the left: Semi-log plot of normalized recovery vs. time. To the right: Linear scale plot of recovery [fraction] vs. time in hours. . Previous flooding sequence: Mg-LSW.

4.2.1.6 Core #11

Core number 11 was not flooded with any brine, a fresh core was saturated with SSW and oil, then aged for 2 weeks. The initial imbibition brine was Mg at increasing temperatures. The recovery at room temperature can be characterized as slow and steady, only reaching 17.9% after 24 hours. Final recovery was 28.3%, and it does seem like the magnesium ion become more active at increased temperatures, especially at 50 ^{0}C.

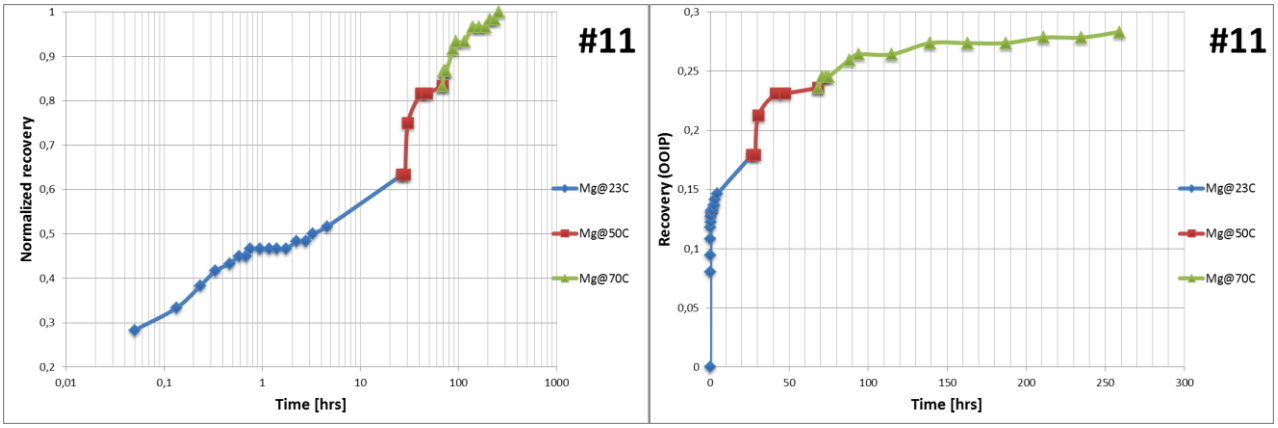

Figure 4.27: SI on core number 11 with Mg as initial imbibition fluid at increasing temperature. To the left: Semi-log plot of normalized recovery vs. time. To the right: Linear scale plot of recovery [fraction] vs. time in hours. No flooding was performed on this core.

4.2.1.7 Core #12

Core number 10 was flooded SO4 brine followed by LSW. Initial imbibing fluid was SSW at increasing temperatures. At room temperature the recovery increased rapidly to 19.8% after about 30 minutes (0.5 hours), after 24 hours the recovery had increased to 22.3%. At 50 ^{0}C the recovery only increased by 0.5% within a few hours, the imbibition then stopped and was stable for several days. The reason

for the small increase is not known, and might be an experimental error. However, as the temperature was increased to 70 ^{0}C there was a large and steady increase in recovery to 29.5%. Switching to SO4 brine at 70 ^{0}C increased the recovery by 1.0% within 24 hours.

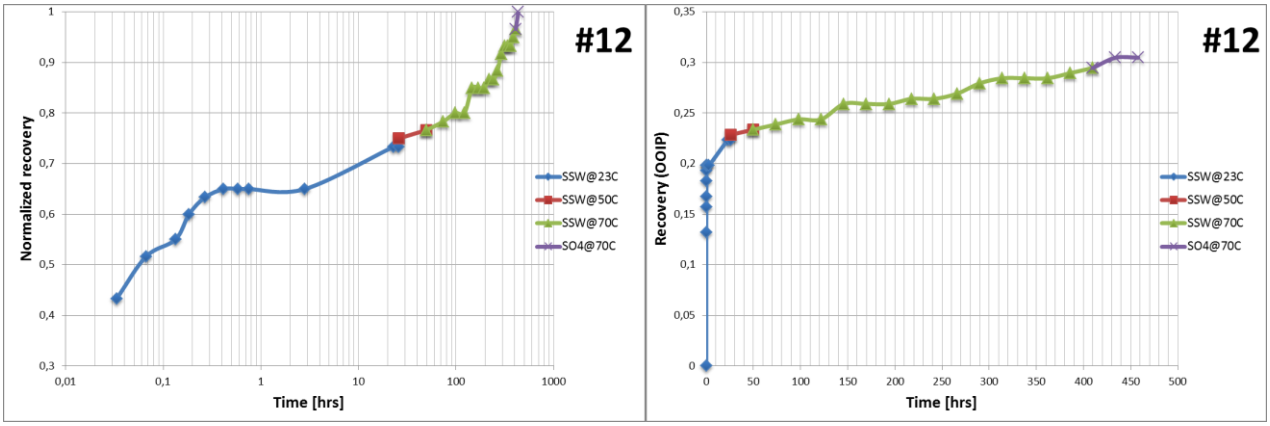

Figure 4.28: SI on core number 12 with SSW as initial imbibition fluid at increasing temperature. To the left: Semi-log plot of normalized recovery vs. time. To the right: Linear scale plot of recovery [fraction] vs. time in hours. Previous flooding sequence: SO4-LSW.

4.2.1.8 Core #13

Core number 13 was not flooded with any brine, a fresh core was saturated with SSW and oil, then aged for 2 weeks. The initial imbibition brine was SO4 at increasing temperatures. Recovery at room temperature reached 23.2% after 1 hour, with a slow increase to 24.1% after 24 hours. At 50 ^{0}C and 70 ^{0}C, the recovery reached 25.4% and 30.2%, respectively.

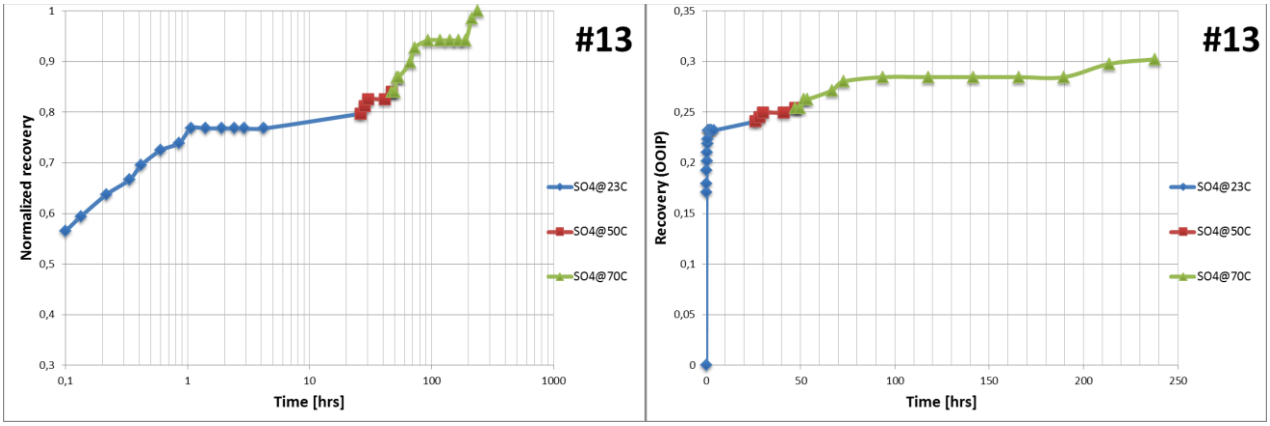

Figure 4.29: SI on core number 13 with SO4 as initial imbibition fluid at increasing temperature. To the left: Semi-log plot of normalized recovery vs. time. To the right: Linear scale plot of recovery [fraction] vs. time in hours. No flooding was performed on this core.

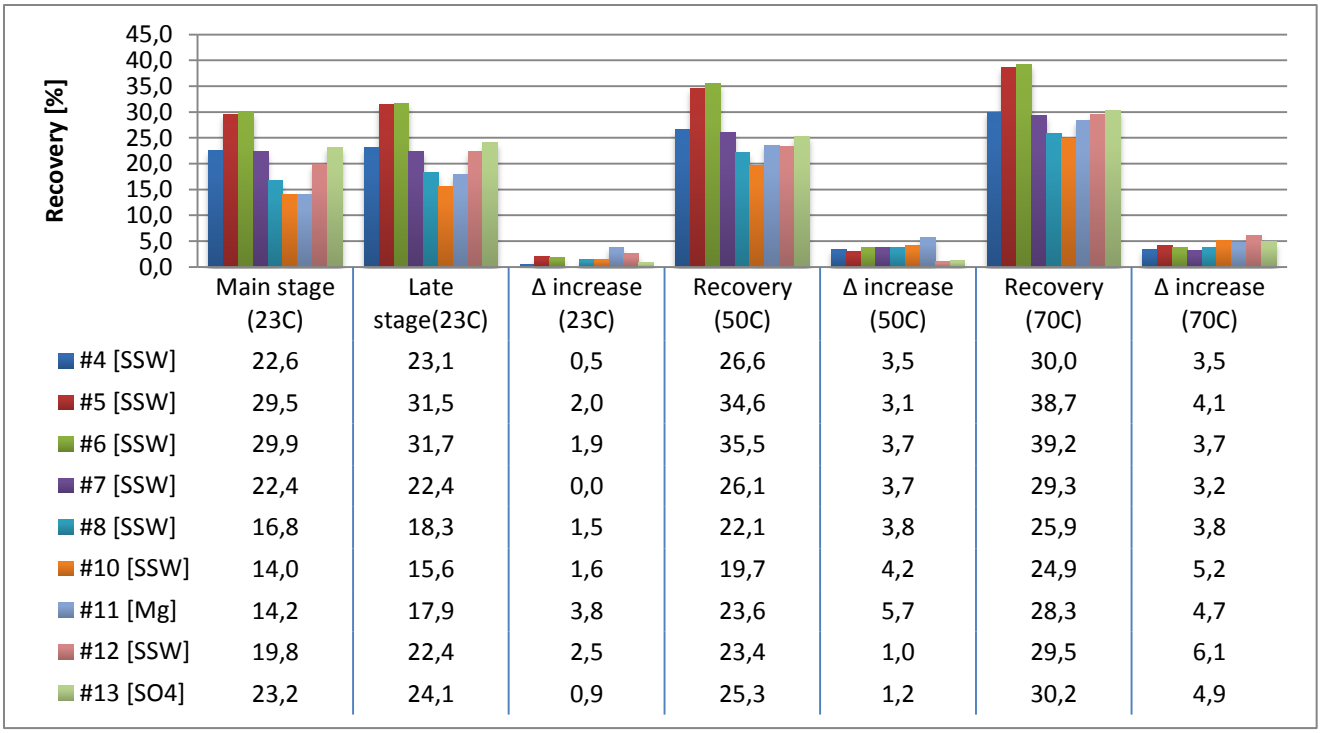

	Main stage (23C)	Late stage(23C)	Δ increase (23C)	Recovery (50C)	Δ increase (50C)	Recovery (70C)	Δ increase (70C)
#4 [SSW]	22,6	23,1	0,5	26,6	3,5	30,0	3,5
#5 [SSW]	29,5	31,5	2,0	34,6	3,1	38,7	4,1
#6 [SSW]	29,9	31,7	1,9	35,5	3,7	39,2	3,7
#7 [SSW]	22,4	22,4	0,0	26,1	3,7	29,3	3,2
#8 [SSW]	16,8	18,3	1,5	22,1	3,8	25,9	3,8
#10 [SSW]	14,0	15,6	1,6	19,7	4,2	24,9	5,2
#11 [Mg]	14,2	17,9	3,8	23,6	5,7	28,3	4,7
#12 [SSW]	19,8	22,4	2,5	23,4	1,0	29,5	6,1
#13 [SO4]	23,2	24,1	0,9	25,3	1,2	30,2	4,9

Table 4.3: Summary of recovery at different temperatures, including delta increase at an increase in temperature. Note: At room temperature, main stage is characterized as the first few hours, late stage is a potential increase in imbibition after this time. Δ increase is the gain between late stage and main stage at room temperature.

pH		
Core	**Initial imbibing fluid**	**Second imbibing fluid**
#4	-	8,20 [LSW]
#5	-	8,14 [SO4]
#6	7,16 [SSW]	7,54 [LSW]
#7	7,52 [SSW]	7,73 [SO4]
#8	7,31[SSW]	7,11 [Mg]
#10	7,3 [SSW]	7,39 [Mg]
#11	6,66 [Mg]	-
#12	7,14 [SSW]	8,06 [SO4]
#13	6,72 [SO4]	-

Table 4.4: Measured pH of the imbibition brine when the experiment was ended.

4.2.2 Effect of flooding brine on spontaneous imbibition

There is a significant difference in spontaneous imbibition for the cores flooded with various brines, even though the same imbibition liquid (SSW) was used. The core flooded with LSW displayed an increase in total recovery (8.7%) when compared to the baseline core (#4) with SSW, both imbibition rate and time is observed to increase, with the highest difference observed at room temperature. The core flooded with Mg brine displayed a small recovery (18.3%) at room temperature, and the imbibition rate was slow. A similar result was observed for the experiment using a non-flooded core with Mg as initial imbibition brine, with a relatively small and slow recovery (17.9%) at room temperature.

These results indicate that the magnesium are slowly reacting with the rock, in addition the increase in recovery at increased temperatures are slightly higher, indicating that it becomes more active at higher temperatures, mainly at 50 ^{0}C. A temperature increase results in a decrease in interfacial tension between oil/brine solution as well as oil viscosity. Capillary imbibition rate are significantly increased by the reduced oil viscosity, interfacial tension affect the capillary imbibition rate in a less degree (Babadagli, 1996).

Flooding with Mg brine somehow reduce the recovery and imbibition rate compared to core #4 flooded with SSW. In contrast to the LSW flooding, the pH did not increase significantly when flooding with Mg brine. Low concentrations of potassium in the effluent and small increase in pH indicate that the brine-rock interactions and dissolution of kaolinite are small, leaving the minerals more or less undisturbed.

The wetting process of sandstone is reported to be dependent on ion binding, and the process is highly temperature dependent (Buckley et. Al., 1998). The mechanism behind ion binding is when cations behave as bridges between the adsorption of negatively charged oil components to the negatively charged sites on the rock surface, like carboxylate and clay surface. The mechanism for ion binding provides the opportunity for negatively charged carboxylates to alter the wetting conditions to less water-wet for the negatively charged clay surface, and it is probably the dominant wetting mechanism in wetting alteration in sandstone reservoirs by acidic oil (Buckley, 1996). A higher concentration of divalent ions, such as Ca^{2+} and Mg^{2+}, have been reported to reduce the low salinity effect (Jerauld et.al., 2008). Aruoture, 2013, based on simulations, showed that the concentration of divalent cations on clay surfaces was higher during injection of the low salinity brine than during injection of the high salinity brine. Explaining why low salinity brine containing relatively high concentrations of divalent cations can also change the wetting state towards a less water-wet state.

The wettability alteration could be explained by molecular diffusion into the initial saturating brine by various ions (sulfate, calcium, magnesium). If the surrounding fluid is different from the one inside the core, molecular diffusion will cause ionic concentrations fronts that move through the open faces of the core. A non-equilibrium state are created in the pore space that may cause chemical reactions in the aqueous phase, water-rock interaction on terms of dissolution/precipitation of minerals, as well as changes in the surface energy / surface charge. These reactions may lead to changes in the wetting state of the porous media, as the water-rock chemistry can have a strong influence on the wetting state.

For the LSW flooded cores imbibition rate are observed to increase, and capillary pressure falls to zero and imbibition stops at an increased water saturation. This could be explained by an alteration in wettability towards more water wet. Both the flooding and resulting simulations performed indicate that the core becomes more water wet as LSW brine is injected, which is partially confirmed by the imbibition results obtained. Some clay dissolution was observed during flooding, less clay is therefore available during the aging process. Released fines, as observed in the flooding, could reduce the permeability, improving the sweep efficiency. Pore throats may also be affected, which may have an effect on the capillary pressure.

No significant changes were observed by flooding a core with SO4 brine. Indicating that SO_4^{2-} initially adsorbed on the pore surface is displaced by the SSW, returning the equilibrium at pore surface.

4.2.3 Characterization of wettability at room temperature

At the end of the aging process, the rock will behave as mixed-wet, as both water-wet and oil-wet pores exist in the core, strongly related to the distribution of connate water within a core (Salathiel, 1973). A wettability alteration toward increased water-wetness is the most frequently suggested cause of increased recovery from LSW, as more oil is released from the rock surface during the alteration. The evidence is however often indirect. Spontaneous imbibition, or more precisely the rate of spontaneous imbibition can be used as a more direct way of comparing the wettability. The results can be scaled to include core and fluid properties.

Babadagli, 1996, used the imbibition recovery curve to quantify wettability characteristics. Equation 2.70 for capillary imbibition recovery was derived in section 2.10.4.

$$(2.70) \quad R_{im}(t) = \frac{1}{V_P(1-S_{wi})}\int_0^t q(t)dt = \frac{2C}{V_p S_{oi}}\sqrt{t}$$

If all other parameters are constant, the slope C, is only a function of wettability. Babadagli, 1996, introduced a wettability index, $f(\theta)$, ranging from 0 to 1, where the highest slope is equal to 1,

representing strongly water wet conditions. The wettability index as introduced does not contain all the parameters affecting imbibition, therefore Shahri et.al., 2012, derived a new index called the Normalization Index, eq. 2.71. Even though the wettability index introduced by Babadagli (1996) would be sufficient in this case, the Normalization Index would make it possible to compare the spontaneous imbibition performed in this study to a wider range of other work.

$$(2.71) \quad R_{im}(t) = \frac{C^* \frac{K}{\phi}}{V_P(1-S_{wi})\sqrt{\mu_o \mu_w} L_C^2} \left[\frac{\sigma}{\sqrt{\frac{K}{\phi}}} + \frac{\Delta \rho g L_C^2}{L_H} \right] \sqrt{t}$$

Imbibition time for water-wet rock is lower than oil-wet rock, however, fluid and rock properties affect the imbibition rate and slope as well. For example both the permeability, interfacial tension, oil and water viscosities affect the slope of the curve. From figure 4.31 it can be observed that there are some deviation between the measurements and the theoretical straight line. There are some experimental errors introduced by both the reading of oil volume, and there will be some accumulation of oil at the surface of the core as the brine imbibes. In addition it is assumed that the core properties are the same as before the flooding, which need not to be the case.However, eq. 2.70 and eq.2.71 are based on the important assumption that capillarity is the main force for imbibition, a deviation would indicate that imbibition is dominated or affected by forces other than capillarity. This is discussed at the end of this section. Nevertheless, a best fit can be used to compare cores.

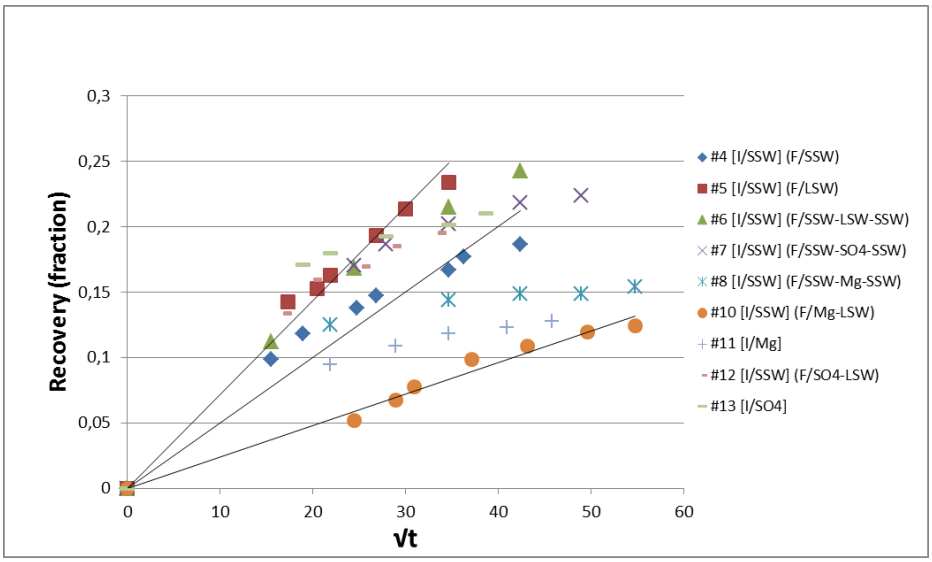

Figure 4.30: Straight line portion according to Babadagli, 1996. Recovery fraction plotted vs. square root of time [Seconds] for spontaneous imbibition at room temperature. Note: In the legend the core number is listed first, and then I for imbibition brine, and last F, for flooding sequence performed on the core.

Core nr.	Slope	C	C*	f(θ)	NI
#4	0,0049	2,49E-08	1,69E-07	0,859	0,900
#5	0,0059	2,9E-08	1,87E-07	1,0	0,991
#6	0,0053	2,84E-08	1,88E-07	0,979	1,0
#7	0,0046	2,16E-08	1,5E-07	0,746	0,797
#8	0,0027	1,4E-08	8,8E-08	0,484	0,468
#10	0,0026	1,25E-08	7,16E-08	0,432	0,381
#11	0,0029	1,54E-08	5,85E-08	0,530	0,311
#12	0,0053	2,57E-08	1,64E-07	0,888	0,872
#13	0,005	2,85E-08	1,28E-07	0,984	0,681

Table 4.5: Wettability index according to Babadagli, 1996, and the Normalization Index (Shahri et.al., 2012).

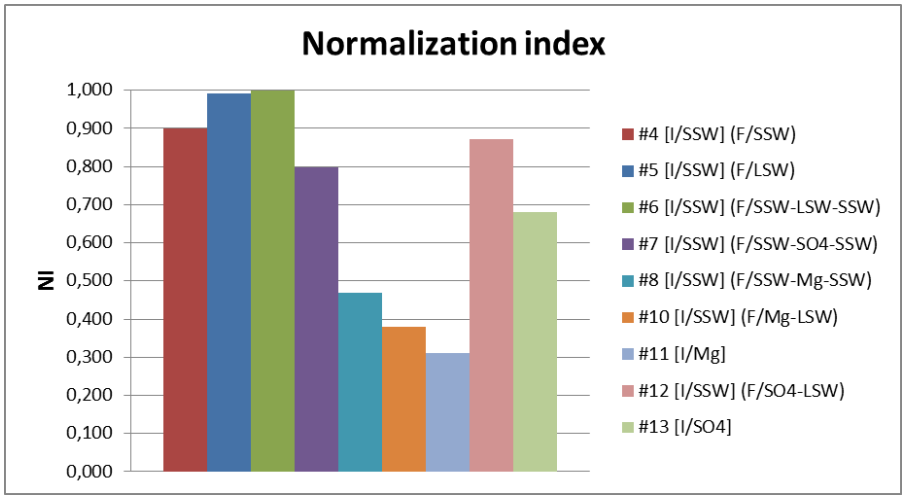

Figure 4.31: Normalization index calculated from the slope of imbibition rate for each core at room temperature. In the legend the core number is listed first, and then I for imbibition brine, and last F, for flooding sequence performed on the core.

4.2.4 Dimensionless scaling

When R(t) is plotted versus $\sqrt{t}$ according to eq.2.70 , the wettability index is obtained from the slope of the straight line, the highest slope, is set equal to 1. A modified capillary dimensionless time containing the normalization index can then be used for an appropriate scaling of data. To be able to take account of all parameters affecting the imbibition rate, a dimensionless time for gravity can be incorporated (Shahri et.al., 2012).

$$t^*_{DMM,C} = \sqrt{\frac{K}{\phi}} \frac{\sigma\, NI}{\sqrt{\mu_o \mu_w}} \frac{1}{L_C^2}\, t \qquad (4.5)$$

$$(4.6) \quad t_{DMM,C} = \sqrt{\frac{K}{\phi}} \frac{\sigma}{\sqrt{\mu_o \mu_w}} \frac{1}{L_C^2} t$$

$$(4.7) \quad t_{DMM,G} = \frac{K \Delta\rho g}{L\phi\sqrt{\mu_o \mu_w}} t$$

$t^*_{DMM,C}$ = Capillary dimensionless time, with normalization index
$t_{DMM,C}$ = Capillary dimensionless time
$t_{DMM,G}$ = Dimensionless time for gravity
t = time
K = absolute permeability
Φ = porosity
σ = interfacial tension
μ = viscosity
L = length of the core
L_C = characteristic length, shape factor
NI = Normalization index, see table 4.5.

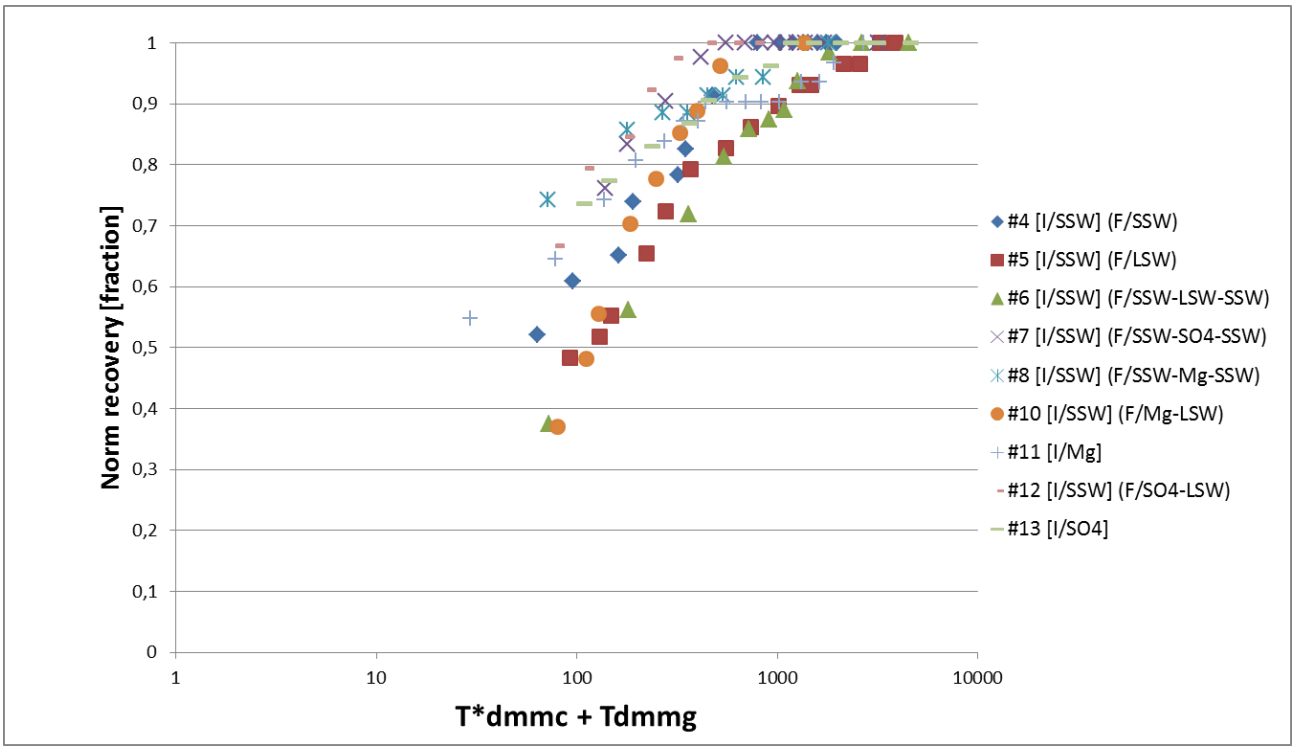

Figure 4.32: Semi-log plot of normalized recovery vs. dimensionless time with wettability index at room temperature. In the legend the core number is listed first, and then I for imbibition brine, and last F, for flooding sequence performed on the core.

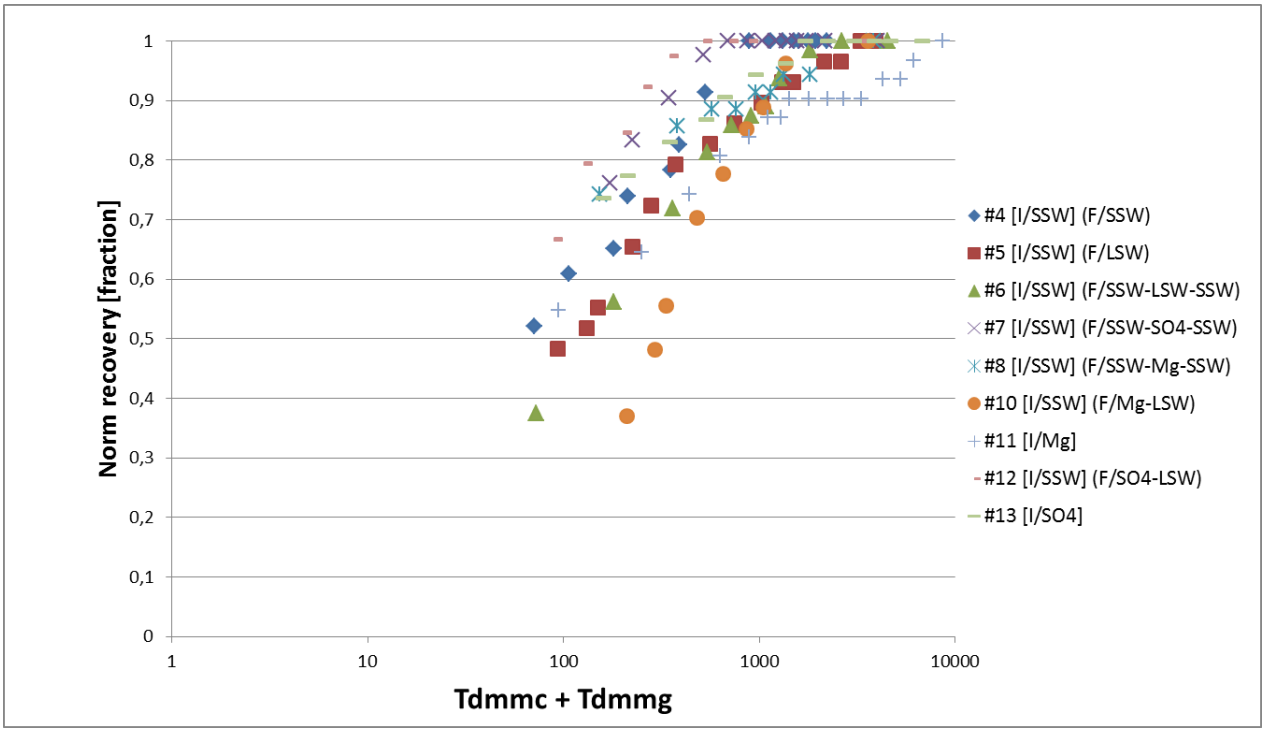

Figure 4.33: Semi-log plot of normalized recovery vs. dimensionless time without wettability index at room temperature. In the legend the core number is listed first, and then I for imbibition brine, and last F, for flooding sequence performed on the core.

The modified dimensionless time, which is the sum of capillary and gravity dimensionless times, are plotted above both with and without the normalization index. Even with the normalization index there is incongruity between the imbibition curves, meaning that other existing factors are affecting the imbibition rate. The recovery data for the different cores have the same trend, but the overall dimensionless time depends on different parameters. Permeability, interfacial tension and density differences have a positive effect on the magnitude of dimensionless time. Negative parameters include porosity, oil water and water viscosities. Wettability could increase the imbibition rate, for example a water wet rock has a higher imbibition rate, which reduces imbibition time and dimensionless time.

Density differences, oil and water viscosities, and IFT should be equal for all the cores with SSW as initial imbibition fluid. According to figure 4.30 core #5 and #6 had the highest imbibition rate, the straight line indicates capillary driven imbibition. The dimensionless time however, are high compared to the other cores, even with the normalization index. This could be due to the overall effect of the different parameters, for example permeability. A reduction in permeability would reduce the dimensionless time, supporting the theory that mobilization of fines from the LSW injection have led to blocking of pores and reduced permeability.

Dissolution, mobilization of fines, release of clay particles and an increase in pH are all reported to increase water-wetness. Adsorption of polar components onto the clay surface is believed to be dependent of pH of initial brine / formation water, if the LSW flooding causes a local pH increase as proposed by Austad et.al., 2010, it might reduce the clays ability to adsorb organic material.

Core #7 was flooded with SO4 brine, and core #13 had SO4 as initial imbibition brine. Both performs similarly to the core flooded with SSW, initial imbibition rate is high, but equilibrium is quickly reached and the SI stops. A decrease in oil recovery is mainly dependent by at which water saturation the capillary pressure falls to zero. Imbibition rate effects are probably related to change in imbibition capillary pressure and mobility to water. As the water saturation increases there are opposing effects determining the imbibition rate; the driving force of capillary pressure decreases, but the mobility of the water phase increases. The relative permeability to water is low and that to oil is high during the beginning of imbibition. Ratio of the capillary to gravity forces is given by the inverse Bond number (NB^{-1}):

$$N_B^{-1} = C\frac{\sigma\sqrt{\frac{\phi}{K}}}{\Delta\rho g H} \quad (2.10)$$

At large inverse bond numbers capillary forces dominate the flow, and as NB^{-1} approaches zero, gravity forces dominate. Numerator is a measure of capillary entry pressure, denominator is the gravity head over the length, H. Al-Lawati et.al., 1996, reported that for high permeability cores with high to intermediate IFT, the imbibition fluid rapidly imbibed into the core. In the low IFT case, imbibition rate was slow, but with a higher oil recovery at the end in comparison with the intermediate and high IFT fluids. The IFT measurements showed that SO4 has a IFT at 31.1 mN/m, compared to SSW at 20.1 mN/m. At low IFT it was observed that gravity forces were the dominant imbibition force. At intermediate values of the inverse bond number, gravity is still strong enough to cause considerable segregation of the flow, keeping relative permeabilities high, while capillary forces are still strong enough to boost the driving force of fluid flow. As a result the imbibition rate can be higher at intermediate IFT values, compared to either capillary of gravity dominated flow. On the other hand, imbibition rate is more rapid for cores with high permeability.

A deviation from a straight line in a log-log plot of recovery versus time (figure 4.34) may indicate that the imbibition process is dominated or affected by forces other than capillarity. It can be observed that the initial imbibition rate is high, but after a period of time the oil recovery more or less ceases. The results indicate that early oil production appears to be obtained from capillary imbibition, as the imbibition process progresses gravity will become more dominant and to a lesser extent from capillarity. Imbibition behavior can be explained on the basis that capillary forces are at

their highest the first instant the imbibition is initiated, caused by imbibition in the smallest pores/capillary tubes, at this instant the capillary force dominate the gravity forces. The rate of imbibition and capillary pressure decreases proportionally to the capillary radius as larger capillaries becomes available, after a certain time a transition occurs, and the capillary forces are no longer the dominating mechanism for oil recovery. It is reported in the literature that residual oil saturation decreases with a reduction in IFT. It seems that a critical IFT value exist, below this value a significant reduction in the oil trapping or increase in oil mobilization were observed, correlated to the breakup of oil into smaller bubbles (Saleh et.al.,1993; Morrow et.al., 1982; Morrow et.al., 1985; Mohanty et.al., 1987).

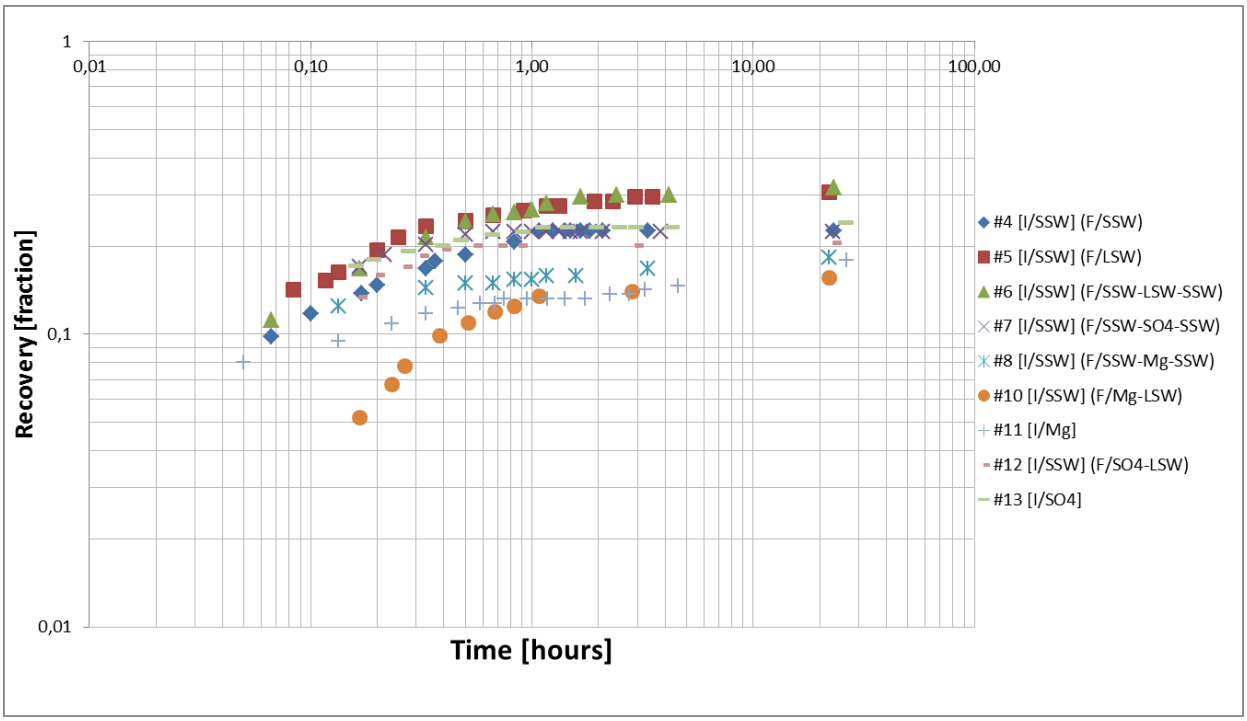

Figure 4.34: Log-log plot of recovery fraction at room temperature vs. time in hours. In the legend the core number is listed first, and then I for imbibition brine, and last F, for flooding sequence performed on the core

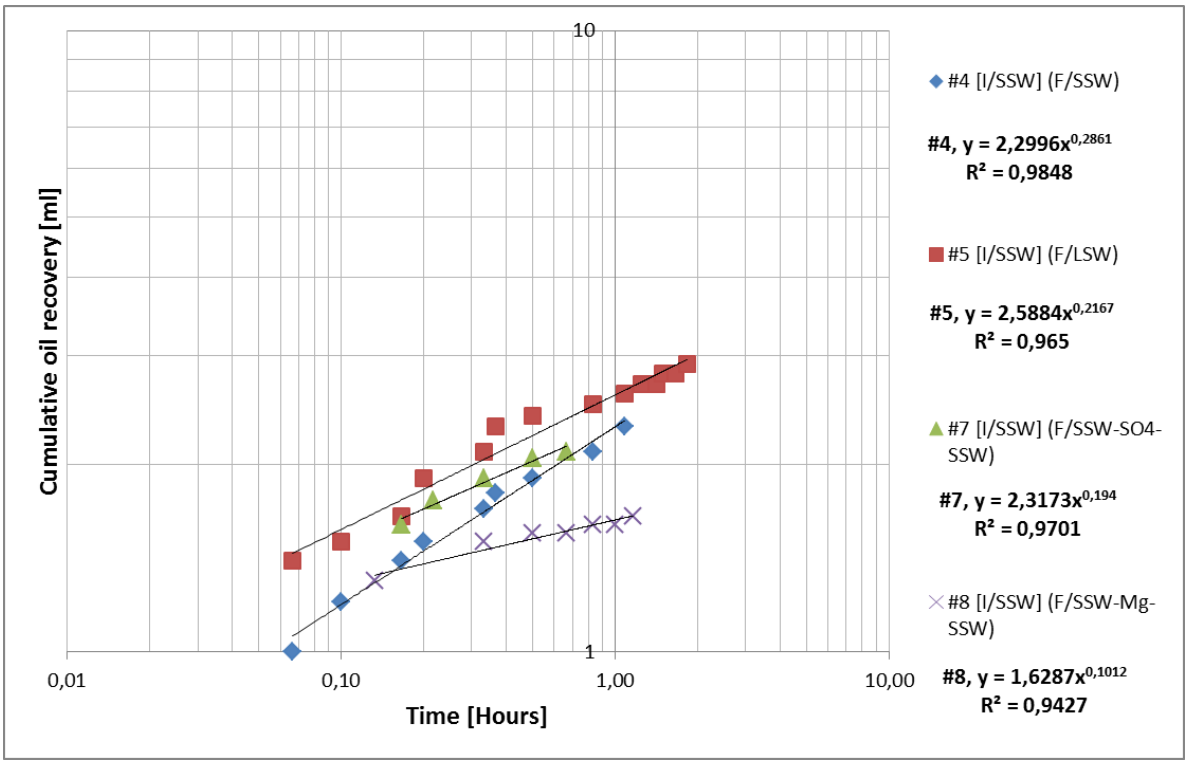

Figure 4.35: Log-log plot of cumulative oil recovery [ml] vs. time in hours. In the legend the core number is listed first, and then I for imbibition brine, and last F, for flooding sequence performed on the core. Equation for each core is listed below the legend key.

$$(2.67) \quad {Q_W}^2 = \left(\frac{2p_C k_w \phi {A_C}^2 S_W}{\mu_W}\right) t$$

According to the eq.2.67, derived in section 2.10.4, a log-log plot of cumulative oil production versus imbibition time should yield a straight line with a slope equal to 0.5. Assuming that gravity forces are negligible compared to capillary forces. However, a countercurrent flow will be slower than a cocurrent flow, as the movement of both oil and water in opposite directions will reduce the total mobility. It is interesting to observe that the different cores maintain a straight slope at early oil production, but the time period before a deviation occurs, differs widely. Especially for core #5, which maintain a straight slope almost twice as long as core #4. Explaining the increase in displacement efficiency observed might be essential to understanding the LSW mechanism.

5. Simulation

5.1 Coreflood history matching

A history match of the production profile and differential pressure curves was obtained for the flooding with SSW and LSW, a set of relative permeability curves and capillary pressure curves are obtained. The match is reasonable, and the resulting curves are shown below for the different cases. Sendra simulator was used to perform the history match (Sendra,2013.1).

5.1.1 Injection of SSW and LSW

Figure 5.1 shows the best fit for production curves and differential pressure for the injection of SSW and LSW.

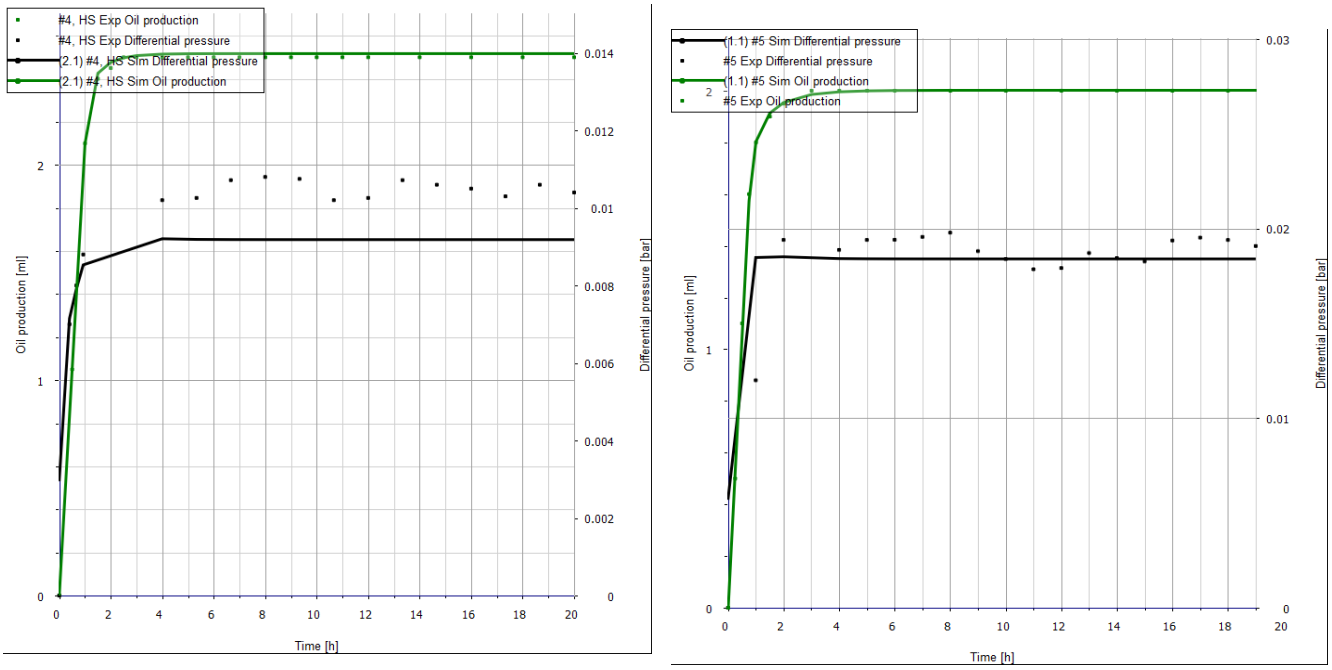

Figure 5.1: Simulated recovery and pressure drop compared to experimental data. To the left: Core number 4 with SSW as injection brine. To the right: Core number 5 with LSW as injection brine.

Estimated relative permeability curves are presented figure 5.2. SSW flooding corresponds to mixed-wet conditions, LSW indicates a more water-wet state, by an increase in k_{ro} and decrease in k_{rw}. As both cores are aged in SSW, they follow a similar shape from S_{wi}, with a cross over at 0.35.

A number of authors have reported that low salinity brine can increase the water-wetness in mixed/ less water wet cores as observed in this case, however, several authors have also reported that low salinity brine can make cores more oil wet. For a more oil wet core an earlier breakthrough of water is expected, and the oil production could continue over a longer period of time than at more water-wet conditions. A wettability change from water-wet to less water-wet can decrease the residual oil

saturation, and contribute to the microscopic sweep efficiency. Such changes could also involve an increase in the negative capillary pressure, which leads to unfavorable increase in the end effects for short core plugs at low injection rates. It should be noted that if the short core become more water-wet, an opposite effect could be observed in corefloods at slow rates, the reduced capillary end effect can appear as a reduction of remaining oil saturations.

For reservoirs conditions a less water-wet state could lead to an earlier breakthrough of water and an extended oil production period. A higher amount of water is therefore required to reach S_{or} compared to more water-wet reservoir. Real life production must be economical justifiable, and if the water cut becomes too high the field must be abandoned, average remaining oil saturation could then be higher at less water-wet conditions compared to more water-wet.

An alteration from mixed-wet to more water-wet can reduce the microscopic sweep efficiency, increasing the remaining oil saturation. This is consistent with the results obtained from the flooding in the experimental section, where recovery was lower for LSW (22%) than SSW (31%). An important note is that the simulation program does not simulate migration of fines, plugging of pores, and salinity of water. Pore plugging reduces the oil mobility, and can lead to a wrong conclusion, stating wettability alteration to more oil wet.

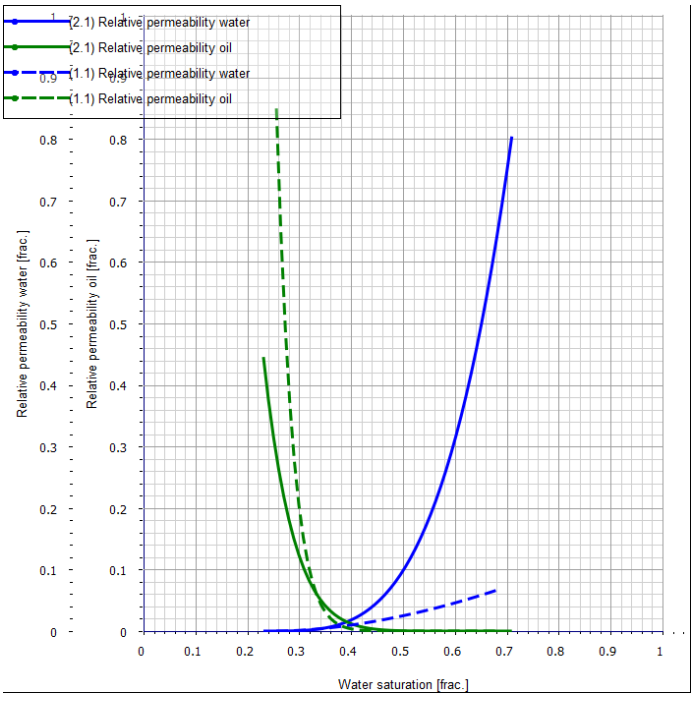

Figure 5.2: Relative permeability curves for SSW (nr 2.1, solid line) and LSW (nr 1.1, dashed line) as injection brines.

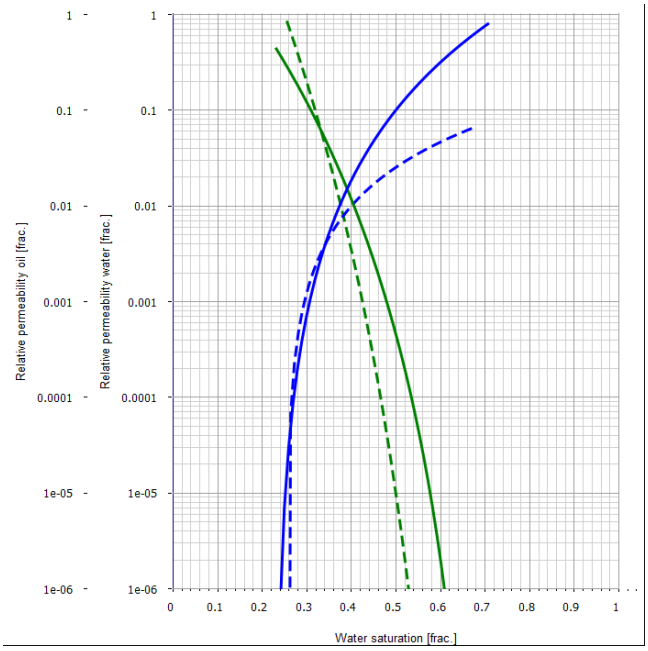

Figure 5.3: Relative permeability curves for SSW (nr 2.1, solid line) and LSW (nr 1.1, dashed line) as injection brines. Semi-log scale.

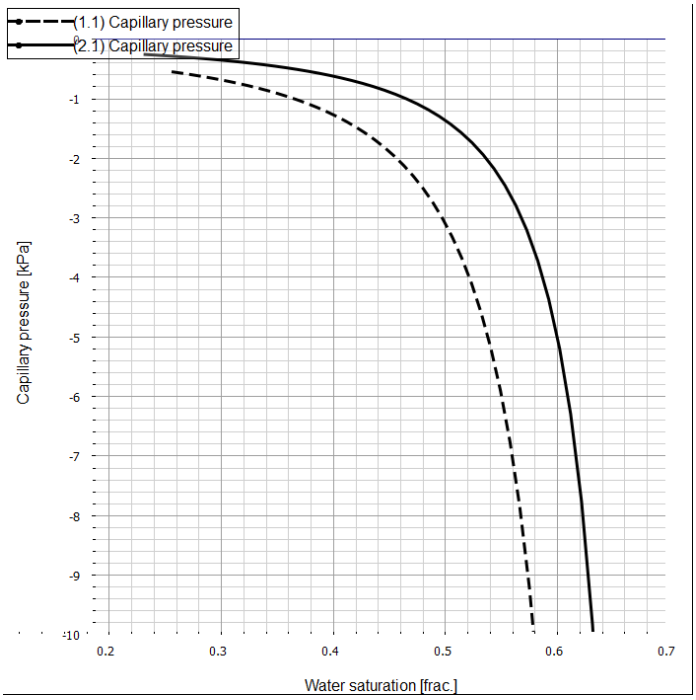

Figure 5.4: Capillary pressure curves for SSW (nr 2.1, solid line) and LSW (nr 1.1, dashed line) as injection brine.

6. Summary of results and mechanism

Low salinity effects are complex and not easily predicted, due to the amount of parameters and complexity behind oil/brine/rock interactions, which the scope of this research work clearly shows. Some main conclusion can still be presented based on the results and theoretical studies. The initially proposed requirements for low salinity effects from Tang et.al., 1999, remains unchanged:

- Negative zeta potential material (clays) must be present in the porous medium.
- Oil must contain polar components to create mixed-wet conditions.
- Presence of connate water containing divalent cations.

In this research it is shown that injection of LSW (25 times diluted SSW), brine containing only Na_2SO_4(0.024 M), and only $MgCl_2$(0.045 M), increases the pH. From the analysis of the effluent it can be concluded that the increase are due to brine-rock interactions, such as ion exchange, and dissolution of carbonate in the form of cementing material.

Huertas et.al., 1999; 1998, investigated the density of negatively and positively charged sites at the kaolinite surface by acid and base titration, a dependence upon pH were observed, the ionic strength in the range of 0.001 to 1M showed very little influence on the results. The dissolution rate constant show inflections at pH ≈ 4 and ≈ 10, above and below these values the dissolution rate displayed strong pH dependence. In neutral conditions the rate was much less dependent upon pH.

The following main observations were made by the experimental work performed:

Core flood studies:

- Initially there is a balanced adsorption of organic material, protons and active cations on the clay surface.
- Dissolution of kaolinite is dependent upon pH, and the injection brine can increases the dissolution rate by increasing the pH. This statement is based on the observations of increase in pH and analysis of the potassium (K^+) concentration in the effluent. Potassium concentration was observed to be increasing with increasing pH levels. Solid analysis of the sandstone used in the experiments shows that Muscovite and Microline are present, both containing potassium.
- SO_4^{2-} containing brine had a higher increase in pH, and consequently the dissolution rate of kaolinite increased as observed by the concentration of potassium in the effluent.
- Increased injection rates of LSW increased the pH, which lead to an increase in the concentration of potassium in the effluent.

- For constant rate water floods there was an increase in pressure with a change in salinity. Fine-grained materials, strained areas on large grains or defects will initially dissolve at a large rate, causing a release of fines which can lead to partial blocking of the pore throat, which increases the pressure. If the pH is sufficiently high, these fines may dissolve.
- The difference in the behavior of the cores suggest that low salinity flooding is related to a shift in wettability towards more water-wet, by a mechanism that involves dissolution of clay and associated release of organic material and other fine material from pore surface, creating new initially water-wet surface.
- No increase in recovery was observed from the LSW, SO_4^{2-} or Mg^{2+} brine. However, an essential physics in EOR is that the mobilized oil cannot pass a zone where the flow velocity is lower than that for the onset of oil mobilization, part or all of the mobilized oil drops will be trapped again. In addition the clay fraction was low in the tested cores.
- Although an increase in pH was observed for the injection of Mg^{2+} brine, indicating some brine-rock interactions, no dissolution of kaolinite was observed. However, the final pH level was low compared to SO_4^{2-} and LSW injections.

Spontaneous imbibition studies:

- LSW brine permanently altered some of the rock properties, as indicated by rate and extent of spontaneous imbibition, the effects could not be reversed by another aging process. Released fines are believed to reduce the permeability and to some extent affect pore throats, resulting in improved sweep efficiency and capillary effect.
- LSW, Na_2SO_4, and $MgCl_2$brine had little to no effect on the previously flooded cores as a second imbibing fluid at 70^oC.
- The core flooded with brine containing only $MgCl_2$had a slower imbibition rate and low recovery from spontaneous imbibition at room temperature. A proposed mechanism is that Mg^{2+} adsorbs on the clay surface, acting as a bridge between Si and oil by chemical bonds. The slow release of oil may be an indication of breaking of the chemical bond.
- No significant changes were observed by flooding a core with Na_2SO_4 brine. Indicating that SO_4^{2-} initially adsorbed on the pore surface is displaced by the SSW, returning the equilibrium at pore surface.

7. Conclusions

This work is done with the intention to contribute to the ongoing discussions about LSW mechanism(s). There are many mechanisms that have been proposed in the literature. However, the mechanisms differ with minerals composition, water composition and temperature. Different brines were, in this work, injected both as a secondary and primary recovery method.

The proposed mechanism from this work may be categorized into two main categories, based on observation and data analysis. Both mechanisms are related to alteration of wettability to more water-wet. One of the mechanisms is based on mineral/ions interaction that may lead to dissolution. This may cause a raise of the pH and as the mineral dissolves, pH increases more. In order to test this hypothesis, brine containing only Na_2SO_4 was injected that caused large increase of pH to 9.65 (from 6.5). The effluent ion analysis showed an average concentration of 3.1 mMole/l for potassium (K^+), which is not in the injected water composition. The ion analysis, also, indicated the presence of average of 0.5 mMole/l of bicarbonate (HCO_3^-). It is interesting to observe that the monitored pH in the effluent increased followed by exponential pH increase that could be explained based on the presence of the HCO_3^-.

Another test was performed in which the injected brine contained only $MgCl_2$, an increase of the pH to 8.0 from 6.8 was observed. The analysis did not show any significant level of K^+ in the effluent, which may indicate low kaolinite dissolution. The pH was at a level where the dissolution rate of kaolinite is low, hence could not be detected. Unlike the case of the $NaSO_4$, where the pH is above the inflection point, and the dissolution rate is pH dependent.

In the case of low salinity water, the dissolution rate showed a slight increase of K^+ compared to the injected water composition at 0.4 mMole/L. As the injection rate increased, the pH increased and K^+ concentration also increased to a maximum of 2.05 mMole/l. Although, the bulk pH is on the boarder of the inflection point, the localized pH may be higher.

Low salinity water also increased the pressure drop, which is believed to be caused by release of fines. This may lead to partial blocking of the pore throat. This reduces the oil mobility that led to wrong conclusion, in literature, stating wettability alteration to more oil wet.

Since the clay fraction of the tested cores, in this work, was low (total of 3%, see table 3.3), no additional oil recovery was observed. Increasing the flow rate was thought to increase the mobile oil, however this was not the case, which may be explained by that the flow rate is not high enough, and the flow followed the water path already established by the low flow rate.

References

A.A. Hamouda , O. Karoussi, E.A. Chukwudeme, **Relative permeability as a function of temperature, initial water saturation and flooding fluid compositions for modified oil-wet chalk**, Journal of Petroleum Science and Engineering, 2008

Abdallah, W., Buckley, J.S., Carnegie, A., Edwards, J., Herold, B., Graue, A., Habashy, T., Seleznev, N., Signer, C., Hussain, H., Montaron, B., Ziauddin, M., **Fundamentals of Wettability**, Oil Field Review, 19, 44-61, 2007

Ahmed, T., **Reservoir Engineering Handbook**, Gulf Publ., Houston, Tex. , 2000

Al-Lawati, S., Oman, P., Saleh, S., **Oil Recovery in Fractured Oil Reservoirs by Low IFT Imbibition Process**, SPE 36688, SPE Annual Technical Conference and Exhibition held In Denver, Colorado, U S.A 6– 9 October, 1996

Al-Lawati, S., Saleh, S., **Oil Recovery in Fractured Oil Reservoirs by Low IFT Imbibition process**, SPE 36688, presented at the 1996 SPE Annual Technical Conference and Exhibition held in Colorado, Canada, 6-9 October, 1996

Anderson, W.G., **Wettability Literature Survey – Part 1: Rock/Oil/brine interactions and the effects of core handling on wettability**, Journal of Petroleum Technology, October, 1986

Arnarson, T.S., Keil, R.G., **Mechanisms of pore water organic matter adsorption to montmorillonite, Marine Chemistry**, 71(3-4):309-320, 2000

Ashraf, A., Hadia, N., & Torsæter, O., **Laboratory investigation of low salinity waterflooding as secondary recovery process: effect of wettability**, SPE Oil and Gas India Conference and Exhibition SPE 129012. Mumbai, India. , 2010

Austad, T., Milter, J., **Spontaneous imbibition of water into low permeable chalk at different wettabilities using surfactants**, SPE 37236, presented at the International Symposium on Oilfield Chemistry, Houston, Texas, 1997

Austad, T., RezaeiDoust, A., Puntervold, T., **Chemical Mechanism of Low Salinity Water Flooding in Sandstone Reservoir**, Paper SPE 129767, 2010

Babadagli, T., **Temperature effect on heavy-oil recovery by imbibition in fractured reservoirs**. Journal of Petroleum Science, Eng. 14, 197-208, 1996

Bailey, G.W., White, J.L. and Rothberg, T., **Adsorption of organic herbicides by montmorillonite: role of pH and chemical character of adsorbate**. Soil Sci. Soc. Am. Proc., 32:222, 1968

Barenblatt, G.I., Zheltov, I.P., Kochina, I.N., **Basic concepts in the theory of seepage of homogeneous liquids in fissured rocks**, J. Appl. Math. Mech. 24(5), 1286-1303., 1960

Batias, J., Hamon, G., Lalanne, B., Romero, C., **Field and Laoratory Observations of Remaining Oil Saturations in a Light Oil Reservoir Flooded by a Low Salinity Aquifer**, SCA2009-01, 2009

Bavière, M., **Basic concepts in enhanced oil recovery processes**. Oxford, Published for the Society of Chemical Industry by Blackwell, 1991

Beaton, N., Havlin, T., **Soil Fertility and Fertilizers**, New Dehli, 2011

Berg, S., Cense, A., Jansen, E., & Bakker, K., **Direct experimental evidence of wettability modification by low salinity**. In International Symposium of the Society of Core Analyst. Noordwijk, The Netherlands, 2009

Bergaya, F., Theng, B.K.G., Lagaly, G., **Handbook of Clay Science**, Elsevier, Amsterdam, 2006

Blum, A. E. and Lasaga A. C., **The role of surface speciation in the dissolution of albite**, Geochim. Cosmochim. Acta 55, 2193–2201, 1991

Boussour, S., Cissokho, M., Cordier, P., Bertin, H., Hamon, G., **Oil Recovery by Low Salinity Brine Injection: Laboratory Results on Outcrop and Reservoir Cores**, Paper SPE 124277, 2009

Buckley, J.S., **Asphaltene Precipitation and Crude Oil Wetting**, SPE Advanced Technology Series., 1995

Buckley, J.S., Liu, Y., Monsterleet, S., **Mechanism of Wetting Alteration by crude oils**, SPE Journal, March: 54-61., 1998

Buckley, J.S., **Mechanism and Consequence of Wettability Alteration by Crude Oils**, PhD Thesis, Heriot-Watt University, Edinburgh, United Kingdom., 1996

Buckley, J.S., **Multiphase Displacement in Micromodels**, Interfacial Phenomena in Oil Recovery, Morrow, N.R. (Editor), Marcel Dekker Inc., New York City, 1991

C.C. Mattax, J.R. Kyte., **Imbibition oil recovery from fractured, water-drive reservoir,** SPE J, pp. 177-184**,**1962

C.Martin, J., **The Effects of Clay on the Displacement of Heavy Oil by Water**, Venezuelan Annual Meeting, Society of Petroleum Engineers of AIME, Caracas, Venezuela., 1959

Carroll-Webb S. A. and Walther J. V., **A surface complex reaction model for the pH-dependence of corundum and kaolinite dissolution rates**, Geochim. Cosmochim. Acta 52, 2609–2623, 1988

Chatzis, I., Morrow, N.R., **Correaltion of Capillary Number Relationships for Sandstone**, 1984

Chatzis, I., Morrow, N.R., Lim, H.T., **Magnitude and Detailed structure of residual oil saturation**, SPE Journal , April, pp, 311-326, 1983

Cissokho, M.,Boussour, S., Cordier, P., Bertin, H., Hamon, G., **Low Salinity Oil Recovery on Clayey Sandstone: Experimental study**, Paper SCA2009-05., 2009

Clementz, D.M., **Interaction of petroleum heavy ends with montmorillonite Clays and Clay minerals**, 1976

Collins, S.H., Melrose, J.C., **Adsorption of Asphaltenes and Water on Reservoir rock minerals**, Paper SPE 11800 presented at the SPE International Symposium on Oilfield and Geothermal Chemistry held in Denver, Colorado, 1-3 June, 1983

Corey, A., **The interrelation between gas and oil relative permeabilities**. Prod. Monthly, 19, 38–41, 1954

Cosse, R., **Basics of reservoir Engineering**, Technip, Paris, 1993

Cuiec, L., **Rock / Crude oil Interactions and wettability: An Attempt to Understand Their Interrelation**, SPE Annual Technical Conference and Exhibition, 1984

Cuiec, L., **Wettability and Rock/Crude-Oil component Interactions**, 21st Intersociety Energy Conversion Engineering Conference, San Diego, USA, 1986

Cuiec, L.E., Bourbiaux, B., and Kalaydjian, F., **Oil recovery by imbibition in low-permeability chalk**, SPE Formation Evaluation 9(3): 200-208, 1994

Cuiec, L.E., **Restoration of the Natural State of Core Samples**, Fall Meeting of the Society of Petroleum Engineers of AIME, Dallas, Texas, 1975

Da Silva, F.V., Belery, P., **Molecular Diffusion in Naturally Fractured Reservoirs: A Decisive Recovery Mechanism**, Paper SPE 19672, presented at the 1989 SPE Annual Technical Conference and Exhibition held in San Antonio, TX, 8-11 October, 1989

Dandekar, A.Y., **Petroleum reservoir rock and fluid properties**, Taylor & Francis, 2006

Denekas, M.O, Mattax, C.C., Davis, G.T., **Effects of Crude Oil Components on Rock Wettability**, SPE, 1959

Dubey, S.T, Doe, P.H., **Base Number and Wetting Properties of Crude Oils**, SPE reservoir engineering, 1993

Ehrlich, R., Wygal Jr, R.J**., Interrelation of Crude Oil and Rock Properties with the Recovery of Oil by Caustic Waterflooding**, 17(4):263-270, 1977

Erle C., Donaldson and Djebbar Tiab, **Petrophysics,** second edition, Elsevier, Inc., 2004

Evje, S., & Hiorth, A., **A mathematical model for dynamic wettability alteration controlled by water-rock chemistry**. Networks and Heterogeneous Media, 5, 217–256, 2010

Evje, S., & Hiorth, A., **A model for interpretation of brine- dependent spontaneous imbibition experiments,** Advances in Water Resources, 34, 1627–1642, 2011

Fabuss, B.M., A. Korosi, and D. F. Othmer, **Viscosities of aqueous solutions of several electrolytes present in sea water**, Chem. Eng. Data 14(2), 192, 1969.

Fanchi, J.R., **Integrated reservoir asset management: principles and best practices**, 2010

Fjelde, I., Asen, S., & Omekeh, A., **Low salinity water flooding experiments and interpretation by simulations**, In SPE Improved Oil Recovery Symposium SPE 154144. Tulsa, Oklahoma, USA. , 2012

Ganor J., Mogollo´n J. L., and Lasaga A. C., **The effect of pH on kaolinite dissolution rates and on activation energy**, Geochim. Cosmochim. Acta 59, 1037–1052, 1995

Gardescu, I.I., **Behavior of gas bubbles in capillary spaces**, Trans. AIME 86, 351–369, 1930

Garg, A., Kovscek, A.R., Nikravesh, M., Castanier, L.M., Patzek, T.W., **CT Scan and Neural Network Technology for Construction of Detailed Distribution of Residual Oil Saturation During Waterflooding**, 35737-MS, SPE Western Regional Meeting, 22-24 May, 1996

Graue, A., Ma, S., Morrow, N.R., Viksund, B.G., Wang, W**., Initial Water Saturation and Oil Recovery from Chalk and Sandstone by Spontaneous Imbibition**, SCA-9814, 1998

Graue, A., Viksund, B.G., Baldwin, B.A., **Reproducible wettability alteration of low-permeable outcrop chalk**, SPE Reservoir Eval. Eng. 2(2), 134-140, 1999

Green, D. W. and G. P. Willhite, **Enhanced oil recovery**, Richardson, TX, Society of Petroleum Engineers, 1998

Hamilton, P. J**., A Review of Radiometric Dating Techniques for Clay Mineral Cements in Sandstones**, In: S.M. Richard H. Worden (Editor), Clay Mineral Cements in Sandstones, pp. 253-287, 2009

Hamon, G, Vidal, J., **Scaling-up the capillary imbibition process from laboratory experiments on homogeneous and heterogeneous samples**, SPE 15852, presented at the 1986 European Petroleum Conf. of SPE, London, 1986

Handy, L.L., **Determination of Effective Capillary Pressure for Porous Media from Imbibition Data**, Petroleum Transactions, AIME, 219, 1960

Hiorth, A., Cathles, L., & Madland, M., **The impact of pore water chemistry on carbonate surface charge and oil wettability**, Transport in Porous Media, 85, 1–21. 10.1007/s11242-010-9543-6, 2010

Hourshad Mohammadi, Gary R. Jerauad, **Mechanistic Modeling of the Benefit of Combining Polymer with Low Salinity Water for Enhanced Oil Recovery**, SPE, 2012

Huertas, F.J., Chou, L., Wollast, R., **Mechanism of kaolinite dissolution at room temperature and pressure Part II: Kinetic study**, PII S0016-7037(99)00249-5, 1999

Hunter, R.J., **Zeta Potential in Colloid Science: Principles and Applications**, Academic Press, London, 1981

IDF, **Clay Chemistry, Technical Manual for Drilling, Completion and Workover Fluids, International Fluids Limited**, 1982

Iler R.K., **The chemistry of silica: solubility, polymerization, colloid and surface properties, and biochemistry**, Wiley, 1979

Israelachvili, J., **Intermolecular and Surface Forces**, Academic Press. Elsevier Science & Technology, 2011

Jadhunandan, P.P., Morrow, N.R., **Effect of Wettability on Waterflood Recovery for Crude oil/brine/rock systems**, SPE Reservoir Engineering, 10(1): 40-46, 1995

Jadhunandan, P.P., Morrow, N.R., **Spontaneous Imbibition of Water by Crude oil/Brine/Rock Systems: In situ**, v.15, no.4, pp. 319-345, 1991

Jamin, J.M., **Memoir on equilibrium and movement of liquids in porous substances,** Compt. Rend. **50**, 172–176,311–314, 385–389, 1860

Jerauld, G. R., Lin, C. Y., Webb, K. J., and Seccombe, J. C., **Modeling Low-Salinity Waterflooding**, SPE Reservoir Evaluation and Engineering, paper SPE 102239, December, 1000-1012, 2008

Khilar, K.C., Fogler, H.S., **Water Sensitivity of sandstones**, SPE 23(1):55-64, 1983

Kleven, R. and Alstad,J., **Interaction of alkali, alkaline-earth and sulphate ions with clay minerals and sedimentary rocks**, Journal of Petroleum Science and Engineering, 15: 181- 200, 1996

Lager, A., Webb, K.J., Black, C.J.J, Singleton, M., Sorbie, K.S., **Low Salinity Oil Recovery – An Experimental Investigation**, Petrophysics, 49(1): 28-35, 2008a

Lager, A., Webb, K.J., Black, C.J.J., **Impact of Brine Chemistry on Oil Recovery**, paper A24 presented at the 14th European Symposium on Improved Oil Recovery, Cairo , Egypt, 2006

Lager, A., Webb, K.J., Collins, I.R., Richmond, D.M., **LoSal Enhanced Oil Recovery: Evidence of Enhanced Oil Recovery at the Reservoir Scale**, SPE/DOE Symposium on Improved Oil Recovery. Society of Petroleum Engineers, Tulsa, Oklahoma, USA, 2008b

Lake, L.W., **Enhanced Oil Recovery**, Prentice hall, Englewood Cliffs, N.J. , 1989

Lebedeva, E., Senden, T., Knackstedt, M., Morrow, N.R., **Improved oil recovery from tensleep sandstone studies of brine-rock interactions by micro−CT and afm**, In European symposium of improved oil recovery. Paris, France, 2009

Legens, C., Palermo, T., Toulhoat, H., Fafet, A., Koutsoukos, P., **Carbonate Rock Wettability changes induced by organic compound adsorption**, Journal of Petroleum Science and Engineering 20: 277-282, 1998

Legens, C., Toulhoat, H., Cuiec, L., Villieras, F., Palermo, T., **Wettability change related to adsorption of organic acids on calcite: experimental and ab initio computational studies**, SPE Journal 4(4): 328-333, 1999

Levitt, D. B., and Pope, G. A., **Selection and Screening of polymers for Enhanced-Oil Recovery**, paper SPE 113845, presented at the SPE Improved Oil recovery Symposium held in Tulsa, Oklahoma, U.S.A., 19-23 April, 2008

Li, M., **Linked Polymer Solution (LPS) and its application in EOR**, The 29th IEA Workshop & Symposium, Beijing, China, 2008

Li, Y., **Oil Recovery by Low Salinity Water Injection into a Reservoir: A new study of Tertiary Oil Recovery Mechanism**, Transp Porous Med (2011) 90:333–362, 2011

Li, Y., **Rebuting enhanced oil recovery by cyclic water and oil floods**, SPE 133154, presented at Trinidad and Tobago energy resources conference, 27–30 June 2010, Port of Spain, Trinidad, 2010

Li, Y., Wardlaw, N.C., **Mechanisms of non-wetting phase trapping during imbibition at slow rates,** J. Colloid Interface Sci. 109(2), 473–485, 1986b

Li, Y., Wardlaw, N.C., **The Influence of wettability and critical pore-throat size ratio on snap-off**, J. Colloid Interface Sci. 109(2), 461–472, 1986a

Ligthelm, D.J., J. Gronsveld, J.P. Hofman, N.J. Brussee, F. Marcelis, and H.A. van der Linde, **Novel waterflooding Strategy by Manipulation of Injection brine composition**, Paper SPE 119835, 2009

M.C. Leverett, **Flow of oil–water mixtures through unconsolidated sands,** Trans AIME, 132 (1939), pp. 151–169, 1939

Ma, S., X. Zhang, N.R. Morrow, **Influence of fluid viscosity on mass transfer between rock matrix and fractures,** J Can Pet Tech, 38 (7) (July 1999), pp. 25–30, 1999

Madsen, L., Grahl-Madsen, L., Grøn, C., Lind, I., Engell, J., **Adsorption of polar aromatic hydrocarbons on synthetic calcite**, Org. Geochem. 24(12): 1151-1155, 1996

McGuire, P.L, Chatham, J.R., Paskvan, F.K., Sommer, D.M., Carini, F.H., **Low Salinity Oil Recovery: An Exciting New EOR Opportunity for Alaska`s North Slope**, Paper SPE 93903, 2005

Melrose, J.C., Brandner, C.F., **Role of capillary forces in determining microscopic displacement efficiency for oil recovery by waterflooding,** J. Can. Pet. Technol. 13(4), 54–62,1974

Mohammadi, H., Jerauld, G.R., **Mechanistic Modeling of the Benefit of Combining Polymer with Low Salinity Water for Enhanced Oil Recovery**, 153161-MS, SPE Improved Oil Recovery Symposium, 14-18 April, 2012

Mohanty, K. K., Davis, H.T., Scriven, L.E., **Physics of oil entrapment in water-wet rock**, SPE Reservoir Engineering, February, pp. 113-128, 1987

Moore, T.F., Slobod, R.L., **The effect of viscosity and capillarity on the displacement of oil by water**, Prod. Mon. 20, 20–30, 1956

Morad, S., Worden, R. H., **Clay Mineral Cements in Sandstone**, Special publication of the international Association of sedimentologist, Blackwell, Oxford, 2003

Morrow, N.R**., Characterization of Wettability and the Effects of Initial Water Saturation and Aging time on Wettability and Oil Recovery by Waterflooding**, Third Intl. Symposium on Evaluation of Reservoir Wettability and Its effect on Oil recovery, Laramie, Wyoming 21-23 September, 1994

Morrow, N.R., Chatzis, I., Taber, J.J., **Entrapment and mobilization of Residual Oil in Bead Packs**, SPE paper 14423, Sept., 1985

Morrow, N.R., Mason, G., **Recovery of oil by spontaneous imbibition**, Current Opinion in Colloid & Interface Science 6(4): 321-337, 2001

Morrow, N.R., **Physics and Thermodynamics of Immiscible Displacement in Porous Media,** Ind. Eng. Chem., Vol. 62, pp. 32-56, 1970

Morrow, N.R., Songkran, B**., Effect of Viscous and Buoyancy forces on Nonwetting Phase Trapping in Porous Media**, Surface Phenomena in Enhanced Oil Recovery, D.O. Shah (ed.), Plenum Press, New York City, P 387-411, 1982

Morrow, N.R., Tang, G.Q., Valat, M., Xie, X., **Prospects of Improved Oil Recovery Related to Wettability and Brine Composition**, Journal of Petroleum Science and Engineering, 1998

Morrow, N.R., Zhang, X., Zhou, X., **Characterization of Wettability from Spontaneous Imbibition Measurements**, Journal of Canadian Petroleum Technology, 1999

Muskat, M., Wyckoff, R.D., **A theoretical analysis of waterflooding networks,** Trans. AIME 107, 62–77, 1934

Newman A. C. D. and Brown G.,**The chemical constitution of clays**, In Chemistry of Clays and Clay Minerals (ed. A. C. D. Newman); Mineral. Soc. Monogr. 6, 1–128, 1987

Nichols, G., **Sedimentology and Stratigraphy**, Wiley-Blackwell, Chichester, X, 419 s. pp, 2009

NPD (2013) from http://www.npd.no/en/About-us/Information-services/Dictionary/.

Olga Vizika and Lombard, J.M., **Wettability and Spreading: Two Key Parameters in Oil Recovery With Three-Phase Gravity Drainage**, SPE, 1996

Pashley, R.M., Karaman, M.E., **Applied colloid and surface chemistry**, wiley, Chichester, 2004

Perkins, T.K., Johnston, O.C., **A review of diffusion and Dispersion in porous media**, SPE Journal 3(1): 70-84, 1963

Pu, H., Xie, X., Yin, P., & Morrow, N.R., **Low salinity waterflooding and mineral dissolution**, In SPE Annual Technical Conference and Exhibition SPE 134042. Florence, Italy, 2010

Pu, H., Xie, X., Yin, P., Morrow, N.R., **Application of Coalbed Methane Water to Oil Recovery By Low Salinity Waterflooding**, Paper SPE 113410, Tulsa, OK, USA, 2008

Puntervold, T., Strand, S., Austad, T., **Water Flooding of Carbonate Reservoirs: Effects of a model base and natural crude oil bases on Chalk wettability**, Energy & Fuels, 21(3): 1606-1616, 2007

Raymond, M. and W. L. Leffler, **Oil and gas production in nontechnical language**, Tulsa, Okla., PennWell., 2006

Reinholdtsen, A. J., RezaeiDoust, A., Strand, S., & Austad, T., **Why such a small EOR-potential from the Snorre field?**, In European symposium on Improved Oil Recovery. Cambridge, UK, 2011

RezaeiDoust, A., **Low Salinity Water Flooding in Sandstone Reservoirs**, PhD Thesis UIS no. 135 – September, 2011

RezaeiDoust, A., Puntervold, T., Strand, S., Austad, T., **Smart Water as Wettability Modifier in Carbonate and Sandstone: A Discussion of Similarities/Differences in the Chemical Mechanisms**, Energy&Fuels, 23(9): 4479-4485, 2009

Robertson, E.P**., Low-Salinity Waterflooding to Improve Oil Recovery – Historical Field Evidence**, Paper SPE-109965 presented at the 2007 SPE Annual Technical Conference and Exhibition held in Anaheim, CA, USA, 11-14 Nov, 2007

Romanuka, J., Hofman, J. P., Ligthelm, D., Suijkerbuijk, B., Marcelis, A., Oedai, S., Brussee, N., van der Linde, H., Aksulu, H., & Austad, T., **Low salinity EOR in carbonates**, In SPE Symposium on Improved Oil Recovery SPE 153869, Tulsa, Oklahoma, USA, 2012

Russel, W.B., Saville, D.A. and Schowalter, W.R., **Colloidal Dispersions**, Cambridge University Press, 1989

Salathiel, R.A., **Oil Recovery by surface film drainage in mixed-wettability rocks**, Journal of Petroleum Technology, October: 1216-1224, 1973

Saleh, T.S., Graves, R.M., **Experimental Investigation of Linear Scaling of Micellar Displacement in Porous Media**, SPE paper 25172, March, 1993

Sandengen, K., Tweheyo, M., Raphaug, M., Kjølhamar, A., Crescente, C., & Kippe, V., **Experimental evidence of low salinity water- flooding yielding a more oil-wet behavior,** In International Symposium of the Society of Core Analysts, Austin, Texas, USA., 2011

Schechter, D.S, Zhou, D., Orr Jr., R.M**., Low IFT drainage and imbibtion**, Journal of Petroleum Science and Engineering 11: 283-300, 1994

Schembre, J., Akin, S., Kovscek, A., **Spontaneous Imbibition in Low Permeability Media**, SUPRI TR 114 Report, U.S. Department of Energy, 1998

Schoefield R. K. and Samson H. R., **Flocculation of kaolinite due to the attraction of oppositely charged crystal faces**, Diss. Faraday Soc. 18, 138–145, 1954

Seccombe, J.C, Lager, A., Webb, K.J., Jerauld, G., Fueg, E**., Improving Waterflood Recovery: LoSal™ EOR Field Evaluation**, Paper SPE 113480 presented at the 2008 SPE/DOE Improved Oil Recovery Symposium held in Tulsa, OK, USA, 19-23 April, 2008

Shahri, P.M., Jamialahmadi, M., Shadizadeh, S.R., **New Normalization Index for Spontaneous Imbibition**, Journal of Petroleum Science and Engineering 82-83 (2012) 130-139, 2012

Sharma, M.M, Filoco, P.R, **Effects of Brine Salinity and Crude-Oil Properties on Oil Recovery and Residual Saturations**, SPE Journal, 5(3):293-300, 2000

Shaw, D.J., **Introduction to colloid and surface chemistry**, Butterworth Heinemann, oxford, 1991

Skauge, A., Fallah, S., McKay, E., **Modeling of LPS Linked Polymer Solutions**, The 29th IEA Workshop & Symposium, Beijing, China, 2008

Skjæveland, S. M., Siqveland, L. M., Kjosavik, A., Hammervold Thomas, W. L., & Virnovsky, G. A., **Capillary pressure correlation for mixed-wet reservoirs**, SPE Reservoir Evaluation & Engineering , 3 , 60–67, 2000

Sposito, G., **The Chemistry of Soils**, Oxford University Press, New York, XII, 277 s.pp, 1989

Springer, N., Korsbech, U., Aage, H.K., **Resistivity Index Measurement without the Porous Plate: A Desaturation Technique Based on Evaporation Produces Uniform Water Saturation Profiles and more Reliable Result for Tight North Sea Chalk**, International Symposium of the Society of Core Analysts Pau, France, 2003

Strand, S., Høgnesen, E.J., Austad, T., **Wettability alteration of carbonates – Effects of potential determining ions (Ca^{2+} and SO_4^{2-}) and temperature**, Colloids and Surfaces A: Physiochem. Eng. Aspects, 275: 1-10, 2006

Strand, S., Puntervold, T., Austad, T**., Effect of Temperature on enhanced oil recovery from mixed-wet chalk cores by spontaneous imbibition and forced displacement using seawater**, Energy and fuels, 22: 3222-3225, 2008

Suijkerbuijk, B., Hofman, J. P., Ligthelm, D., a, J. R., Brussee, N., van der Linde, H., & Marcelis, A., **Fundamental investigation into wettability and low salinity flooding by parameter isolation,** In SPE Symposium on Improved Oil Recovery SPE 154204. Tulsa, Oklahoma, USA., 2012

Taber, J.J., **Dynamic and Static Forces Required To Remove a Discontinuous Oil Phase from Porous Media Containing Both Oil and Water**, SPE 2098-PA, 1969

Tang, G.Q., Morrow, N.R., **Influence of Brine Composition And Fines Migration on Crude Oil/brine/rock interactions and Oil Recovery**, Journal of Petroleum Science and Engineering, 1999a

Tang, G.Q., Morrow, N.R., **Oil Recovery by Waterflooding and Imbibition – Invading brine Cation Valency and Salinity**, Paper SCA9911, 1999b

Tang, G.Q., Morrow, N.R., **Salinity, Temperature, Oil Composition and Oil Recovery by Waterflooding**, SPE Reservoir Engineering, 1997

Tripathi, I., & Mohanty, K., **Instability due to wettability alteration in displacements through porous media,** Chemical Engineering Science, 63, 5366 – 5374, 2008

Tripathi, I., and Monhanty, K. K., **Flow Instability Associated with Wettability Alteration**, paper SPE 110202, presented at the SPE Annual Technical Conference and Exhibition held in Anaheim, California, U.S.A., 11-14 November, 2007

Vermolen, E.C.M., Van Haasterecht, M.J.T., Masalmeh, S.K., Faber, M.J., Boersma, D.M., and Gruenenfelder, M., **Pushing the Envelope for Polymer Flooding Towards High-Temperature and High-Salinity Reservoirs with Polyacrylamide Based Ter-polymers**, paper SPE 141497, presented at the SPE Middle East Oil and Gas Show and Conference held in Manama, Bahrain, 25-28 September, 2011

Viksund, B.G., Morrow, N.R., Ma, S., Wang, W., and Graue, A., **Initial Water Saturation and Oil Recovery from Chalk and Sandstone by Spontaneous Imbibition**, Paper SCA-1998-14, presented at

the 1998 International Sumposium of the Society of Core Analysts, held in Hamburg, Germany, 14-16 September, 1998

Vledder, P., Fonseca, J. C., Wells, T., Gonzalez, I., & Ligthelm, D., **Low salinity water flooding: Proof of wettability alteration on a field wide scale**, Presented in the 17th Symposium on Improved Oil Recovery SPE 129564, Tulsa, Oklahoma, USA, 2010

Wardlaw, N.C., McKellar, M., **Oil blob populations and mobilization of trapped oil in unconsolidated packs,** Can. J. Chem. Eng. 63:525–532 (1985), 1985

Wardlaw, N.C., **The effects of geometry, wettability, viscosity and interfacial tension on trapping in single pore-throat pairs**, The Journal of Canadian Petroleum Technology, May-June, pp. 21-27, 1982

Wardlaw, N.C**., The effects of pore structure on displacement efficiency in reservoir rocks and in glass micromodels**, Paper SPE 8843 presented at the first joint SPE/DOE Symposium on EOR held in Tulsa, OK, USA, April 20-23, 1980

Warren, J.E., Root, P.J., **The behavior of naturally fractured reservoirs**, SPE J. 3(3), 245-255, 1963

Webb, K.J., Black, C.J.J., Al-Ajeel, H., **Low Salinity Oil Recovery – Log-Inject-Log**, Paper SPE 89379 presented at the 2004 SPE/DOE Fourteenth Symposium on Improved Oil Recovery held in Tulsa, OK, USA, 17-21 April, 2004

Webb, K.J., Lager, A., Black, C.J.J., **Comparison of High/Low Salinity Water/Oil Relative Permeability**, Paper SCA2008-39, 2008

Willhite, G., **Waterflooding**, Spe Textbook Series. Society of Petroleum Engineers, 1986

Xie, X., Morrow, N.R., **Oil Recovery by Spontaneous Imbibition from weakly water-wet rocks**, Petrophysics 42(4), 313-322, 2001

Yousef, A. A., Al-Saleh, S., Al-Kaabi, A., & Al-Jawfi, M., **Laboratory investigation of the impact of injection water salinity and ionic content on oil recovery from carbonate reservoirs**, SPE Reservoir Evaluation & Engineering, 15, 578–593, 2011

Yu, L., **Wettability Alteration During Spontaneous Imbibition of Seawater Into Preferentially Oil-Wet Chalk**, PhD Thesis UiS no.55 – August, 2008

Yu-shu, W., & Baojun, B., **Efficient simulation for low salinity waterflooding in porous and fractured reservoirs**, In SPE Reservoir Simulation Symposium SPE 118830, The Woodlands, Texas, USA, 2009

Zeinijahromia, A., Vazb, A., Bedrikovetsky, P., **Well impairment by fines migration in gas fields**, Journal of Petroleum Science and Engineering, Volume 88-89, June 2012, Pages 125-135, 2012

Zeppieri, S., Rodrigeuz, J., Lopez de Ramos, A.L., **Interfacial tension of alkane + water systems**, J. Chem. Eng., Data 2001, 46, 1086-1088, 2001

Zhang, P., Tweheyo, M.T., Austad, T., **Wettability Alteration and Improved oil recovery by spontaneous imbibition of seawater into chalk: Impact of the potential determining ions: Ca^{2+}, Mg^{2+} and So_4^{2-}**, Colloids and surfaces A: Physiochem. Eng. Aspects, 301: 199-208, 2007a

Zhang, X., N.R. Morrow, S. Ma, **Experimental verification of a modified scaling group for spontaneous imbibition,** SPE Reservoir Eng, 11 (4) (November 1996), pp. 280–285, 1996

Zhang, Y., Morrow, N.R., **Comparison of Secondary and Tertiary Recovery With Change in Injection Brine Composition for Crude Oil/Sandstone Combinations**, SPE/DOE, Symposium on Improved Oil Recovery, Society of Petroleum Engineers, Tulsa, OK, USA, 2006a

Zhang, Y., Morrow, N.R., **Comparison of Secondary and Tertiary Recovery with Change in Injection Brine Composition for Crude Oil / Sandstone Combinations**, Paper SPE 99757, 2006b

Zhang, Y., Xie, X., Morrow, N.R., **Waterflood Performance by Injection of Brine with Different Salinity for Reservoir Cores**, Paper SPE 109849, presented at the 2007 SPE Annual Technical Conference and Exhibition, Anaheim, CA, USA, 2007b

Zhou, X., Morrow, N.R., Ma, S.M**., Interrelationship of Wettability, Initial Water Saturation, Aging Time, and Oil Recovery by Spontaneous Imbibition and Waterflooding**, SPE Journal 5(2): 199-207, 2000

Zolotuchin, A.B. and Ursin, J.R., **Introduction to petroleum reservoir engineering**, Kristiansand Høyskoleforlag, 2000

Picture 1: Wikipedia, http://en.wikipedia.org/wiki/File:DoubleLayer.gif

Picture 2: Wikipedia, http://en.wikipedia.org/wiki/File:Double_Layer.png

Appendix

Solid analysis of the sandstone

Parameter	Results	Unit	PQL			Uncertainty	
Elements in solids, XRF			Lower	Upper	Method/Standard	Rel	Abs
Aluminum, Al	1.8	wt%	0.1	-	X-021 (XRF)	10%	-
Barium, Ba	<0.1	wt%	0.1	-	X-021 (XRF)	10%	-
Calcium, Ca	0.1	wt%	0.1	-	X-021 (XRF)	10%	-
Chromium, Cr	<0.1	wt%	0.1	-	X-021 (XRF)	10%	-
Copper, Cu	<0.1	wt%	0.1	-	X-021 (XRF)	10%	-
Iron, Fe	0.2	wt%	0.1	-	X-021 (XRF)	10%	-
Potassium, K	0.6	wt%	0.1	-	X-021 (XRF)	10%	-
Magnesium, Mg	<0.1	wt%	0.1	-	X-021 (XRF)	10%	-
Manganese, Mn	<0.1	wt%	0.1	-	X-021 (XRF)	10%	-
Sodium, Na	<0.1	wt%	0.1	-	X-021 (XRF)	10%	-
Nickel, Ni	<0.1	wt%	0.1	-	X-021 (XRF)	10%	-
Phosphorus, P	<0.1	wt%	0.1	-	X-021 (XRF)	10%	-
Lead, Pb	<0.1	wt%	0.1	-	X-021 (XRF)	10%	-
Silicon, Si	44	wt%	0.1	-	X-021 (XRF)	10%	-
Strontium, Sr	<0.1	wt%	0.1	-	X-021 (XRF)	10%	-
Titanium, Ti	<0.1	wt%	0.1	-	X-021 (XRF)	10%	-
Zinc, Zn	<0.1	wt%	0.1	-	X-021 (XRF)	10%	-
Sulphur, S	<0.1	wt%	0.1	-	X-021 (XRF)	10%	-
Chlorine, Cl	0.1	wt%	0.1	-	X-021 (XRF)	10%	-

Table A.1: Content solid analysis of the sandstone used in the experiments. Analyzed by XRF.

Composition of synthetic seawater, SSW.

Salt	**m [g/l]**	**m [mole/l] (molar)**
SSW	38.67	-
NaCl	23.38	0.400
Na2SO4	3.41	0.024
NaHCO3	0.17	0.002
KCl	0.75	0.010
MgCl2	4.24	-
$CaCl_2$ (dry)	1.44	-
$MgCl_2 \times 6H_2O$	9.05	0.045
$CaCl_2 \times 2H_2O$	1.91	0.013
BaCl2 x 2H2O	-	-
SrCl2 x 6H2O	-	-
Density $[\frac{g}{cm^3}]$	1.024	-
Weight [%]	3.42	-
TDS [g/l]	33.39	-
Ionic Strength	-	0.657
$\boldsymbol{Ca^{2+}}$ **/** $\boldsymbol{SO_4^-}$	-	0.542
Ions	**m [g/l]**	**m [mole/l] (molar)**
HCO_3^-	0.12	0.002
Cl^-	18.62	0.525
SO_4^{2-}	2.31	0.0240
Mg^{2+}	1.08	0.045
Ca^{2+}	0.52	0.013
Na^+	10.35	0.450
K^+	0.39	0.010

Table A.2: Composition of synthetic seawater, SSW

Composition of low salinity water, LSW

Salt	**m [g/l]**	**m [mole/l] (molar)**
SSW	1.5468	-
NaCl	0.9352	0.016
Na2SO4	0.1364	0.00096
NaHCO3	0.0068	0.00008
KCl	0.03	0.0004
MgCl2	0.1696	-
$CaCl_2$ (dry)	0.0576	-
$MgCl_2 \times 6H_2O$	0.362	0.0018
$CaCl_2 \times 2H_2O$	0.0764	0.00052
BaCl2 x 2H2O	-	-
SrCl2 x 6H2O	-	-
Density $[\frac{g}{cm^3}]$	1.024	-
Weight [%]	0.1368	-
TDS [g/l]	1.3356	-
Ionic Strength	-	0.05104
Ca^{2+} / SO_4^-	-	0.542
Ions	**m [g/l]**	**m [mole/l] (molar)**
HCO_3^-	0.0048	0.00008
Cl^-	0.7448	0.021
SO_4^{2-}	0.0924	0.00096
Mg^{2+}	0.0432	0.0018
Ca^{2+}	0.0208	0.00052
Na^+	0.414	0.018
K^+	0.0156	0.0004

Table A.3: Composition of low salinity water, LSW

Standard deviation

Standard deviation shows how much variation or dispersion exists from the average, mean or expected value. A low standard deviation indicates that the data points tend to be very close to the mean, high standard deviation indicates that the data points are spread out over a large range of values.

$$\sigma_s = \sqrt{\frac{1}{N}\sum_{i=1}^{N}(X_i - \bar{X})^2}$$

$$\sigma_{s,c} = \sqrt{\frac{1}{N-1}\sum_{i=1}^{N}(X_i - \bar{X})^2}$$

σ_s = Standard deviation

$\sigma_{s,c}$ = Corrected standard deviation

N = Number of samples

X_i = Observed value

$\bar{X}$ = Mean value of observations

Results from ion analysis

All data is given in milli mole/l.

#5		Sodium [Na]	Potassium [K]	Magnesium [Mg]	Calcium [Ca]	Chloride [Cl]	Carbonate [HCO3]	Sulfate [SO4]
Porevolume	#							
0,00	0	23,526	0,813	2,172	0,871	25,393	0,357	1,020
0,50	1	322,776	7,682	30,307	14,719	376,087	0,622	18,004
2,00	2	108,176	4,062	8,237	4,081	122,441	0,604	5,624
2,33	3	21,960	3,438	1,675	1,041	25,885	0,586	0,977
2,58	4	20,509	0,672	1,737	1,046	21,838	0,586	0,880
2,83	5	24,028	1,996	2,182	1,236	27,334	0,610	1,050
3,33	6	23,851	3,300	2,054	1,251	28,503	0,570	1,035
4,33	7	25,970	4,251	2,346	1,363	32,228	0,562	1,150
5,67	8	21,073	1,966	1,670	1,144	22,509	0,699	0,835

Table A.4: Results from ion analysis on core #5, LSW-flooding.

#6		Sodium [Na]	Potassium [K]	Magnesium [Mg]	Calcium [Ca]	Chloride [Cl]	Carbonate [HCO3]	Sulfate [SO4]
Porevolume	**#**							
0,00	**0**	432,668	8,798	43,635	14,501	501,299	1,758	22,773
1,43	**1**	451,553	10,558	44,350	16,255	521,659	2,229	23,900
1,76	**2**	412,898	12,043	41,125	14,180	473,062	1,865	21,316
1,98	**3**	463,981	9,056	46,145	15,803	528,336	2,317	24,179
2,29	**4**	453,313	10,146	45,318	15,320	527,303	1,820	24,033
2,61	**5**	456,003	9,502	45,849	15,157	531,269	1,953	24,153
3,16	**6**	480,185	10,052	48,965	15,777	561,527	1,882	25,472
3,47	**7**	446,192	9,030	44,519	14,727	513,242	1,261	23,304
3,87	**8**	467,104	10,292	46,864	15,457	538,915	1,252	24,477
4,42	**9**	461,190	10,470	47,115	14,327	541,979	0,704	25,950
4,74	**10**	464,186	10,496	47,477	15,872	548,679	0,668	26,389
5,05	**11**	466,832	11,054	50,152	16,436	574,082	0,821	30,271
5,38	**12**	351,912	7,948	33,928	11,357	406,968	0,772	19,527
6,95	**13**	69,579	2,084	4,904	1,929	74,806	0,726	3,297
7,26	**14**	27,448	0,693	2,535	1,232	30,685	0,306	1,258
7,58	**15**	26,108	0,648	2,510	1,238	29,095	0,477	1,171
7,90	**16**	27,119	0,792	2,482	1,276	29,628	0,508	1,193
8,92	**17**	26,734	0,655	2,471	1,249	28,951	0,575	1,194
9,87	**18**	25,624	0,717	2,516	1,098	29,267	0,473	1,177
10,82	**19**	27,112	0,951	2,454	1,173	29,217	0,644	1,165
11,77	**20**	27,771	2,056	2,522	1,165	30,558	0,604	1,172
12,40	**21**	28,135	0,715	2,495	1,184	29,614	0,748	1,198
13,02	**22**	302,737	5,901	32,833	10,995	357,682	0,471	16,941
13,34	**23**	403,274	8,850	41,924	13,989	472,659	0,570	22,538
14,21	**24**	437,576	9,624	44,686	14,822	511,601	0,544	24,445

Table A.5: Results from ion analysis on core #6, SSW-LSW-SSW flooding, respectively.

#7		Sodium [Na]	Potassium [K]	Magnesium [Mg]	Calcium [Ca]	Chloride [Cl]	Carbonate [HCO3]	Sulfate [SO4]
Porevolume	#							
0,00	0	448,259	11,458	45,210	13,289	521,166	1,608	23,743
0,83	1	442,342	11,676	42,163	16,567	514,124	1,922	23,378
1,17	2	458,028	12,911	45,825	13,904	530,984	2,060	24,203
1,50	3	458,360	11,154	45,874	13,519	533,842	1,570	24,295
3,17	4	455,835	10,585	46,053	12,881	530,583	1,796	24,236
3,50	5	452,978	10,177	45,161	13,363	524,602	1,947	24,000
3,83	6	454,425	13,043	44,842	12,666	527,286	1,960	23,935
4,17	7	448,996	15,920	44,832	12,959	526,098	1,909	23,772
4,50	8	398,505	17,985	39,752	13,386	471,390	0,666	25,515
6,33	9	135,181	5,133	9,921	2,927	112,374	0,669	27,091
6,67	10	50,240	1,915	0,583	0,748	2,383	0,546	26,293
7,00	11	49,579	3,603	0,365	0,715	3,793	0,490	26,108
7,33	12	50,487	2,454	0,296	0,666	2,835	0,603	26,156
7,67	13	49,738	3,980	0,323	0,615	4,188	0,559	26,068
8,33	14	49,129	1,388	0,216	0,575	1,799	0,502	25,708
9,33	15	49,164	0,204	0,180	0,578	0,743	1,046	25,851
10,67	16	48,855	1,191	0,162	0,550	1,602	0,509	25,504
12,00	17	111,717	2,665	6,919	2,141	81,232	0,562	25,943
12,67	18	268,142	4,426	21,738	7,153	274,996	0,449	27,711
13,33	19	393,819	10,886	38,876	11,421	452,335	0,666	26,675
14,20	20	438,787	10,744	45,069	13,166	511,586	0,656	26,249

Table A.6: Results from ion analysis on core #7, SSW-S04-SSW flooding, respectively.

#8		Sodium [Na]	Potassium [K]	Magnesium [Mg]	Calcium [Ca]	Chloride [Cl]	Carbonate [HCO3]	Sulfate [SO4]
Porevolume	#							
0,00	0	442,508	10,177	43,471	11,671	514,768	2,186	23,622
0,67	1	464,249	12,388	43,713	14,944	540,868	2,085	25,030
1,00	2	466,876	15,132	44,798	13,830	544,443	1,269	24,566
1,33	3	454,351	11,021	45,103	13,693	524,652	1,972	24,080
2,00	4	465,705	10,955	45,258	12,932	540,305	2,035	24,577
2,83	5	453,724	10,063	45,723	13,289	525,604	2,588	24,238
3,83	6	457,696	10,832	45,501	13,179	529,665	1,746	24,086
4,17	7	453,945	9,901	44,769	12,840	522,427	2,625	24,201
4,50	8	439,937	9,816	44,667	13,014	512,253	1,947	23,258
4,83	9	259,667	7,585	41,616	8,286	336,026	0,637	14,263
5,17	10	83,236	3,517	44,269	3,618	169,129	0,606	4,322
6,83	11	16,248	1,058	46,106	1,259	104,617	0,562	0,793
7,17	12	6,355	0,434	47,349	0,762	95,782	0,603	0,294
7,50	13	2,587	0,071	47,756	0,390	93,393	0,502	0,037
7,83	14	2,643	0,040	47,850	0,328	93,162	0,515	0,024
8,83	15	2,373	0,026	48,624	0,440	93,314	0,458	0,020
11,20	16	1,733	0,028	49,009	0,366	94,047	0,531	0,024
11,67	17	1,855	0,017	48,822	0,419	93,723	0,455	0,031
12,13	18	101,595	3,429	52,970	2,556	195,506	0,358	5,163

Table A.7: Results from ion analysis on core #8, SSW-Mg-SSW flooding, respectively.